AD-A058 385 ARMY MISSILE RESEARCH AND DEVELOPMENT COMMAND REDSTO--ETC F/G 20/3
AN INVESTIGATION OF RADIATION TRANSFER THROUGH AEROSOLS.(U)
JUN 78 B W FOWLER

UNCLASSIFIED DRDMI-C-78-3 NL

1 OF 3
AD
A058 385

LEVEL II

12

ADA058385

TECHNICAL REPORT C-78-3

AN INVESTIGATION OF RADIATION TRANSFER THROUGH AEROSOLS

Bruce W. Fowler
Advaned Systems Concepts Office

U.S. ARMY
MISSILE
RESEARCH
AND
DEVELOPMENT
COMMAND

Redstone Arsenal, Alabama 35809

JUNE 1978

DISPOSITION INSTRUCTIONS

DESTROY THIS REPORT WHEN IT IS NO LONGER NEEDED. DO NOT RETURN IT TO THE ORIGINATOR.

DISCLAIMER

THE FINDINGS IN THIS REPORT ARE NOT TO BE CONSTRUED AS AN OFFICIAL DEPARTMENT OF THE ARMY POSITION UNLESS SO DESIGNATED BY OTHER AUTHORIZED DOCUMENTS.

TRADE NAMES

USE OF TRADE NAMES OR MANUFACTURERS IN THIS REPORT DOES NOT CONSTITUTE AN OFFICIAL INDORSEMENT OR APPROVAL OF THE USE OF SUCH COMMERCIAL HARDWARE OR SOFTWARE.

UNCLASSIFIED
SECURITY CLASSIFICATION OF THIS PAGE (When Data Entered)

REPORT DOCUMENTATION PAGE	READ INSTRUCTIONS BEFORE COMPLETING FORM
1. REPORT NUMBER C-78-3	2. GOVT ACCESSION NO. / 3. RECIPIENT'S CATALOG NUMBER
4. TITLE (and Subtitle) (6) AN INVESTIGATION OF RADIATION TRANSFER THROUGH AEROSOLS	5. TYPE OF REPORT & PERIOD COVERED
	6. PERFORMING ORG. REPORT NUMBER
7. AUTHOR(s) (10) Bruce W. Fowler	8. CONTRACT OR GRANT NUMBER(s)
9. PERFORMING ORGANIZATION NAME AND ADDRESS Commander US Army Missile Research & Development Command Attn: DRDMI-C Redstone Arsenal, Alabama 35809	10. PROGRAM ELEMENT, PROJECT, TASK AREA & WORK UNIT NUMBERS
11. CONTROLLING OFFICE NAME AND ADDRESS Commander US Army Missile Research & Development Command Attn: DRDMI-TI Redstone Arsenal, Alabama 35809	12. REPORT DATE (11) June 1978 / 13. NUMBER OF PAGES 196
14. MONITORING AGENCY NAME & ADDRESS(if different from Controlling Office)	15. SECURITY CLASS. (of this report) Unclassified / 15a. DECLASSIFICATION/DOWNGRADING SCHEDULE

16. DISTRIBUTION STATEMENT (of this Report)

Approved for public release; distribution unlimited. (12) 202 p.

17. DISTRIBUTION STATEMENT (of the abstract entered in Block 20, if different from Report)

(14) DRDMI-C-78-3

18. SUPPLEMENTARY NOTES

(9) Technical rept.

19. KEY WORDS (Continue on reverse side if necessary and identify by block number)

Radiative transfer
Aerosols
Cylindrically symmetric nonspherical particle
Prolate spheroids
Two-dimensional radiative transfer equation
Numerical algorithm
Image propagation
Uniform and gaussian profile

20. ABSTRACT (Continue on reverse side if necessary and identify by block number)

Some aspects of the problem of radiative transfer through aerosols are investigated. The scattering of a plane wave of light of arbitrary wavelength by a cylindrically symmetric nonspherical particle of arbitrary size and refractive index is addressed. The Hertz vector formalism originally used by Mie to treat the spherical particle problem is extended to nonspherical particles. The electromagnetic boundary conditions are reduced to become a set of linear algebraic equations that are solved numerically. All computer code implementing the solution is developed and calculations for selected non-

DD FORM 1 JAN 73 1473 EDITION OF 1 NOV 65 IS OBSOLETE

UNCLASSIFIED
SECURITY CLASSIFICATION OF THIS PAGE (When Data Entered)

20. ABSTRACT (Concluded)

spherical particles are presented. It is shown that the agreement between exact and approximate calculations for prolate spheroids is good. Additionally, the validity and utility of the Mie solution modification recently proposed by Chylek, Grams, and Pinnick are examined. Experimental data for polydisperse nonspherical aerosols are examined.

The multiple scattering of light by aerosols is also addressed through the Radiative Transfer equation. Previously, the Radiative Transfer equation had been primarily used to consider only one-dimensional problems associated with planetary and stellar atmospheres. To consider more general problems associated with laser beam and image propagation, a solution of the two-dimensional Radiative Transfer equation is developed in the form of a numerical algorithm. A computer code implementing this algorithm is presented. Calculations are presented for both uniform and gaussian profile beams. These calculations were performed for a uniform Deirmendjian C.3 fog model at three wavelengths; 1.06 μm, 3.0 μm., 10.6 μm. The effects of multiple scattering on the transmission, backscatter, and contrast transmission of these beams are discussed.

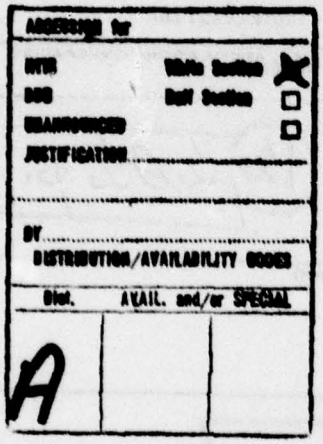

TABLE OF CONTENTS

ACKNOWLEDGMENT

The author would like to acknowledge the unrelenting patience and assistance of his advisor, C. C. Sung over the period 1972-1978. The financial support of the U. S. Army in providing tuition funds and computer time is gratefully acknowledged. The support of the author's parents, friends, and coworkers in the Advanced Systems Concepts Office, U. S. Army Missile Research and Development Command was no small factor in the completion of this dissertation.

Specifically, the author wishes to acknowledge the assistance and support rendered by Emery L. Atkins, Donald R. Peterson, and O. Fred Kezer. This dissertation would not have been possible without the advice and sympathy accorded the author by these three.

CHAPTER I

INTRODUCTION

This dissertation describes the results of an investigation of radiation transfer through aerosols. Aerosols have been studied for many years, and several good reference works on the physical properties of aerosols are available. (Green and Lane, 1964; Sedunov, 1974; Fuchs and Sutugin, 1970; Junge, 1963; Voloshchuk and Sedunov, 1973; Friedlander, 1977.) Sedunov presents a concise, useful definition of an aerosol: a solid and/or liquid substrate in a gaseous superstrate. Basically an aerosol is a collection of solid and/or liquid particles suspended in a gas. The gas involved is usually an atmosphere such as that of the earth, and the particles are suspended due to some act of nature or man. Aerosols may be generated by meteorological conditions (condensation fog), by the wind (dust or near surface haze), and by combustion (most smokes).

Most liquid aerosols are comprised of water, often with impurities. Solid aerosols are more varied, being comprised of such varied materials as minerals (dust), elemental carbon, or organic compounds (spores). In some situations, it is possible for an aerosol particle to be both solid and liquid. An example of this would be a dust aerosol that is exposed to varying humidity conditions: a gust of wind raises a cloud of dust, the particles, which are irregular in shape,

are carried into a region of greater humidity and water is adsorbed on the surface of the particle(s). This adsorbtion has the effect of making the particle more spherical in shape and increasing its size. If the particle is insoluble, it may continue to adsorb water until equilibrium is reached. Sufficient water may be adsorbed to completely cover the particle. Then this particle would be layered, with an irregular, solid core, and coated with liquid that is externally spherical. If the particle were water soluble, the water solution would eventually form a spherical water particle with impurities.

In general, liquid aerosol particles are spherical until they become large enough for gravity and aerodynamic drag to deform them. Solid aerosol particles are usually nonspherical, although spores, some forms of carbon, and some plastics may be spherical.

Aerosols are, of course, a collection of particles, and in addition to their shape, must be described in terms of their sizes. (Aerosol collections made up of particles of only one size are monodisperse, those of particles of several sizes are polydisperse.) The number of particles per unit volume per unit size is usually described by a particle size distribution function, size usually being expressed in terms of the particle radius, although particle diameter, area, volume or mass may be used (Corn, 1976). Because the radius representation is the most common, and is well suited to radiation transfer calculations, the radius representation will be used in this dissertation.

There are three main types of particle size distribution functions in common use. These are the Junge (Junge, 1963),

$$n(r) = C/r^{\eta} \tag{1.1}$$

where $n(r)$ = number of particles per unit volume per unit radius,

r = particle radius,

C = a constant, and

η = coefficient,

the Deirmendjian modified gamma (Deirmendjian, 1964),

$$n(r) = Ar^{\gamma}\exp\,[-Br^{\delta}] \tag{1.2}$$

where A, B, γ, δ, are the parameters, and

the log normal (Corn, 1976),

$$n(r) = \frac{D}{r}\exp\,[-\{\ln(r) - \ln(\langle r\rangle)\}^2/2\ln(\sigma)^2] \tag{1.3}$$

where D = coupling constant,

$\langle r\rangle$ = average particle radius, and

σ = standard deviation.

The Junge distribution is commonly used to describe atmospheric aerosols (haze), is defined with an upper and lower limit on particle radius, and has a coefficient η that is observed to vary between the limits of 2.5 and 4. A Junge distribution is shown in Figure (1.1).

The Deirmendjian distribution is commonly used to describe fog,

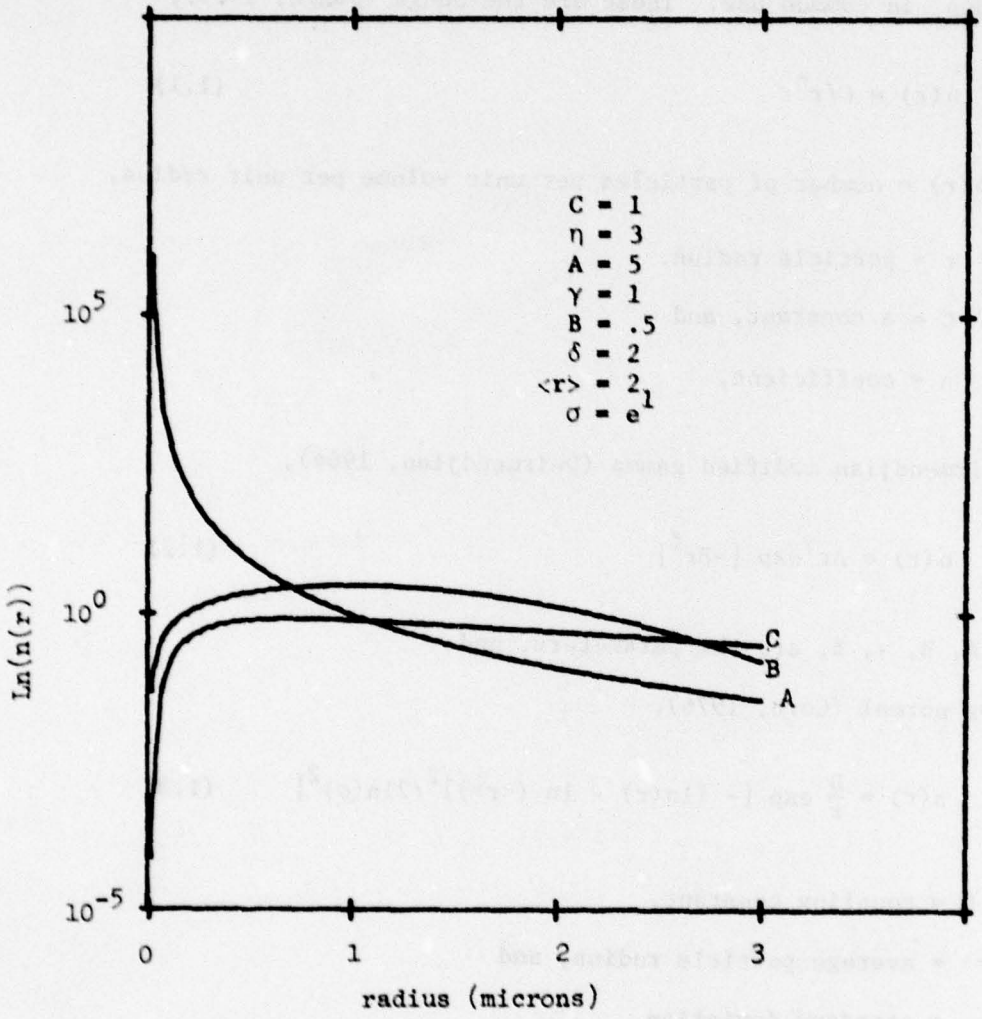

Figure (1.1) Particle Size Distributions for Junge (A), Deirmendjian (A), and Log Normal (C) Distributions.

haze, and rain. An example of the Deirmendjian distribution is shown in Figure (1.1). The log normal distribution is also commonly used to describe fogs and hazes as well as many smokes. This distribution enjoys much experimental popularity due to the ease it affords data analysis. An example of a log normal distribution is also shown in Figure (1.1).

While nonspherical aerosols exist and are commonplace, they are usually described in terms of one of these three distributions and rules exist for determining the "equivalent" spherical size of the particles (Cadle, 1965). No attempt is made by Cadle to describe the shape distribution of the particles as a function of size.

Aerosols are also described by their refractive indices. This quantity is usually complex and because of the difficulty of measuring it, is assumed to be constant for any one aerosol with respect to particle size and shape. The refractive index of water is shown as an example in Figure (1.2) (Deirmendjian, 1975).

The first step in treating the problem of radiation transfer through aerosols is to solve the problem of the scattering of light by a single particle. This problem has been studied with notable success since the formulation of the Maxwell Equations (Rayleigh, 1871; Mie, 1908; Debye, 1909). While an analytic solution for the scattering and absorption of a plane wave of light of arbitrary wavelength by a sphere of arbitrary radius and refractive index (the Mie solution) has long been known, the extent of the numerical calculations has precluded extensive use of the solution until the recent advent of the digital computer. The Rayleigh solution for particles small in radius compared to the wavelength is relatively simple and has

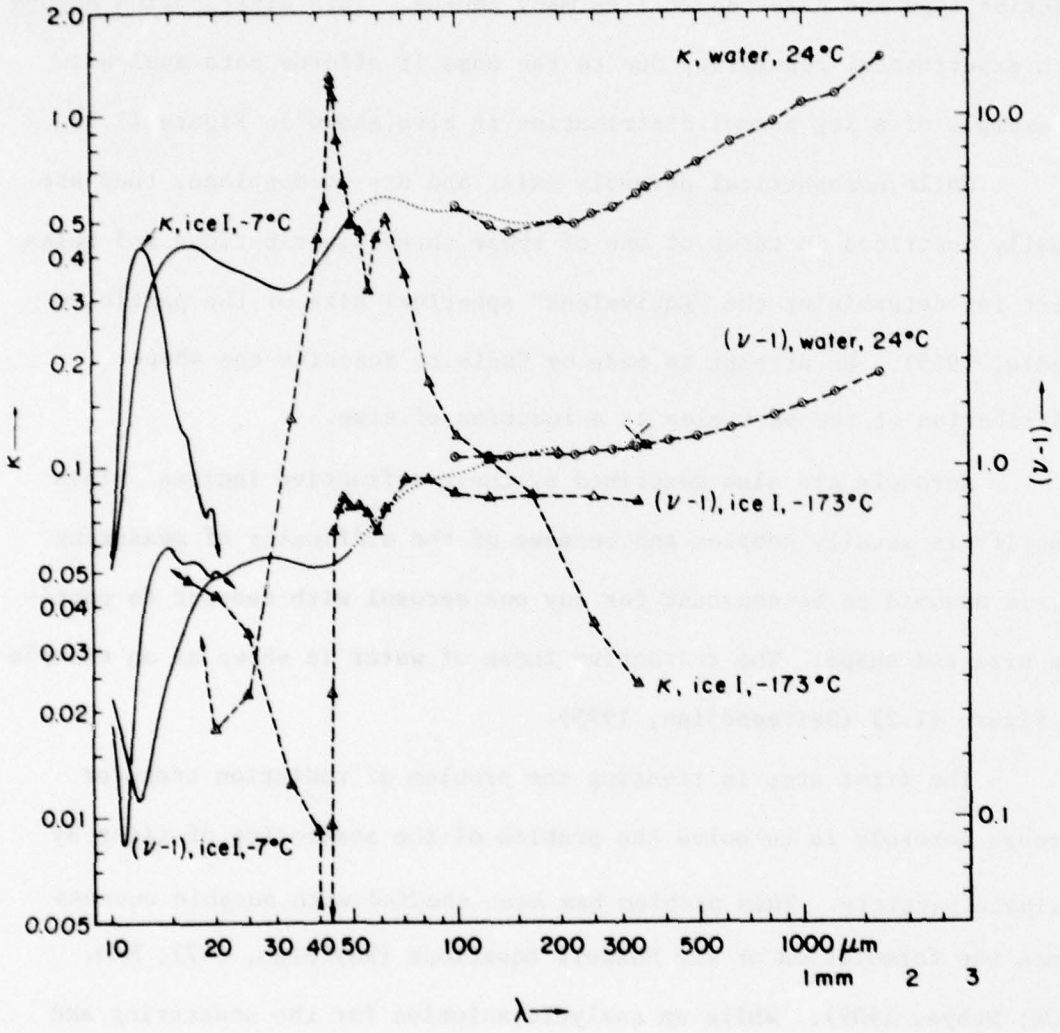

Figure (1.2). Refractive Index of Water.

LEGEND: k = Re(m)
ν = -Im(m)
m = refractive index
λ = wavelength

therefore enjoyed much wider use prior to the computer's advent. While the Rayleigh solution is not applicable to most aerosols for wavelengths shorter than the submillimeter (100 μm.), it is applicable to gas molecules even into the ultraviolet, and much work on the single and multiple scattering properties of clear atmospheres has been conducted.

At this time, no elegant solution to rival Mie theory has appeared to describe the scattering properties of general nonspherical particles except for small size particles which may be treated by Rayleigh-Gans theory (Gans, 1925). Attempts have been made to adjust particle size distributions used with Mie theory to reproduce experimental data, but these efforts have met with limited success (Cadle, 1965).

In recent years, several treatments of the problem of single scattering by irregular particles have been advanced. These treatments have included extensions of the Mie solution into other coordinate systems where Helmholtz's equation is separable. One notable example of this type of effort is the solution for prolate and oblate spheriods (Asano and Yamamoto, 1975).

Perturbation techniques have been applied by expanding the electric and magnetic fields, and the particle's shape in perturbation series. Application of the boundary conditions results in a perturbation equation that allows the corrections to the electric and magnetic fields to be calculated in a bootstrap manner (Yeh, 1964). Unfortunately, this method suffers from the usual limitation of perturbation theory -- the perturbations must be small.

A technique that has enjoyed some use in describing conductors is the use of the last-squares regression technique to solve for the

scattered electric and magnetic fields (Davies, 1973). This technique, however, does not exactly satisfy the boundary conditions of electrodynamics.

One recent technique of note has been the use of an integral equation formalism (Eyres and Nelson, 1976; Uzonoglu and Holt, 1977; Waterman, 1971). While integral equation formalisms have been used before, these latest treatments are notable because the boundary conditions are properly accounted for, and the numerical solution is obtained, not by iteration, but by reducing the integral equations to linear equations and obtaining the expansion coefficients.

An empirical treatment recently advanced is a modification of the Mie solution based on the correlation of resonances in the analytical solution with glories in the experimental data (Chylek, Grams, and Pinnick, 1976). Although calculations performed using this modification have displayed better agreement with experimental data than Mie calculations, the validity of the modification has been criticized (Kerker, 1977). While this treatment offers a possibility of widespread usefulness because of its computational simplicity, the modification's basis has not been substantiated by more exact calculations.

The second step in treating the radiation transfer problem is to extend the calculations of the single scattering of light by a single particle to the single scattering of light by a collection of particles. In most cases, notably for naturally occuring aerosols and the visible wavelengths of light, aerosol particles are sufficiently large that the Mie solution is required. Fortunately, the aerosols are also sufficiently dilute so that during any reasonably long period of

time, the particles are in the far fields of all the other particles. Deirmendjian has shown that under these circumstances, the particles are independent and the scattered intensities rather than the scattered electric and magnetic fields may be added (Diermendjian, 1964). As a result, the scattering properties of most aerosols may be described in terms of an average particle. It should be noted, however, that work has been done to include the interparticle correlations (Foldy, 1945). As the submillimeter and millimeter regions of the spectrum become more accessable and utilized, the importance of this problem should become more apparent.

The third step in treating the problem of radiation transfer through aerosols is the calculation of the multiple scattering effects that may occur in an aerosol medium. To perform this calculation, the theory of radiative transfer (RT) developed by Chadrasekhar may be used (Chandrasekhar, 1960). This theory has enjoyed extensive use in describing the propagation of light through stellar and planetary atmospheres. These two problems are characterized by three notable conditions: first, the illumination incident onto and/or from the atmosphere is uniform; second, the scattering medium varies in only one direction at most; and third, the scattering phase function of a gas (the Rayleigh solution) has a simple analytic form. These conditions allowed the general form of the RT equation to be reduced to a one-dimensional form that could in a few cases be solved analytically and, for the Rayleigh phase function, could be solved numerically without the computer. Indeed, this numerical solution represented the essential state-of-the-art prior to the computer's advent about 1960.

The digital computer has permitted the RT equation in its one-dimensional form to be solved for other, more complicated phase functions so that the problems of light transmission through a hazy atmosphere or an atmosphere with uniform cloud cover could be solved.

While this one-dimensional form of the RT equation was adequate for describing the brightness of a star, or the amount of light reaching the surface of a planet, advances in detector/source technology have uncovered problems that the existing RT techniques cannot treat. The availability of both visible and infrared imaging devices and of the laser have introduced a new class of problems involving nonuniform incident illumination. The determination of laser beam broadening or imaging contrast degradation due to multiple scattering is beyond the scope of the uniform illumination formulation of RT.

To date, however, only limited attempts have been made to solve the general RT equation. Notable among these is a calculation using the four-dimensional RT equation simplified for small angle scattering only (Weinman and Shipley, 1972). This calculation, which was performed to predict laser pulse stretching in clouds, is valid only when the aerosol particles are much larger than the wavelength. (The phase function is sharply peaked.) This approach is not valid for scattering by atmospheric gases because the Rayleigh phase function is not sharply peaked.

Another notable calculation was performed to support the optical measurement of the particle size distribution in a chamber (Deepak and Green, 1975). Although this calculation was valid for general scattering angle, it was carried out only to third order in scattering. While third order scattering is adequate for the optical depths observed in

the experiment, the technique of Deepak and Green is not readily applicable to problems that require that higher orders of scattering and/or more general boundary conditions be considered.

As a result of these considerations, this dissertation investigation was begun to determine the effects of aerosol and atmospheric gas multiple scattering on imaging and laser beam transmission. These transmission calculations involve nonuniform incident illuminations and aerosol media that had not, to date, been generally treated, either analytically or numerically. This phase of investigation has resulted in a two-dimensional RT code for the treatment of imaging and laser beam transmission. This code constitutes the contribution of this investigation to the third step of the radiation transfer problem.

As calculations with this code proceeded from liquid aerosols to solid aerosols, the problem of single scattering by irregular particles surfaced. As has been noted earlier, several techniques for treating the problem were known, but none provided the necessary information for solution of the RT equation. This information includes the extinction coefficient, the albedo, and the phase functions for irregularly shaped dielectric aerosols. Considerable effort has been made to extend the Mie solution to irregular particles to provide this information. This extension was implemented into a code for solving the single scattering problem for cylindrically symmetric irregular dielectric particles. This restriction is imposed, not by limitations of the theory, but by limitations of the computer. The development, implementation and use of this code is described in this dissertation.

This code constitutes the contribution of this investigation to the first part of the problem of radiation transfer through aerosols. Thus, of three parts to the problem, two have been addressed in this investigation: the single scattering by an irregular dielectric particle, and the multiple scattering effects for nonuniform boundary conditions.

In Chapter II of this dissertation, the Hertz vector formalism is developed from the Maxwell Equations. This formalism has the advantage of reducing the vector differential equations (which are derived directly from the Maxwell Equations) for describing the single scattering to scalar differential equations. This Hertz vector formalism is then used in Chapter III to derive the Mie solution. The extension of the Mie solution to aerosols is reviewed in Chapter IV.

Several of the previous formalisms for treating scattering by irregular particles are reviewed and discussed in Chapter V. Chapter VI then presents the theory for single scattering by irregular particles used in this investigation. This is an extension of the differential equation, Hertz vector formalism of Mie to "slightly" irregular particles with cylindrical symmetry. Unlike the Mie solution for the spherical particle, which has an analytic solution that can be evaluated, this formalism requires a numerical solution because the radius of the particle is itself a function of angle. This solution may be obtained by the computer, however, and a code to perform this calculation is described in Appendix (I).

The calculations performed using this code for spheres and spheroids are compared with exact calculations in Chapter VII. Additionally, sample calculations for a variety of irregular particles are

presented. In Chapter VIII, the validity of the Mie modification of Chylek, Grams and Pinnick is addressed (Chylek, Grams, and Pinnick, 1976). This modification is first examined by calculation of the electric and magnetic field expansion coefficients. Following this, polydisperse aerosol phase functions are calculated for several types of irregular particles after incorporating the techniques of Chapter IV into the code. These phase functions are then combined using linear regression techniques to fit experimental data.

Chapter IX begins the discussion of the multiple scattering part of this investigation. In this chapter, the general RT equation is presented and its reduction to one-dimensional form for the treatment of plane-parallel atmospheres is outlined. An approximate solution of the two-dimensional unpolarized RT equation suitable for imaging and steady-state laser beam transmission calculations is presented in Chapter X, together with an algorithm for its numerical solution. This algorithm is implemented in a code described in Appendix (IV). Calculations performed for transmission through a Deirmendjian C.3 fog using this code are presented in Chapter XI and discussed. Chapter XII is a summary of the results of this dissertation investigation with emphasis on the various limitations of the calculations. A few problems to be treated as future efforts are indicated.

CHAPTER II

ELECTROMAGNETIC WAVES AND HERTZ VECTORS

The Hertz vector formalism for electromagnetic waves may be derived from Maxwell's Equations (Jackson, 1962),†

$$\nabla \cdot \underset{\sim}{D} = 4\pi\rho, \tag{2.1}$$

$$\nabla \cdot \underset{\sim}{B} = 0, \tag{2.2}$$

$$\nabla \times \underset{\sim}{H} = \frac{4\pi}{c}\underset{\sim}{J} + \frac{1}{c}\frac{\partial \underset{\sim}{D}}{\partial t}, \tag{2.3}$$

and

$$\nabla \times \underset{\sim}{E} = -\frac{1}{c}\frac{\partial \underset{\sim}{B}}{\partial t}, \tag{2.4}$$

where: $\underset{\sim}{D}$ = the electric displacement,

$\underset{\sim}{E}$ = the electric field,

$\underset{\sim}{B}$ = the magnetic flux intensity,

$\underset{\sim}{H}$ = the magnetic field,

ρ = the charge density, and

c = the speed of light.

The constitutive equations are

$$\underset{\sim}{D} = \varepsilon\underset{\sim}{E}, \tag{2.5}$$

$$\underset{\sim}{J} = \sigma\underset{\sim}{E}, \tag{2.6}$$

and

$$\underset{\sim}{B} = \mu\underset{\sim}{H}, \tag{2.7}$$

† Gaussian units are used throughout this dissertation.

where: ε = the dielectric function (constant),

σ = the conductivity, and

μ = the permeability.

The dielectric function and the conductivity are restricted in this treatment to be scalar functions that change value only at known, definite boundaries. It is assumed that $\mu = 1$, and $\rho = 0$.

As a result of these restrictions, Eqs. (2.1) and (2.2) may be written as

$$\nabla \cdot \underset{\sim}{E} = 0, \tag{2.8}$$

and

$$\nabla \cdot \underset{\sim}{H} = 0. \tag{2.9}$$

For monochromatic light of wavelength, λ, $\underset{\sim}{E}$ and $\underset{\sim}{H}$ may be taken to have time dependence of the form $e^{i\omega t}$ where $\omega = 2\pi c/\lambda$. The modulus of the wave vector, k, and the refractive index, m, may be defined by

$$k = \omega/c = 2\pi/\lambda, \tag{2.10}$$

and

$$m^2 = \varepsilon - 4\pi i\sigma/\omega, \tag{2.11}$$

since the permeability is one (Born and Wolf, 1975; Van de Hulst, 1957).

Equations (2.3) and (2.4) may be rewritten using these caveats and Eqs. (2.5) and (2.6) as

$$\nabla \times \underset{\sim}{H} = -ikm^2 \underset{\sim}{E}, \tag{2.12}$$

and

$$\nabla \times \underset{\sim}{E} = ik\underset{\sim}{H} \ . \tag{2.13}$$

This set of Maxwell Equations, Eqs. (2.8), (2.9), (2.12), and (2.13) may be used to calculate the light scattering properties of individual particles.

In particular, Equations (2.8) and (2.9) admit the solution of the Maxwell Equations by Hertz vector. Because the divergence of the curl of a vector is zero ($\nabla \cdot \nabla \times \underset{\sim}{A} = 0$), the magnetic and electric Hertz vectors may be defined as

$$\underset{\sim}{E} = a\nabla \times \underset{\sim}{\Pi}, \tag{2.14}$$

and

$$\underset{\sim}{H} = b\nabla \times \underset{\sim}{\Sigma} \ , \tag{2.15}$$

where a and b are coefficients to be determined. It may be noted that $\underset{\sim}{\Pi}$ and $\underset{\sim}{\Sigma}$ are two independent solutions of the second order vector partial differential equations derivable from the Maxwell Equations. Because $\underset{\sim}{E}$ and $\underset{\sim}{H}$ must be transverse in the far field, $\underset{\sim}{\Pi}$ and $\underset{\sim}{\Sigma}$ must be radial vector functions and any linear differential equations in $\underset{\sim}{\Pi}$ and $\underset{\sim}{\Sigma}$ must be reducable to scalar equations.

The magnetic field due to $\underset{\sim}{\Pi}$ may be found by substituting Eq. (2.14) into Eqs. (2.12) and (2.13) to yield

$$\nabla \times \underset{\sim}{H} = - ikam^2 \nabla \times \underset{\sim}{\Pi} \ , \tag{2.16}$$

and

$$a\nabla \times \nabla \times \underset{\sim}{\Pi} = ik\underset{\sim}{H} \ , \tag{2.17}$$

so that

$$\underset{\sim}{H} = -i k a m^2 \underset{\sim}{\Pi} + \underset{\sim}{\nabla}\Phi \ , \tag{2.18}$$

where Φ is a scalar potential that is consistent with Eq. (2.16) since the curl of the gradient of a scalar is zero. This potential is included to insure that $\underset{\sim}{\Pi}$ will satisfy the Lorentz condition (Jackson, 1962; Tyras, 1969),

$$\Phi = \underset{\sim}{\nabla}\cdot\underset{\sim}{\Pi} \ . \tag{2.19}$$

Equation (2.17) may be rewritten using the vector identity,

$$\underset{\sim}{\nabla}x\underset{\sim}{\nabla}x\underset{\sim}{A} = \underset{\sim}{\nabla}(\underset{\sim}{\nabla}\cdot\underset{\sim}{A}) - \nabla^2\underset{\sim}{A} \ , \tag{2.20}$$

to become

$$a\underset{\sim}{\nabla}(\underset{\sim}{\nabla}\cdot\underset{\sim}{\Pi}) - a\underset{\sim}{\nabla}^2\Pi = i k \underset{\sim}{H} \ , \tag{2.21}$$

which may be combined with Eq. (2.18) to yield

$$a\underset{\sim}{\nabla}(\underset{\sim}{\nabla}\cdot\underset{\sim}{\Pi}) - a\nabla^2\underset{\sim}{\Pi} = a k^2 m^2 \underset{\sim}{\Pi} + i k \underset{\sim}{\nabla}\Phi. \tag{2.22}$$

Equation (2.22) may be combined with Eq. (2.19), the Lorentz condition, to yield

$$a\underset{\sim}{\nabla}(\underset{\sim}{\nabla}\cdot\underset{\sim}{\Pi}) - a\nabla^2\underset{\sim}{\Pi} = a k^2 m^2 \underset{\sim}{\Pi} + i k \underset{\sim}{\nabla}(\underset{\sim}{\nabla}\cdot\underset{\sim}{\Pi}) \ . \tag{2.23}$$

Since a is an arbitrary constant, it may be identified as ik, so that Eq. (2.23) reduces to

$$\nabla^2\underset{\sim}{\Pi} + k^2 m^2 \underset{\sim}{\Pi} = 0 \ , \tag{2.24}$$

Helmholtz's wave equation. Equations (2.14) and (2.18) may be rewritten as

$$\underset{\sim}{E} = ik\underset{\sim}{\nabla}\times\underset{\sim}{\Pi} \ , \tag{2.25}$$

and

$$\underset{\sim}{H} = k^2m^2\underset{\sim}{\Pi} + \underset{\sim}{\nabla}(\underset{\sim}{\nabla}\cdot\underset{\sim}{\Pi}) \ . \tag{2.26}$$

The electric Hertz vector, $\underset{\sim}{\Sigma}$, may be derived in a similar manner, starting with the substitution of Eq. (2.15) into Eqs. (2.12) and (2.13). This substitution yields

$$b\underset{\sim}{\nabla}\times\underset{\sim}{\nabla}\times\underset{\sim}{\Sigma} = - ikm^2\underset{\sim}{E} \tag{2.27}$$

and

$$\underset{\sim}{\nabla}\times\underset{\sim}{E} = ikb\underset{\sim}{\nabla}\times\underset{\sim}{\Sigma} \ . \tag{2.28}$$

Equation (2.28) may be exploited to admit

$$\underset{\sim}{E} = ikb\underset{\sim}{\Sigma} + \underset{\sim}{\nabla}\Psi \ , \tag{2.29}$$

where Ψ is a scalar potential that satisfies the Lorentz condition

$$\Psi = \underset{\sim}{\nabla}\cdot\underset{\sim}{\Sigma} \ . \tag{2.30}$$

Equation (2.27) may be rewritten using Eq. (2.20) as

$$b\underset{\sim}{\nabla}(\underset{\sim}{\nabla}\cdot\underset{\sim}{\Sigma}) - b\nabla^2\underset{\sim}{\Sigma} = bk^2m^2\underset{\sim}{\Sigma} - ikm^2\underset{\sim}{\nabla}\Psi \ . \tag{2.31}$$

Equation (2.27) allows b to be identified as $-ikm^2$, and Eq. (2.31) becomes

$$\nabla^2\underset{\sim}{\Sigma} + k^2m^2\underset{\sim}{\Sigma} = 0 \ , \tag{2.32}$$

the Helmholtz's wave equation for the Magnetic Hertz vector. Further, Equations (2.15) and (2.29) may be rewritten as

$$\underset{\sim}{H} = -ikm^2\underset{\sim}{\nabla}\times\underset{\sim}{\Sigma} \ , \tag{2.33}$$

and

$$\underset{\sim}{E} = k^2 m^2 \underset{\sim}{\Sigma} + \underset{\sim}{\nabla}(\underset{\sim}{\nabla}\cdot\underset{\sim}{\Sigma}) \ . \tag{2.34}$$

The Maxwell Equations, Equations (2.8), (2.9), (2.12), and (2.13) may now be replaced by the equations

$$\nabla^2 \underset{\sim}{\Pi} + k^2 m^2 \underset{\sim}{\Pi} = 0 \ , \tag{2.35}$$

$$\nabla^2 \underset{\sim}{\Sigma} + k^2 m^2 \underset{\sim}{\Sigma} = 0 \ , \tag{2.36}$$

$$\underset{\sim}{E} = ik\underset{\sim}{\nabla}\times\underset{\sim}{\Pi} + k^2 m^2 \underset{\sim}{\Sigma} + \underset{\sim}{\nabla}(\underset{\sim}{\nabla}\cdot\underset{\sim}{\Sigma}) \ , \tag{2.37}$$

and

$$\underset{\sim}{H} = k^2 m^2 \underset{\sim}{\Pi} + \underset{\sim}{\nabla}(\underset{\sim}{\nabla}\cdot\underset{\sim}{\Pi}) - ikm^2 \underset{\sim}{\nabla}\times\underset{\sim}{\Sigma} \ . \tag{2.38}$$

Equations (2.35) and (2.36) may be reduced to scalar differential equations because $\underset{\sim}{E}$ and $\underset{\sim}{H}$ must be transverse in the far field, and $\underset{\sim}{\Pi}$ and $\underset{\sim}{\Sigma}$ can therefore only be radial. The scalar potentials may be defined in relation to the Hertz vectors (Born and Wolf, 1975) by

$$\underset{\sim}{\Pi} = \hat{r}\pi \ , \tag{2.39}$$

and

$$\underset{\sim}{\Sigma} = \hat{r}\sigma \ , \tag{2.40}$$

where $\hat{r}$ is the unit vector in the radial direction. Equations (2.35) and (2.36) may be rewritten as

$$\nabla^2 \pi + k^2 m^2 \pi = 0 \ , \tag{2.41}$$

and

$$\nabla^2 \sigma + k^2 m^2 \sigma = 0 \ , \tag{2.42}$$

which have general solutions of the forms (Born and Wolf, 1975)

$$S = \sum_{\ell,m} \left(a_\ell \psi_\ell(kmr) + b_\ell \eta_\ell(kmr) \right) P_\ell^m(\cos\theta) \left[c_m \sin(m\phi) + d_m \cos(m\phi) \right], \tag{2.43}$$

and

$$S' = \sum_{\ell,m} \left(a'_\ell \rho_\ell^1(kmr) + b'_\ell \rho_\ell^2(kmr) \right) P_\ell^m(\cos\theta) \left[c_m' \sin(m\phi) + d_m' \cos(m\phi) \right] \tag{2.44}$$

depending on the boundary conditions to be applied. The angular function P_ℓ^m is the m^{th} associated Legend polynomial of order ℓ, and the cylinder functions ψ_ℓ, η_ℓ, ρ_ℓ^1, and ρ_ℓ^2 are related to the usual spherical Bessel functions (Abramowitz and Stegun, 1964) by

$$\psi_\ell(x) = x j_\ell(x), \tag{2.45}$$

$$\eta_\ell(x) = x y_\ell(x), \tag{2.46}$$

$$\rho_\ell^1(x) = x h_\ell^1(x), \tag{2.47}$$

$$\rho_\ell^2(x) = x h_\ell^2(x), \tag{2.48}$$

Equations (2.37) and (2.38) may be explicitly written as

$$E_r = k^2 m^2 \sigma + \frac{\partial^2 \sigma}{\partial r^2}, \tag{2.49}$$

$$E_\theta = \frac{k}{r\sin(\theta)} \frac{\partial \pi}{\partial \phi} + \frac{1}{r} \frac{\partial^2 \sigma}{\partial \theta \partial r} , \tag{2.50}$$

$$E_\phi = \frac{-ik}{r} \frac{\partial \pi}{\partial \theta} + \frac{1}{r\sin(\theta)} \frac{\partial^2 \sigma}{\partial \phi \partial r} , \tag{2.51}$$

$$H_r = k^2 m^2 \pi + \frac{\partial^2 \pi}{\partial r^2} , \tag{2.52}$$

$$H_\theta = \frac{1}{r} \frac{\partial^2 \pi}{\partial \theta \partial r} - \frac{ikm^2}{r\sin(\theta)} \frac{\partial \sigma}{\partial \theta} \tag{2.53}$$

$$H_\phi = \frac{1}{r\sin(\theta)} \frac{\partial^2 \pi}{\partial \phi \partial r} + \frac{ikm^2}{r} \frac{\partial \sigma}{\partial \theta} \tag{2.54}$$

Equations (2.41) - (2.54) constitute most of the basic mathematics for the solution of the Mie type problems to be discussed in subsequent chapters.

CHAPTER III

SPHERICAL PARTICLES:MIE THEORY

The Mie problem is that of describing the scattered electric and magnetic fields due to the interaction of a plane wave of light with a spherical object. The boundary conditions for this problem require that the components of the fields tangent to the sphere at its surface be continuous. Because the surface normal for a sphere is purely radial, the boundary conditions require that E_θ, E_ϕ, H_θ, and H_ϕ be continuous at the sphere's surface. Examination of Eqs. (2.49) - (2.55) reveals that if π and σ are continuous and once radially differentiable continuous at the surface, the boundary conditions will be satisfied since the angular dependence of Equations (2.43) and (2.44) are identical.

The plane wave is taken to be incident along the z axis with components

$$E_x = e^{ikz}, \tag{3.1}$$

and

$$H_y = ie^{ikz}, \tag{3.2}$$

which give rise to scalar potentials (in spherical coordinates) of

$$\sigma^i = k^{-2} \sum_\ell i^{\ell-1} \frac{2\ell + 1}{\ell(\ell + 1)} \psi_\ell (kr) P_\ell^1 (\cos \theta) \cos (\phi), \tag{3.3}$$

and

$$\pi^i = k^{-2} \sum_\ell i^{\ell-1} \frac{2\ell + 1}{\ell(\ell + 1)} \psi_\ell (kr) P_\ell^1 (\cos \theta) \sin (\phi), \tag{3.4}$$

where the superscript "i" denotes the incoming wave (solution) and m = 1 (free space) outside the sphere. The assymptotic behavior of the cylinder functions in the limits $r \to 0$, and $r \to \infty$ allow the internal ("w") and scattered ("s") potentials to be written as

$$\sigma^w = k^{-2} m^{-2} \sum_\ell a_\ell \psi_\ell (kmr) P_\ell^1 (\cos\theta) \cos(\phi), \tag{3.5}$$

$$\pi^w = k^{-2} m^{-1} \sum_\ell b_\ell \psi_\ell (kmr) P_\ell^1 (\cos\theta) \sin(\phi), \tag{3.6}$$

$$\sigma^s = k^{-2} \sum_\ell c_\ell \rho_\ell^1 (kr) P_\ell^1 (\cos\theta) \cos(\phi), \tag{3.7}$$

$$\pi^s = k^{-2} \sum_\ell d_\ell \rho_\ell^1 (kr) P_\ell^1 (\cos\theta) \sin(\phi). \tag{3.8}$$

The difference of a factor m^{-1} between Eqs. (3.5) and (3.6) arises from the fact that if $\underset{\sim}{E} = \hat{e}_1 A e^{ikmz}$ and $\underset{\sim}{H} = \hat{e}_2 B e^{ikmz}$, then Eqs. (2.12) and (2.13) require that B = mA. The boundary conditions, that the tangential components of the $\underset{\sim}{E}$ and $\underset{\sim}{H}$ fields be continuous, may be determined by examination of Eqs. (2.49) - (2.54). Since π and σ are already continuous in angles, the tangential continuity is satisfied by: E_θ, π and $\frac{\partial\sigma}{\partial r}$; E_ϕ, π and $\frac{\partial\sigma}{\partial r}$; H_θ, $\frac{\partial\pi}{\partial r}$ and $m^2\sigma$; and H_ϕ, $\frac{\partial\pi}{\partial r}$ and $m^2\sigma$. Thus, the boundary conditions are specifically,

$$\frac{\partial}{\partial r} (\sigma^i + \sigma^s) \Big|_{r=a} = \frac{\partial}{\partial r} \sigma^w \Big|_{r=a}, \tag{3.9}$$

$$\frac{\partial}{\partial r} (\pi^i + \pi^s) \Big|_{r=a} = \frac{\partial}{\partial r} \pi^w \Big|_{r=a}, \tag{3.10}$$

$$(\sigma^i + \sigma^s) \Big|_{r=a} = m^2 \sigma^w \Big|_{r=a}, \tag{3.11}$$

$$(\pi^i + \pi^s)\big|_{r = a} = \pi^w\big|_{r = a}, \tag{3.12}$$

where a is the radius of the sphere.

The orthogonality properties of $\sin(\phi)$, $\cos(\phi)$, and the $P_\ell^1(\cos\phi)$ may be exploited to reduce Eqs. (3.3) - (3.12) to

$$i^{\ell-1}\frac{2\ell+1}{\ell(\ell+1)}\psi_\ell'(ka) + c_\ell \rho_\ell^{1\,\prime}(ka) = m^{-1}a_\ell\psi_\ell'(kma) \tag{3.13}$$

$$i^{\ell-1}\frac{2\ell+1}{\ell(\ell+1)}\psi_\ell'(ka) + d_\ell \rho_\ell^{1\,\prime}(ka) = b_\ell\psi_\ell'(kma), \tag{3.14}$$

$$i^{\ell-1}\frac{2\ell+1}{\ell(\ell+1)}\psi_\ell(ka) + c_\ell \rho_\ell^{1}(ka) = a_\ell\psi_\ell(kma), \tag{3.15}$$

$$i^{\ell-1}\frac{2\ell+1}{\ell(\ell+1)}\psi_\ell(ka) + d_\ell \rho_\ell^{1}(ka) = m^{-2}b_\ell\psi_\ell(kma), \tag{3.16}$$

where: $\psi'(y) = \dfrac{\partial\psi_\ell(x)}{\partial x}\Big|_{x = y}$

Equations (3.13) - (3.16) may be combined to solve for the expansion coefficients of the scattered wave scalar potentials,

$$c_\ell = i^{\ell-1}\frac{2\ell+1}{\ell(\ell+1)}\left(\frac{m\psi_\ell(kma)\,\psi_\ell'(ka) - \psi_\ell(ka)\,\psi_\ell'(kma)}{\rho_\ell^{1}(ka)\psi_\ell'(kma) - m\rho_\ell^{1\,\prime}(ka)\,\psi_\ell(kma)}\right), \tag{3.17}$$

and

$$d = i^{\ell-1}\frac{2\ell+1}{\ell(\ell+1)}\left(\frac{m\psi_\ell(ka)\psi_\ell'(kma) - \psi_\ell'(ka)\psi_\ell(kma)}{\psi_\ell(kma)\rho_\ell^{1\,\prime}(ka) - m\psi_\ell'(kma)\rho_\ell^{1}(ka)}\right) \tag{3.18}$$

By combining Eqs. (2.50), (2.51), (2.53), (2.54), (3.7), (3.8), (3.17), and (3.18), the scattered electric and magnetic field and components may be written as

$$E_\theta = (kr)^{-1} \sum_\ell \left(i d_\ell \rho_\ell^{1}(kr) \frac{P_\ell^1(\cos\theta)}{\sin(\theta)} + c_\ell \rho_\ell^{1'}(kr) \frac{\partial P_\ell^{1}(\cos\theta)}{\partial\theta} \right) \times \cos(\phi), \quad (3.19)$$

$$E_\phi = -(kr)^{-1} \sum_\ell \left(i d_\ell \rho_\ell^{1}(kr) \frac{\partial P_\ell^1(\cos\theta)}{\partial\theta} - c_\ell \rho_\ell^{1'}(kr) \frac{P_\ell^{1}(\cos\theta)}{\sin(\theta)} \right) \times \sin(\phi), \quad (3.20)$$

$$H_\theta = (kr)^{-1} \sum_\ell \left(d_\ell \rho_\ell^{1'}(kr) \frac{\partial P_\ell^1(\cos\theta)}{\partial\theta} - i c_\ell \rho_\ell^{1}(kr) \frac{P_\ell^{1}(\cos\theta)}{\sin(\theta)} \right) \times \sin(\phi), \quad (3.21)$$

$$H_\phi = (kr)^{-1} \sum_\ell \left(d_\ell \rho_\ell^{1'}(kr) \frac{P_\ell^{1}(\cos\theta)}{\sin(\theta)} + i c_\ell \rho_\ell^{1}(kr) \frac{\partial P_\ell^{1}(\cos\theta)}{\partial\theta} \right) \times \cos(\phi). \quad (3.22)$$

The radial components may be calculated in the same manner, but are not included because they decrease as r^{-2} rather than as r^{-1} and will be vanishingly small in the far field when compared to Eqs. (3.19) - (3.22).

The asymptotic properties of the ρ_ℓ^{1}'s are

$$\rho_\ell^{1}(x) = (-i)^{\ell+1} e^{ix}, \quad x \to \infty \quad (3.23)$$

$$\rho_\ell^{1'}(x) = (-i)^{\ell} e^{ix}, \quad x \to \infty \quad (3.24)$$

which may be used to write the far field components as

$$E_\theta = -\frac{e^{ikr}}{kr} \sum_\ell (-i)^{\ell+1} \left[d_\ell \frac{P_\ell^1(\cos\theta)}{\sin(\theta)} + c_\ell \frac{\partial P_\ell^1(\cos\theta)}{\partial\theta} \right] \cos(\phi), \tag{3.25}$$

$$E_\phi = -\frac{e^{ikr}}{kr} \sum_\ell (-i)^{\ell+1} \left[d_\ell \frac{\partial P_\ell^1(\cos\theta)}{\partial\theta} + c_\ell \frac{P_\ell^1(\cos\theta)}{\sin(\theta)} \right] \sin(\phi), \tag{3.26}$$

$$H_\theta = \frac{e^{ikr}}{kr} \sum_\ell (-i)^{\ell+1} \left[d_\ell \frac{\partial P_\ell^1(\cos\theta)}{\partial\theta} + c_\ell \frac{P_\ell^1(\cos\theta)}{\sin(\theta)} \right] \sin(\phi), \tag{3.27}$$

$$H_\phi = -\frac{e^{ikr}}{kr} \sum_\ell (-i)^{\ell+1} \left[d_\ell \frac{P_\ell^1(\cos\theta)}{\sin(\theta)} + c_\ell \frac{\partial P_\ell^1(\cos\theta)}{\partial\theta} \right] \sin(\phi). \tag{3.28}$$

It may be noted that

$$E_\theta = H_\phi, \tag{3.29}$$

and

$$E_\phi = -H_\theta. \tag{3.30}$$

Equations (3.25) and (3.26) may conveniently be rewritten (Van de Hulst, 1957) as

$$E_\theta = -\frac{e^{ikr}}{kr} S_1(\theta) \cos(\phi), \tag{3.31}$$

and

$$E_\phi = -\frac{e^{kr}}{kr} S_2(\theta) \sin(\phi) \tag{3.32}$$

where

$$S_1(\theta) = \sum_\ell (-i)^{\ell+1} \left(d_\ell \frac{P_\ell^1(\cos\theta)}{\sin(\theta)} + c_\ell \frac{\partial P_\ell^1(\cos\theta)}{\partial\theta} \right) , \tag{3.33}$$

and

$$S_2(\theta) = \sum_\ell (-i)^{\ell+1} \left(c_\ell \frac{P_\ell^1(\cos\theta)}{\sin(\theta)} + d_\ell \frac{\partial P_\ell^1(\cos\theta)}{\partial\theta} \right) . \tag{3.34}$$

A new set of angular functions are commonly defined (Van de Hulst, 1957; Deirmendjian, 1964),

$$\eta_\ell(\theta) = \frac{P_\ell^1(\cos\theta)}{\sin(\theta)} , \tag{3.35}$$

and

$$\tau_\ell(\theta) = \frac{\partial P_\ell^1(\cos\theta)}{\partial\theta} . \tag{3.36}$$

It is also convenient to define new coefficients α_ℓ and β_ℓ,

$$\alpha_\ell = (-i)^{\ell+1} c_\ell \frac{\ell(\ell+1)}{2\ell+1} , \tag{3.37}$$

$$= \left[\frac{\psi_\ell'(kma)\psi_\ell(ka) - m\psi_\ell(kma)\psi_\ell'(ka)}{\psi_\ell'(kma)\rho_\ell^1(ka) - m\psi_\ell(kma)\rho_\ell^{1'}(ka)} \right] , \tag{3.38}$$

and

$$\beta_\ell = (-i)^{\ell+1} d_\ell \frac{\ell(\ell+1)}{2\ell+1} , \tag{3.39}$$

$$= \left[\frac{m\psi_\ell'(kma)\psi_\ell(ka) - \psi_\ell(kma)\psi_\ell'(ka)}{m\psi_\ell'(kma)\rho_\ell^1(ka) - \psi_\ell(kma)\rho_\ell^{1'}(ka)} \right] . \tag{3.40}$$

Equations (3.33) and (3.34) may now be rewritten as

$$S_1(\theta) = \sum_\ell \frac{2\ell+1}{\ell(\ell+1)} \left[\beta_\ell \eta_\ell(\theta) + \alpha_\ell \tau_\ell(\theta) \right] , \tag{3.41}$$

and

$$S_2(\theta) = \sum_\ell \frac{2\ell+1}{\ell(\ell+1)} \left[\alpha_\ell \eta_\ell(\theta) + \beta_\ell \tau_\ell(\theta) \right] . \tag{3.42}$$

It is now possible to develop the cross sections and phase functions by introducing the Stokes vector formalism (Van de Hulst, 1957). The components of the Stokes vector are defined as

$$I_\ell = \overline{E_\ell^2} , \tag{3.43}$$

$$I_r = \overline{E_r^2} , \tag{3.44}$$

$$U = 2\overline{E_\ell E_r}\cos(\delta), \tag{3.45}$$

$$V = 2\overline{E_\ell E_r}\sin(\delta), \tag{3.46}$$

where the bar indicates an average over polarization angle, and E_ℓ and

E_r are field components. For the spherical (Mie) problem treated here, $E_\ell = -E_\phi$, and $E_r = E_\theta$, so that

$$E_\ell^2 = \frac{S_1 S_1^* \cos^2(\phi)}{k^2 r^2}, \tag{3.47}$$

$$E_r^2 = \frac{S_2 S_2^* \cos^2(\phi)}{k^2 r^2}, \tag{3.48}$$

$$E_\ell E_r = \frac{(S_1 S_2^* + S_1^* S_2)\sin(\phi)\cos(\phi)}{k^2 r^2}, \tag{3.49}$$

$$E_r E_\ell = \frac{i(S_1 S_2^* - S_1^* S_2)\sin(\phi)\cos(\phi)}{k^2 r^2}, \tag{3.50}$$

By averaging over ϕ, the differential cross sections may be derived as

$$\sigma_1(a, \lambda, m, \theta) = \frac{S_1 S_1^*}{k^2}, \tag{3.51}$$

$$\sigma_2(a, \lambda, m, \theta) = \frac{S_2 S_2^*}{k^2} \tag{3.52}$$

$$\sigma_3(a, \lambda, m, \theta) = \frac{(S_1 S_2^* + S_1^* S_2)}{2k^2} \tag{3.53}$$

$$\sigma_4(a, \lambda, m, \theta) = \frac{i(S_1 S_2^* - S_1^* S_2)}{2k^2} \tag{3.54}$$

where the cross sections σ_i have been written with all explicit dependence on particle radius, wavelength, refractive index, and scattering angle. The cross sections are related to the Stokes vector components by the matrix equation

$$\begin{pmatrix} I_\ell \\ I_r \\ U \\ V \end{pmatrix} = \begin{pmatrix} \sigma_1 & 0 & 0 & 0 \\ 0 & \sigma_2 & 0 & 0 \\ 0 & 0 & \sigma_3 & \sigma_4 \\ 0 & 0 & -\sigma_4 & \sigma_3 \end{pmatrix} \begin{pmatrix} I_{\ell o} \\ I_{ro} \\ U_o \\ V_o \end{pmatrix} \tag{3.55}$$

where the subscript "o" indicates the pre-scattering value.

The total scattering cross section is given by

$$\sigma_{sc}(a, \lambda, m) = \int_{4\pi} \frac{d\Omega}{2} (\sigma_1 + \sigma_2) \tag{3.56}$$

where the integral is over solid angle. Equation (3.56) may be integrated exactly for the Mie problem because of the orthogonality properties of the Legendre polynomials, yielding

$$\sigma_{sc}(a, \lambda, m) = \frac{2\pi}{k^2} \sum_\ell (2\ell + 1) \left[\alpha_\ell \alpha_\ell^* + \beta_\ell \beta_\ell^* \right]. \tag{3.57}$$

The extinction cross section may be evaluated using the optical theorem (Van de Hulst, 1957) as

$$\sigma_{ex}(a, \lambda, m) = \frac{2\pi}{k^2} \mathrm{Re} \left[S_1(0) + S_2(0) \right]. \tag{3.58}$$

The two angular functions $\eta_\ell(\theta)$ and $\tau_\ell(\theta)$ may be evaluated at $\theta = 0$ as

$$\eta_\ell(0) = \tau_\ell(0) = \frac{\ell(\ell + 1)}{2}, \tag{3.59}$$

reducing Eqs. (3.41) and (3.42) to

$$S_1(0) = S_2(0) = \frac{1}{2} \sum_{\ell} (2\ell + 1)\left[\alpha_\ell + \beta_\ell\right]. \tag{3.60}$$

Equation (3.58) then becomes

$$\sigma_{ex}(a, \lambda, m) = \frac{2\pi}{k^2} \sum_{\ell} (2\ell + 1) \{Re(\alpha_\ell) + Re(\beta_\ell)\} . \tag{3.61}$$

These equations may be used to calculate the extinction properties of the entire medium of aerosols as will be discussed in the next chapter.

CHAPTER IV

SINGLE SCATTERING FOR MANY SPHERICAL PARTICLES

Chapter III discussed the scattering of light of arbitrary wavelength by a single spherical particle of arbitrary radius a and refractive index m. In nature, aerosol particles are generally distributed in size (radius) although the particles are usually either spherical as in the case of fog, or are treated as spherical as in the case of atmospheric haze or dust. Some of the aspects of light scattering by nonspherical particles will be discussed in subsequent chapters.

In this chapter, the aerosol particles will not only be assumed to be spherical, but also each particle will be in the far field of all other particles. If d is the average distance between particles, then it is required that $\lambda \ll d$, $a \ll d$. Since the aerosol particles are moving, it is assumed that the average time between collisions is sufficiently large that the number of particles for which $\lambda \not\ll d$ at any instant is small with respect to the total number of particles. These restrictions allow the particles to be treated as independent and the resulting intensity quantities, rather than the field amplitudes, are summed over all particles.

It will be further assumed that there exists a usable analytic or numeric (piecewise analytic) function $N(\underset{\sim}{r}, a, t)$ such that $N(\underset{\sim}{r}, a, t)\, d^3\underset{\sim}{r}\, da\, dt$ is the number of particles of radius between a and a+da within the volume $d^3\underset{\sim}{r}$ during the time interval between t and t+dt. While this function may in principle be calculated, this

calculation has never been performed exactly, although several approximate calculations have been performed (Voloshchuk and Sedunov, 1973; Sedunov, 1974).

While the refractive index for any one particle is assumed constant, the refractive index may vary in position, time, or particle size, corresponding to such cases as an evolving acid fog or a mixture of water haze and dust haze. This variation is represented by a function $m(\underset{\sim}{r}, a, t)$ representing the refractive index of particles of size a at position $\underset{\sim}{r}$ at time t. Because of the difficulties in measuring refractive index, most calculations are performed with a constant refractive index. Only in some special cases when it is known that two types of aerosol are mixed, such as from a gun blast on land, is the refractive index varied in practice.

Further, most experimental data on the particle distribution function is limited to one (or at best a few) measurements of the size distribution at a point averaged over some measurement time and the total concentration of aerosols at several points. As a result, the particle distribution function $N(\underset{\sim}{r}, a, t)$ is commonly factored

$$N(\underset{\sim}{r}, a, t) = f(\underset{\sim}{r}, t)n(a), \tag{4.1}$$

where $f(\underset{\sim}{r}, t)$ is the concentration of particles and n(a) is called the particle size distribution. While Eq. (4.1) is known to be true for only limited, special cases, it is commonly used as an approximation for $N(\underset{\sim}{r}, a, t)$.

Given $N(\underset{\sim}{r}, a, t)$ and $m(\underset{\sim}{r}, a, t)$, the extinction coefficient per unit length is given by

$$\alpha(\underset{\sim}{r}, t) = \int_0^\infty \sigma_{sc}(a, \lambda, m(\underset{\sim}{r}, a, t))N(\underset{\sim}{r}, a, t)\, da, \tag{4.2}$$

and the scattering coefficient per unit length is

$$\beta(\underset{\sim}{r}, t) = \int_0^\infty \sigma_{ex}(a, \lambda, m(\underset{\sim}{r}, a, t))N(\underset{\sim}{r}, a, t)\, da, \tag{4.3}$$

where $\sigma_{sc}(a, \lambda, m)$ and $\sigma_{ex}(a, \lambda, m)$ were defined in Eqs. (3.57) and (3.61). The scattering phase functions are defined by

$$p_j(\underset{\sim}{r}, t, \theta) = \int_0^\infty \sigma_j(a, \lambda, m(\underset{\sim}{r}, a, t), \theta)N(\underset{\sim}{r}, a, t)\, da, \tag{4.4}$$

where the $\sigma_j(a, \lambda, m, \theta)$ were defined in Eqs. (3.51) - (3.54). The unpolarized light phase function is defined by

$$P(\underset{\sim}{r}, t, \theta) = \beta(\underset{\sim}{r}, t)^{-1} \int_0^\infty \sigma_{sc}(a, \lambda, m(\underset{\sim}{r}, a, t)), \theta) \times N(\underset{\sim}{r}, a, t)\, da. \tag{4.5}$$

It may be noted that $P(\underset{\sim}{r}, t, \theta)$ has unit integral over solid angle.

It is convenient to define the albedo of single scattering as

$$\omega(\underset{\sim}{r}, t) = \beta(\underset{\sim}{r}, t)/\alpha(\underset{\sim}{r}, t). \tag{4.6}$$

As noted previously, Eq. (4.1), the particle distribution function is often factored into two parts, $f(\underset{\sim}{r}, t)$ and $n(a)$. The concentration may frequently be represented by either a uniform cloud, either of infinite extent (fog) or of finite extent (patchy fog), or by some concentration function such as a gaussian plume (smoke). The particle size distribution is most commonly represented by one of three functions; the Junge distribution, the log normal distribution, or the Deirmendjian modified gamma distribution. The Junge distribution has the form

$$n(a) = C/a^{\eta}, \tag{4.7}$$

where C is an adjustable coefficient to reconcile the concentration, and η is usually of the order of 3 for most atmospheric hazes (Junge, 1963). This type of distribution is most commonly used to describe atmospheric hazes. The log normal distribution has the form

$$n(a) = \frac{D}{a}\exp[-\{(\ln(a) - \ln(\langle r\rangle))/\ln(\sigma)\}^2/2], \tag{4.8}$$

where D is again a coefficient to reconcile the concentration, $\langle r\rangle$ is the average particle radius, and σ is the standard deviation (Green and Lane, 1964). This distribution is commonly used to describe fogs and smokes. The Deirmendjian modified gamma distribution has the form

$$n(a) = Aa^{\gamma}\exp(-Ba^{\delta}), \tag{4.9}$$

where A is again a coefficient to reconcile the concentration and B, γ, and δ are parameters to characterize the aerosol. This distribution has been used to describe fog, haze, snow, rain, clouds, dust, and smoke (Deirmendjian, 1964). In most cases, the parameters η, $\langle r \rangle$, σ, B, γ, and δ are measured experimentally. While the log normal and Deirmendjian distributions may be reconciled with the overall concentration by a direct integration, this reconciliation for the Junge distribution requires the specification of the minimum radius to avoid the pole. (This lower size limit also applied to Eqs. (4.2) - (4.5).

When $N(\underset{\sim}{x}, a, t)$ is separable, and m is a constant, Eqs. (4.2) and (4.3) reduce to

$$\alpha(\underset{\sim}{x}, t) = f(\underset{\sim}{x}, t)\int_0^\infty \sigma_{ex}(a, \lambda, m)n(a)da, \tag{4.10}$$

and

$$\beta(\underset{\sim}{x}, t) = f(\underset{\sim}{x}, t)\int_0^\infty \sigma_{sc}(a, \lambda, m)n(a)da, \tag{4.11}$$

and $\omega(\underset{\sim}{x}, t)$ and $P(\underset{\sim}{x}, t, \theta)$ become constant with respect to $\underset{\sim}{x}$ and t. In this case, the notation ω and $P(\theta)$ is commonly used for the albedo and unpolarized phase function.

When $N(\underset{\sim}{\chi}, a, t)$ is not separable, an effective albedo ω^* that is the maximum value of $\omega(\underset{\sim}{\chi}, t)$ is commonly defined. Since $\omega(\underset{\sim}{\chi}, t) \leq 1$, $\omega^* \leq 1$. A modified phase function

$$Q(\underset{\sim}{\chi}, t, \theta) \equiv \frac{\omega(\underset{\sim}{\chi}, t)P(\underset{\sim}{\chi}, t, \theta)}{\omega^*} \tag{4.12}$$

is defined that has integral value ≤ 1 for all $\underset{\sim}{\chi}$, t. The effective albedo and modified unpolarized phase function are commonly used in Radiative Transfer to permit an order-of-scattering analysis to be performed even when the albedo is not constant.

CHAPTER V

PREVIOUS STUDIES OF NONSPHERICAL PARTICLE SCATTERING

While the solution for the scattering of a plane wave of light of arbitrary wavelength by a sphere of arbitrary radius and refractive index has long been known, (Mie, 1908; Debye, 1909) no such elegant formalism has existed for nonspherical particles of arbitrary size and shape. There are only a few geometric shapes where the Mie problem can be solved exactly by using the standard separation of variables method (Jackson, 1962). An excellent example of this type of effort is the recent work on prolate and oblate spheroids (Asano and Yamamoto, 1975). It must be noted, however, that even when the analytical solution is available, the results are extremely complicated.

Particles that are small may be treated with Rayleigh-Gans theory (Rayleigh, 1881; Gans, 1925). This theory requires that

$$|m - 1| \ll 1, \tag{5.1}$$

the refractive index of the particle be only slightly different from one (free space) and that

$$\frac{4\pi b}{\lambda} |m - 1| \ll 1, \tag{5.2}$$

where b is an effective radius; that the phase shifts be small. As a result of this latter requirements, the particle may be broken up into volume elements (subparticles) which interact only in terms of the phase of the light scattered from each volume element. The scattering intensities may be calculated by integrating over the volume of the

particle without regard for any further interaction of the internal electric and magnetic fields.

When the particles are large,

$$a >> \lambda, \tag{5.3}$$

geometric optics is, of course, valid.

Thus the problem of light scattering by particles of size approximating the wavelength remains to be solved. The modern digital computer has permitted several approximate techniques for the solution of this problem to be developed. The remainder of this chapter will be concerned with a brief review of some of these techniques.

One of the earliest of these techniques was that developed by Yeh (Yeh, 1964). This technique makes use of perturbation theory, expanding the particle radius (as a function of angles), the normal to the surface, and the electric and magnetic fields in perturbation series. The boundary conditions on the fields are applied and the resulting expressions are separated in orders of perturbation.

Yeh's calculations are limited to only slightly nonspherical particles that could be accurately treated with first order perturbation theory (preserving the cylindrical symmetry found in Mie theory). Little additional work appears to have been done using this technique, perhaps due to the burden of explicitly developing the analytic formulae of the perturbation series.

It is obvious that for slightly irregular particles whose radius differs from a constant by much less than the wavelength, some type of perturbation solution is available. For more irregular

particles, it is necessary that the Rayleigh Hypothesis be introduced. Because of its importance, Millar's statement of the Rayleigh Hypothesis for a two-dimensional scalar field will be paraphrased here (Millar, 1973). The extension to the three-dimensional vector field is straightforward.

> "Consider a two-dimensional configuration (Figure (5.1)) with origin inside the scatterer S. The domain exterior to S is denoted by D. Let C be the circle with center O inscribed in S and let C' be the corresponding circumscribed circle. A field is incident on S. Then at all points outside C', the scattered field may be expressed as
>
> $$u^s = \sum_m A_m H_m^{(1)}(r)\exp(im\phi)$$
>
> (where $H_m^{(1)}(r)$ = Hankel function of the first kind of order m, and the A_m may be determined on C'.")

Millar investigated the validity of the hypothesis for both the bounded particle problem and the irregular surface problem. His conclusions may be briefly summarized by noting that boundary value type scattering problems may be validly solved if the particle has no sharp corners and is sufficiently smooth so that light scattered from one surface region of the particle is not rescattered by another surface region of the particle (no multiple scattering). All of the techniques described in this chapter and the next assume that the Rayleigh Hypothesis is valid. Any assessment of the validity of the Rayleigh Hypothesis is difficult. While the limits of its validity have been quantified for certain special irregular, infinite surfaces, its validity for irregular particles is usually inferred from comparison of approximate calculations with exact calculations such as the Mie solution.

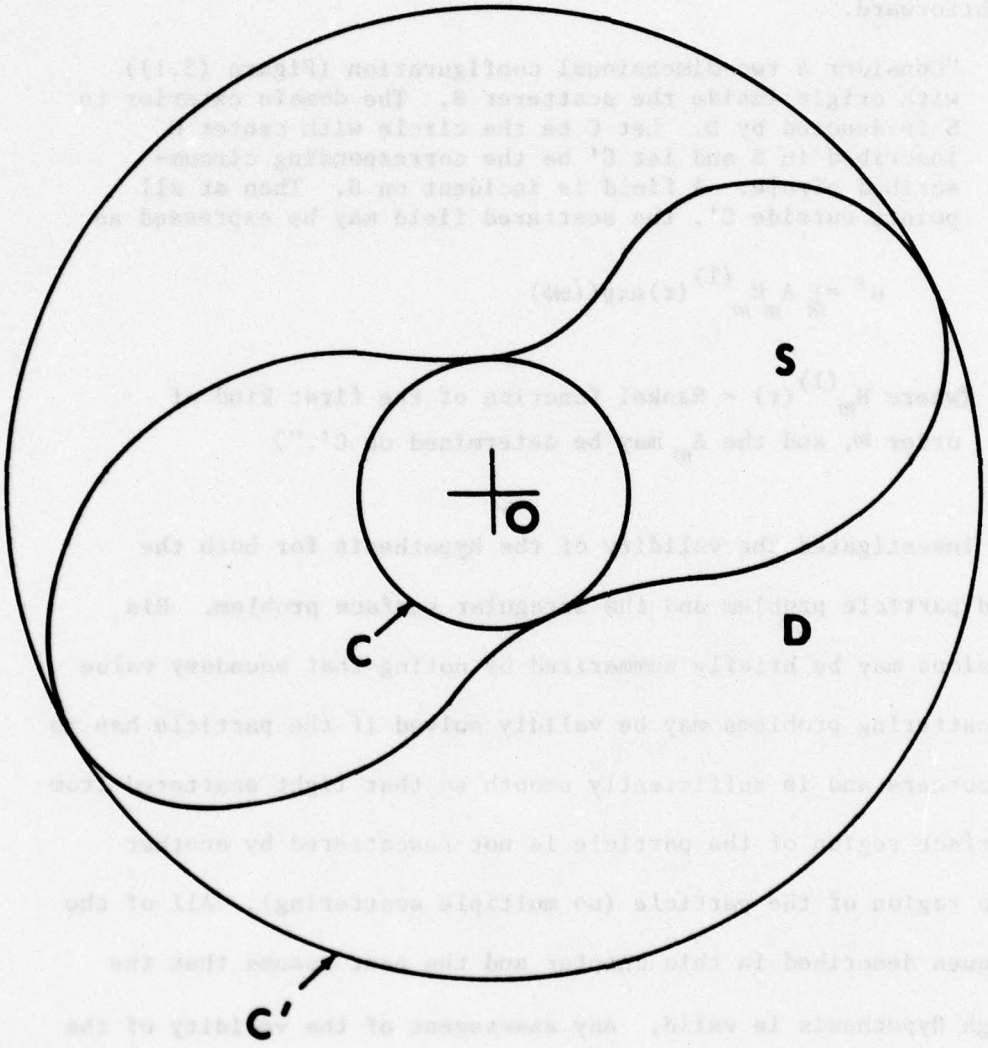

Figure (5.1) Irregular Particle Showing Inscribed (C) = Circle (Sphere) and Circumscribed (C') Circle (Sphere).

One technique for irregular particle scattering, due to Reilly, is a direct extension of Millar's statement of Rayleigh's Hypothesis (Reilly, 1973). For simplicity, the description here will be limited to the scalar wave case. The actual vector wave case of interest follows directly in a like manner, but with additional complexity that obscures the methodology.

The scalar Helmholtz equation has the form

$$\nabla^2\phi + k^2m^2\phi = 0. \tag{5.4}$$

The solution ϕ^i for the incident field is known and the form of the solution ϕ^s for the scattered field is known. The solution ϕ^s is assumed to be valid on and outside the circumscribed sphere around the particle. The refractive index m in the region outside the circumscribed sphere is assumed to be constant with the value m_o.

The refractive index m inside the circumscribed sphere is not constant and has the form

$$\begin{aligned} m &= m_1 \text{ inside the particle} \\ &= m_o \text{ outside the particle.} \end{aligned} \tag{5.5}$$

(Actually m may vary in any manner inside the circumscribed sphere, thus incorporating refractive index gradients and voids or impurities in addition to the nonspherical shape.) The interior solution ϕ^w is assumed to have the form

$$\phi^w = R(r)G(r, \theta, \phi), \tag{5.6}$$

where: R = an unknown function, and

G = a test function that is usually chosen to be a weighted sum of orthogonal polynomials so that R may be determined without recourse to Galerkin's method.

The interior Helmholtz equation has the form

$$\nabla^2(RG) + k^2m^2RG = 0, \tag{5.7}$$

which may be expanded as

$$G\nabla^2R + 2\underset{\sim}{\nabla}G\cdot\underset{\sim}{\nabla}R + R\nabla^2G + k^2m^2RG = 0. \tag{5.8}$$

Since R is purely radial, Eq. (5.8) may be simplified as

$$G\frac{\partial^2R}{\partial r^2} + 2\frac{\partial R}{\partial r}\frac{\partial G}{\partial r} + R\nabla^2G + k^2m^2G = 0. \tag{5.9}$$

Equation (5.9) may be converted to a radial (one-dimensional) differential equation by multiplying by G* , the complex conjugate of G and integrating over angles,

$$\frac{\partial^2R}{\partial r^2}\int G^*Gd\Omega + 2\frac{\partial R}{\partial r}\int G^*\frac{\partial G}{\partial r}d\Omega + R\int G^*\nabla^2Gd\Omega + k^2R\int m^2G^*Gd\Omega = 0, \tag{5.10}$$

where $d\Omega$ indicates integration over 4π. By defining the integrals

$$A(r) = \int G^*\frac{\partial G}{\partial r}d\Omega/\int G^*Gd\Omega \tag{5.11}$$

$$B(r) = \int G^*\nabla^2Gd\Omega/\int G^*Gd\Omega \tag{5.12}$$

$$C(r) = \int m^2G^*Gd\Omega/\int G^*Gd\Omega\,, \tag{5.13}$$

Equation (5.10) may be reduced to

$$\frac{\partial^2 R}{\partial r^2} + 2A(r)\frac{\partial R}{\partial r} + [B(r) + k^2 C(r)]R = 0 \qquad (5.14)$$

which may be solved, usually numerically, for R(r). Once R(r) has been calculated, the scattered field Φ^s may be calculated by matching the fields at the circumscribed spherical boundary as shown in Figure (5.1).

While this technique is both elegant and conceptually simple, it does not rigorously satisfy the boundary conditions of electrodynamics. Perhaps for this reason, this technique has not enjoyed extensive use to date.

Another technique that has been demonstrated by Millar (Millar, 1973) and others (Davies, 1973) is the least-squares technique that is used to approximately satisfy the boundary conditions on the electric and magnetic fields. The technique is employed in the following manner; the electric and magnetic fields are assumed to have some functional form in terms of series of N linearly independent functions and N expansion coefficients for each of the fields; incident, interior, and scattered. Of course, for a conducting particle, the interior fields are zero, and for either a conducting or dielectric particle, the incident fields are known. The radius of the particle is assumed to have some functional form in terms of the angles,

$$r = f(\theta, \phi) \qquad (5.15)$$

so that the surface normal vector may be calculated

$$\underset{\sim}{n} = \underset{\sim}{\nabla}[r - f(\theta, \phi)] \tag{5.16}$$

and the boundary conditions written,

$$\underset{\sim}{n}\times(\underset{\sim}{E}^{i} + \underset{\sim}{E}^{s} - \underset{\sim}{E}^{w})\Big|_{r = f(\theta,\phi)} = 0, \tag{5.17}$$

and

$$\underset{\sim}{n}\times(\underset{\sim}{H}^{i} + \underset{\sim}{H}^{s} - \underset{\sim}{H}^{w})\Big|_{r = f(\theta,\phi)} = 0. \tag{5.18}$$

To this point, this technique does not greatly differ from either the Mie solution, or the technique to be presented in the next chapter. The difference will arise as a result of the way in which the boundary conditions, Eqs. (5.17) and (5.18) are "satisfied". To illustrate the distinction, consider how the boundary conditions are satisfied in the Mie solution by requiring that the equivalent of Eqs. (5.17) and (5.18) be satisfied exactly at all points on the surface of the particle. This type of "satisfaction" is known as collocative and is characterized by no error being introduced at the points where the boundary conditions are satisfied. In the Mie case, this collocation is performed analytically so that no error is introduced at all points on the surface of the particle. Collocation may, of course, be used numerically (called the boundary matching method) but this is done at a finite number of points and error may be introduced at those points where the boundary conditions are not explicitly satisfied.

Least-squares boundary condition "satisfaction" introduces an error in satisfying the boundary conditions. On the surface of the particle, a number of points in the form of angle pairs, $\{\theta_i, \phi_i\}$, $i = 1..I$, are selected. Often, these points are uniformly spaced over the surface of the particle, although the spacing may be adjusted to be less in regions of greater curvature, and greater in regions of less curvature. The accuracy of the solution is influenced by this spacing and it is a matter of obvious note that the solution is not unique, varying with the placement and number of points and the number of functions included in the field representation.

These angle pairs are used to form radii $\{r_i\}$ and normal vectors $\{\underset{\sim}{n}_i\}$. The errors ε_{i1} and ε_{i2} are defined by

$$\varepsilon_{i1}^2 = [\underset{\sim}{n}_i \times (\underset{\sim}{E}^i + \underset{\sim}{E}^s - \underset{\sim}{E}^w)\big|_{r=r_i}]^2, \tag{5.19}$$

and

$$\varepsilon_{i2}^2 = \left(\underset{\sim}{n}_i \times (\underset{\sim}{H}^i + \underset{\sim}{H}^s - \underset{\sim}{H}^w)\big|_{r=r_i} \right)^2, \tag{5.20}$$

and the sum

$$\varepsilon^2 = \sum_{i=1}^{I} (\varepsilon_{i1}^2 + \varepsilon_{i2}^2) \tag{5.21}$$

is required to be minimal with respect to the expansion coefficients.

This requirements of minimal sum square of errors may be used to formulate the solution in matrix algebra (Draper and Smith, 1967).

To illustrate this, consider the scalar equivalent of either Eq. (5.17) or (5.18)

$$[f^i(\underline{r}) + g^s(\underline{r}) - h^w(\underline{r})]\Big|_{r=f(\theta,\,\phi)} = 0 \tag{5.22}$$

where:

$$g^s(\underline{r}) = \sum_{n=1}^{N} a_n \Psi_n(r,\,\theta,\,\phi)$$

$$h^w(r) = \sum_{n=1}^{N} b_n \Phi_n(r,\,\theta,\,\phi)$$

and Ψ_n, Φ_n = known linearly independent functions. The least-squares matrix equation is

$$AB = C \tag{5.23}$$

where

$$A = \begin{pmatrix} \Psi_1(r_1,\,\theta_1,\,\phi_1) & \Psi_2(r_1,\,\theta_1,\,\phi_1) & \cdots & \Phi_N(r_1,\,\theta_1,\,\phi_1) \\ \Psi_1(r_2,\,\theta_2,\,\phi_2) & \Psi_2(r_2,\,\theta_2,\,\phi_2) & \cdots & \Phi_N(r_2,\,\theta_2,\,\phi_2) \\ \vdots & \vdots & & \vdots \\ \Psi_1(r_I,\,\theta_I,\,\phi_I) & \Psi_2(r_I,\,\theta_I,\,\phi_I) & \cdots & \Phi_N(r_I,\,\theta_I,\,\phi_I) \end{pmatrix} \tag{5.24}$$

$$B = \begin{pmatrix} a_1 \\ a_2 \\ \vdots \\ a_n \\ -b_1 \\ -b_2 \\ \vdots \\ -b_n \end{pmatrix} \tag{5.25}$$

$$C = \begin{pmatrix} -f^i(r_1, \theta_1, \phi_1) \\ -f^i(r_2, \theta_2, \phi_2) \\ \vdots \\ -f^i(r_I, \theta_I, \phi_I) \end{pmatrix}. \tag{5.26}$$

The solution may be found by the matrix equation

$$B = (A^+A)^{-1}A^+C \tag{5.27}$$

where $A^\dagger$ = transpose of A, and

$(A^+A)^{-1}$ = inverse of A^+A .

Solution of Eq. (5.27) does introduce an error source into the satisfaction of the boundary conditions compared to the analytical collocative. However, the numerical collocative satisfaction would be to solve Eq. (5.23) for the expansion coefficients when I = N.

It may be seen that the least-squares technique admits more points than the numerical collocative technique and despite the inherent error in the technique, less total error may result, expecially if the solution is constrained by the size of the matrix that can be inverted.

Additionally $A^{+}A$ is a symmetric matrix whereas A(I=N) is not and $A^{+}A$ may therefore be inverted more easily. This has been a crucial factor for many computations in the past.

In summary, the least-squares technique does not exactly satisfy the boundary conditions, but it may be more accurate in terms of overall error than a numerical collocation satisfaction, and it does offer some computational advantages. Nonetheless, some additional error is introduced because the boundary conditions are satisfied numerically rather than analytically.

Another technique is the use of an integral equation rather than a differential equation formalism. Although the use of this type of formalism is not new (Shifrin, 1964), several recent treatments deserve special attention since not only are the boundary conditions accounted for, but numerical results are presented (Eyres and Nelson, 1976; Uzonoglu and Holt, 1977; Waterman, 1971). Although these three formalisms are similar in development, their applicability differs. The formalisms of Eyres and Nelson and of Uzonoglu and Holt are based on the scalar rather than the vector wave equation. Alternately, the formalism of Waterman is completely general, but was applied to conducting particles only.

In these three efforts, the electric (and magnetic) field is represented as a series of orthogonal polynomials and expansion coefficients that permit the integral equation to be reduced to a set of linear algebraic equations that may be solved for the expansion coefficients.

An interesting modification to Mie theory to account for the nonspherical character has recently been advanced (Chylek, Grams, and Pinnick, 1976). They suggest that the most notable difference between spherical and nonspherical polydisperse phase functions is the presence of glories in the spherical aerosols. Because the glory may be associated with the sharp resonance in the c_ℓ and the d_ℓ in the region $\ell \sim 2\pi a/\lambda$ they suggest that the difference between the spherical and the nonspherical phase functions is the presence (absence) of these resonances. By replacing the c_ℓ and the d_ℓ Mie calculated values with the modulo values in these regions, agreement with experimental data superior to that enjoyed by Mie calculations has been demonstrated.

Chylek et al. continue to explain that the glory is due to surface waves and that in an irregular particle, these surface waves would disappear. While the agreement has been noteworthy, the validity of this theory has been questioned (Kerker, 1977) and will be addressed in Chapter VIII.

Before concluding this chapter, some discussion of the nature of the experimental data is in order (Holland and Gagne, 1970; Pinnick, Carroll and Hoffman, 1976). These data are limited, and in many cases

no supplemental data on refractive indices, size and/or shape distributions, or polarization are available. The following features are present in many cases; the phase function is broadened about the forward peak relative to the Mie theory, the backscatter decreases, and the amount of structure decreases but some structure is still present. It should be emphasized that even for data reported for a monodisperse aerosol, averaging over particle orientation has already been conducted during the measurement process. As a result theoretical calculations should be averaged over particle orientations.

CHAPTER VI

NONSPHERICAL PARTICLE SCATTERING FORMALISM

While the Mie theory formalism developed in Chapter III is applicable to spherical particles only, the boundary conditions for $\underset{\sim}{E}$ and $\underset{\sim}{H}$ used to solve the problem are general and applicable to any shape particle providing the Rayleigh Hypothesis holds. This hypothesis, reviewed in Chapter V, is valid if the mathematical representations of the scattered fields accurately describe the scattered field outside and on the boundary of the particle. Millar has shown the validity of the hypothesis for conducting particles when the scattered field is continuous across the surface and all singularities of the scattered field are inside the particle. For the dielectric particles to be considered here, it is adequate to require that the interior and scattered fields are convergent and that the surface is sufficiently simple that no secondary (or higher order) scattering from one region of the particle surface to another region occur.

This discussion will be concerned only with nonspherical particles that are cylindrically symmetric with respect to the z axis, and incident fields will propagate only along the z axis. These restrictions allow retention of the Hertz vector solutions derived in Chapter III for the spherical problem and in addition, are forced by the computational requirements of the problem. This computational restriction is described in Appendix(I). If the particle considered does not exhibit this symmetry,

or the incident fields propagate in some other direction, higher order angular functions must be included in the solution with a proportional increase in the number of expansion coefficients to be determined.

The surface of the nonspherical particle is defined by its radius

$$a(\theta) = \Sigma S_n P_n(\cos\theta). \tag{6.1}$$

The function describing the surface is then

$$\begin{aligned} h(r,\theta) &= r - a(\theta) = 0 \\ &= r - \Sigma S_n P_n(\theta) \end{aligned} \tag{6.2}$$

which has a nonunitized surface normal vector

$$\begin{aligned} \underset{\sim}{n} &= \underset{\sim}{\nabla} h((r,\theta) \\ &= \hat{r} - \hat{\theta} \frac{\partial \ln a(\theta)}{\partial \theta} . \end{aligned} \tag{6.3}$$

It may be noted that the "normalization" or unitization of the surface normal is unnecessary for this calculation.

By introducing the notation

$$\Delta \underset{\sim}{E} = \underset{\sim}{E}^i + \underset{\sim}{E}^s - \underset{\sim}{E}^w \tag{6.4}$$

and

$$\Delta \underset{\sim}{H} = \underset{\sim}{H}^i + \underset{\sim}{H}^s - \underset{\sim}{H}^w \tag{6.5}$$

where the superscripts i, s, and w indicating the incident, scattered, and interior ("within") fields were introduced in Chapter III, the boundary conditions are

$$\underset{\sim}{n}\times\Delta\underset{\sim}{E} = 0, \tag{6.6}$$

and

$$\underset{\sim}{n}\times\Delta\underset{\sim}{H} = 0. \tag{6.7}$$

In determinant form, Equations (6.6) and (6.7) may, by use of Equation (6.3), be written as

$$\underset{\sim}{n}\times\Delta\underset{\sim}{E} = \begin{vmatrix} \hat{r} & 1 & \Delta E_r \\ \hat{\theta} & -\frac{\partial \ln a(\theta)}{\partial\theta} & \Delta E_\theta \\ \hat{\phi} & 0 & \Delta E_\phi \end{vmatrix} = 0. \tag{6.8}$$

and

$$\underset{\sim}{n}\times\Delta\underset{\sim}{H} = \begin{vmatrix} \hat{r} & 1 & \Delta H_r \\ \hat{\theta} & -\frac{\partial \ln a(\theta)}{\partial\theta} & \Delta H_\theta \\ \hat{\phi} & 0 & \Delta H_\phi \end{vmatrix} = 0. \tag{6.9}$$

Equations (6.8) and (6.9) may be written in component form as

$$(\underset{\sim}{n}\times\Delta\underset{\sim}{E})_r = -\frac{\partial \ln a(\theta)}{\partial\theta}\Delta E_\phi = 0 \tag{6.10}$$

$$(\underset{\sim}{n}\times\Delta\underset{\sim}{H})_r = -\frac{\partial \ln a(\theta)}{\partial\theta}\Delta H_\phi = 0 \tag{6.11}$$

$$(\underset{\sim}{n}\times\Delta\underset{\sim}{E})_\theta = -\Delta E_\phi = 0 \tag{6.12}$$

$$(\underset{\sim}{n}\times\Delta\underset{\sim}{H})_\theta = -\Delta H_\phi = 0 \tag{6.13}$$

$$(\underset{\sim}{n}\times\Delta\underset{\sim}{E})_\phi = \Delta E_\theta + \frac{\partial \ln a(\theta)}{\partial\theta}\Delta E_r = 0 \tag{6.14}$$

$$(\underset{\sim}{n}\times\Delta\underset{\sim}{H})_\phi = \Delta H_\theta + \frac{\partial \ln a(\theta)}{\partial\theta}\Delta H_r = 0. \tag{6.15}$$

Obviously, Equations (6.10) and (6.12), and Equations (6.11) and (6.13) are redundant, so that the boundary conditions reduce to

$$\Delta E_\phi = 0 \tag{6.16}$$

$$\Delta H_\phi = 0 \tag{6.17}$$

$$\Delta E_\theta + \frac{\partial \ln a(\theta)}{\partial\theta}\Delta E_r = 0 \tag{6.18}$$

$$\Delta H_\theta + \frac{\partial \ln a(\theta)}{\partial\theta}\Delta H_r = 0. \tag{6.19}$$

When the regular Mie problem for spherical particles is solved, the orthogonality of $\sin(\phi)$, $\cos(\phi)$, and the P_ℓ^1's is used to solve for the coefficients c_ℓ and d_ℓ, Equations (3.13) - (3.16). This technique cannot be used for the nonspherical particle problem because the radial functions ψ_ℓ and ρ_ℓ^1, Equations (2.45) and (2.47), are now also functions of angle θ. The orthogonality of the ϕ functions is still valid for the nonspherical particles considered in this chapter, but the field components will be seen to be already resolved in ϕ, so that no advantage is derived from this orthogonality. By combining Equations (2.49) - (2.54) and (3.3) - (3.8), the field of components for the three waves may be written as

$$E_r^i = \sum_\ell \gamma_\ell [\psi_\ell(kr) + \psi_\ell''(kr)] P_\ell^1(\cos\theta)\cos(\phi) \tag{6.20}$$

$$E_\theta^i = (kr)^{-1} \sum_\ell \gamma_\ell \left[i\psi_\ell(kr) \frac{P_\ell^1(\cos\theta)}{\sin\theta} + \psi_\ell'(kr) \frac{\partial P_\ell^1(\cos\theta)}{\partial\theta} \right] \cos(\phi) \tag{6.21}$$

$$E_\phi^i = (kr)^{-1} \sum_\ell \gamma_\ell \left[-i\psi_\ell(kr) \frac{\partial P_\ell^1(\cos\theta)}{\partial\theta} - \psi_\ell'(kr) \frac{P_\ell^1(\cos\theta)}{\sin(\theta)} \right] \sin(\phi) \tag{6.22}$$

$$H_r^i = \sum_\ell \gamma_\ell \left[\psi_\ell(kr) + \psi_\ell''(kr) \right] P_\ell^1(\cos\theta)\sin(\phi) \tag{6.23}$$

$$H_\theta^i = (kr)^{-1}\sum_\ell \gamma_\ell\left(i\psi_\ell(kr)\frac{P_\ell^1(\cos\theta)}{\sin(\theta)} + \psi_\ell'(kr)\frac{\partial P_\ell^1(\cos\theta)}{\partial\theta}\right)\sin(\phi) \quad (6.24)$$

$$H_\phi^i = (kr)^{-1}\sum_\ell \gamma_\ell\left(-i\psi_\ell(kr)\frac{\partial P_\ell^1(\cos\ )}{\partial\theta} - \psi_\ell'(kr)\frac{P_\ell^1(\cos\theta)}{\sin(\theta)}\right)\cos(\phi) \quad (6.25)$$

$$E_r^w = \sum_\ell a_\ell\left(\psi_\ell(kmr) + \psi_\ell''(kmr)\right)P_\ell^1(\cos\theta)\cos(\phi) \quad (6.26)$$

$$E_\theta^w = (kmr)^{-1}\sum_\ell\left(a_\ell\psi_\ell'(kmr)\frac{\partial P_\ell^1(\cos\theta)}{\partial\theta} + ib_\ell\psi_\ell(kmr)\frac{P_\ell^1(\cos\theta)}{\sin(\theta)}\right)\cos(\phi)$$

(6.27)

$$E_\phi^w = (kmr)^{-1}\sum_\ell\left(-a_\ell\psi_\ell'(kmr)\frac{P_\ell^1(\cos\theta)}{\sin(\theta)} - ib_\ell\psi_\ell(kmr)\frac{\partial P_\ell(\cos\theta)}{\partial\theta}\right)\sin(\phi)$$

(6.28)

$$H_r^w = \sum_\ell mb_\ell\left(\psi_\ell(kmr) + \psi_\ell''(kmr)\right)P_\ell^1(\cos\theta)\sin(\phi) \quad (6.29)$$

$$H_\theta^w = (kr)^{-1}\sum_\ell\left(ia_\ell\psi_\ell(kmr)\frac{P_\ell^1(\cos\theta)}{\sin(\theta)} + b_\ell\psi_\ell'(kmr)\frac{\partial P_\ell^1(\cos\theta)}{\partial\theta}\right)\sin(\phi)$$

(6.30)

$$H_\phi^w = (kr)^{-1}\sum_\ell \left[ia_\ell \psi_\ell(kmr)\frac{\partial P_\ell^1(\cos\theta)}{\partial\theta} + b_\ell \psi_\ell'(kmr)\frac{P_\ell^1(\cos\theta)}{\sin(\theta)}\right]\cos(\phi) \quad (6.31)$$

$$E_r^s = \sum_\ell c_\ell \left[\rho_\ell^1(kr) + \rho_\ell^{1''}(kr)\right] P_\ell^1(\cos\theta)\cos(\phi) \quad (6.32)$$

$$E_\theta^s = (kr)^{-1}\sum_\ell \left[c_\ell \rho_\ell^{1'}(kr)\frac{\partial P_\ell^1(\cos\theta)}{\partial\theta} + id_\ell \rho_\ell^1(kr)\frac{P_\ell^1(\cos\theta)}{\sin(\theta)}\right]\cos(\phi) \quad (6.33)$$

$$E_\phi^s = (kr)^{-1}\sum_\ell \left[-c_\ell \rho_\ell^{1'}(kr)\frac{P_\ell^1(\cos\theta)}{\sin\theta} - id_\ell \rho_\ell^1(kr)\frac{\partial P_\ell^1(\cos\theta)}{\partial\theta}\right]\sin(\phi)$$

(6.34)

$$H_r^s = \sum_\ell d_\ell \left[\rho_\ell^1(kr) + \rho_\ell^{1''}(kr)\right] P_\ell^1(\cos\theta)\sin(\phi) \quad (6.35)$$

$$H_\theta^s = (kr)^{-1}\sum_\ell \left[ic_\ell \rho_\ell^1(kr)\frac{P_\ell^1(\cos\theta)}{\sin\theta} + d_\ell \rho_\ell^{1'}(kr)\frac{\partial P_\ell^1(\cos\theta)}{\partial\theta}\right]\sin(\phi)$$

(6.36)

$$H_\phi^s = (kr)^{-1}\sum_\ell \left[ic_\ell \rho_\ell^1(kr)\frac{\partial P_\ell^1(\cos\theta)}{\partial\theta} + d_\ell \rho_\ell^{1'}(kr)\frac{P_\ell^1(\cos\theta)}{\sin(\theta)}\right]\cos(\phi) \quad (6.37)$$

where the prime on the radial functions indicates differentiation with respect to total argument, and $\gamma_\ell = i^{\ell-1}\frac{2\ell+1}{\ell(\ell+1)}$.

While the boundary conditions, Eqs. (6.16) - (6.19), may not be solved simply because of the angular dependence of the ψ_ℓ and the ρ_ℓ^1 functions, these equations may be rewritten as

$$E_\phi^w - E_\phi^s = E_\phi^i \tag{6.38}$$

$$H_\phi^w - H_\phi^s = H_\phi^i \tag{6.39}$$

$$E_\theta^w - E_\theta^s + \frac{\partial \ln a(\theta)}{\partial\theta}\left(E_r^w - E_r^s\right) = E_\theta^i + \frac{\partial \ln a(\theta)}{\partial\theta}E_r^i \tag{6.40}$$

$$H_\theta^w - H_\theta^s + \frac{\partial \ln a(\theta)}{\partial\theta}\left(E_r^w - E_r^s\right) = H_\theta^i + \frac{\partial \ln a(\theta)}{\partial\theta}E_r^i \tag{6.41}$$

and each side multiplied by P_ℓ^1, and integrated with respect to $\cos(\theta)$. As an example, Eq. (6.38) becomes

$$\int P_\ell^1,(\cos\theta)\left(E_\phi^w - E_\phi^s\right)d\cos\theta = \int P_\ell^1,(\cos\theta)E^i d\cos\theta. \tag{6.42}$$

If each series in Eqs. (6.20) - (6.37) is truncated at $\ell = L$, then there exist L a_ℓ, b_ℓ, c_ℓ, and d_ℓ; 4L unknowns. There are 4 boundary conditions, Eqs. (6.38) - (6.41), and integration of each with P_ℓ^1, yields L equations for a total of 4L. Thus there are 4L equations in 4L unknowns. The a_ℓ, b_ℓ, c_ℓ, and d_ℓ may be solved for by using some coefficient of equation algorithm such as a Gauss-Jordan reduction

(Carnahan, Luther, and Wilkes, 1969), as will be used in the calculations described in the next two chapters. It may be noted that the a_ℓ and the b_ℓ are unwanted quantities as far as the desired result is concerned, but their calculation is dictated by the structure of the formalism.

By defining the integrals

$$A_{\ell\ell',1} = \gamma_\ell \int_{+1}^{+1} \left[\psi_\ell(ka) + \psi''_\ell(ka)\right] \frac{\partial \ln a}{\partial \theta} P_\ell^1 P_{\ell'}^1 d\cos\theta \tag{6.43}$$

$$A_{\ell\ell',2} = \gamma_\ell \int \frac{\psi_\ell(ka)}{ka} \frac{P_\ell^1 P_{\ell'}^1}{\sin(\theta)} d\cos\theta \tag{6.44}$$

$$A_{\ell\ell',3} = \gamma_\ell \int \frac{\psi'_\ell(ka)}{ka} \frac{\partial P_\ell^1}{\partial \theta} P_{\ell'}^1 d\cos\theta \tag{6.45}$$

$$A_{\ell\ell',4} = \gamma_\ell \int \frac{\psi_\ell ka)}{ka} \frac{\partial P_\ell^1}{\partial \theta} P_{\ell'}^1 d\cos\theta \tag{6.46}$$

$$A_{\ell\ell',5} = \gamma_\ell \int \frac{\psi_{\ell'}(ka)}{ka} \frac{P_\ell^1 P_{\ell'}^1}{\sin(\theta)} d\cos\theta \tag{6.47}$$

$$A_{\ell\ell',6} = \int \left[\psi_\ell(kma) + \psi''_\ell(kma)\right] P_\ell^1 P_{\ell'}^1 \frac{\partial \ln a}{\partial \theta} d\cos\theta$$

$$A_{\ell\ell',7} = \int \frac{\psi_\ell(kma)}{kma} \frac{P_\ell^1 P_{\ell'}^1}{\sin(\theta)} d\cos\theta \tag{6.49}$$

$$A_{\ell\ell',8} = \int \frac{\psi'_\ell(kma)}{kma} \frac{\partial P^1_\ell}{\partial\theta} P^1_{\ell'}, dcos \tag{6.50}$$

$$A_{\ell\ell',9} = \int \frac{\psi_\ell(kma)}{kma} \frac{\partial P^1_\ell}{\partial\theta} P^1_{\ell'}, dcos \tag{6.51}$$

$$A_{\ell\ell',10} = \int \frac{\psi'_\ell(kma)}{kma} \frac{P^1_\ell P^1_{\ell'}}{\sin(\theta)} dcos\theta \tag{6.52}$$

$$A_{\ell\ell',11} = \int \left(\rho^1_\ell\ (ka) + \rho^{1''}_\ell(ka)\right) P^1_\ell P^1_{\ell'}, \frac{\partial lna}{\partial\theta} dcos\theta \tag{6.53}$$

$$A_{\ell\ell',12} = \int \frac{\rho^1_\ell(ka)}{ka} \frac{P^1_\ell P^1_{\ell'}}{\sin(\theta)} dcos\theta \tag{6.54}$$

$$A_{\ell\ell',13} = \int \frac{\rho^{1'}_\ell(ka)}{ka} \frac{\partial P^1_\ell}{\partial\theta} P^1_{\ell'}, dcos\theta \tag{6.55}$$

$$A_{\ell\ell',14} = \int \frac{\rho^1{}'_\ell(ka)}{ka} \frac{\partial P^1_\ell}{\partial\theta} P^1_{\ell'}, dcos\theta \tag{6.56}$$

$$A_{\ell\ell',15} = \int \frac{\rho^{1'}_\ell(ka)}{ka} \frac{P^1_\ell P^1_{\ell'}}{\sin(\theta)} dcos\theta, \tag{6.57}$$

where the θ dependence has not been explicitly shown for the P^1_ℓ's, the $P^1_{\ell'}$'s, and a. The 4L equations formed form Eqs. (6.20) - (6.37) and (6.38) - (6.41) may be written as

$$\sum_{\ell}(a_{\ell}A_{\ell\ell',10} + ib_{\ell}A_{\ell\ell',9} - c_{\ell}A_{\ell\ell',15} - id_{\ell}A_{\ell\ell',14}) =$$

$$\sum_{\ell}(iA_{\ell\ell',4} + A_{\ell\ell',5}) \tag{6.58}$$

$$\sum_{\ell}(-ia_{\ell}{}^{m}A_{\ell\ell',9} - b_{\ell}{}^{m}A_{\ell\ell',10} + ic_{\ell}A_{\ell\ell',14} + id_{\ell}A_{\ell\ell',15}) =$$

$$\sum_{\ell}(-iA_{\ell\ell',4} - A_{\ell\ell',5}) \tag{6.59}$$

$$\sum_{\ell}(-a_{\ell}A_{\ell\ell',8} - a_{\ell}A_{\ell\ell',6} - ib_{\ell}A_{\ell\ell',7} + c_{\ell}A_{\ell\ell',13} + c_{\ell}A_{\ell\ell',11}$$

$$+ id_{\ell}A_{\ell\ell',12}) = \sum(-iA_{\ell\ell',2} - A_{\ell\ell',3} - A_{\ell\ell',1}) \tag{6.60}$$

$$\sum_{\ell}(-ia_{\ell}{}^{m}A_{\ell\ell',7} - b_{\ell}{}^{m}A_{\ell\ell',8} - b_{\ell}{}^{m}A_{\ell\ell',6} + ic_{\ell}A_{\ell\ell',12} + d_{\ell}A_{\ell\ell',13}$$

$$+ d_{\ell}A_{\ell\ell',11}) = \sum_{\ell}(-A_{\ell\ell',3} + A_{\ell\ell',1} - iA_{\ell\ell',2}) \tag{6.61}$$

Equations (6.58) - (6.61) may be written in matrix form as

$$B\,G = F \tag{6.62}$$

where B is a 4L by 4L matrix given by

$$B = \begin{pmatrix} A_{\ell\ell',10} & iA_{\ell\ell',9} & -A_{\ell\ell',15} & -iA_{\ell\ell',14} \\ -imA_{\ell\ell',9} & mA_{\ell\ell',10} & iA_{\ell\ell',14} & A_{\ell\ell',15} \\ -(A_{\ell\ell',6}+A_{\ell\ell',8}) & -iA_{\ell\ell',7} & A_{\ell\ell',11}+A_{\ell\ell',13} & iA_{\ell\ell',12} \\ -imA_{\ell\ell',7} & -m(A_{\ell\ell',6}+A_{\ell\ell',8}) & iA_{\ell\ell',12} & A_{\ell\ell',11}+A_{\ell\ell',13} \end{pmatrix} \tag{6.63}$$

where each entry is an L by L array with ℓ variation along the columns and ℓ' variation along the rows. The matrix G is a 4L by 1 (one) matrix given by

$$G = \begin{pmatrix} a_\ell \\ b_\ell \\ c_\ell \\ d_\ell \end{pmatrix} \tag{6.64}$$

where each entry is an L by 1 matrix, and F is a 4L by 1 matrix given by

$$F = \begin{pmatrix} \sum(iA_{\ell\ell',4} + A_{\ell\ell',5}) \\ -\sum(iA_{\ell\ell',4} + A_{\ell\ell',5}) \\ \sum(-A_{\ell\ell',1} - iA_{\ell\ell',2} - A_{\ell\ell',3}) \\ \sum(-A_{\ell\ell',1} - iA_{\ell\ell',2} - A_{\ell\ell',3}) \end{pmatrix} \tag{6.65}$$

where each entry is an L (in ℓ') by 1 matrix. The coding of Eqs. (6.63) - (6.65) and their solution is described in Appendix (I), along

with a listing of the code. A demonstration that Eqs. (6.61) - (6.65) reduce to Mie theory for spherical particles is given in Appendix (II). Some special considerations involved in calculating the radial functions ψ_ℓ and ρ_ℓ^1 are discussed in Appendix (III).

After the c_ℓ and the d_ℓ have been calculated, it is necessary to form the α_ℓ and the β_ℓ used in the cross section and phase function calculations, Eqs. (3.41), (3.42), (3.57), and (3.61). These quantities were defined in Eqs. (3.37) and (3.39) as

$$\alpha_\ell = (-i)^{\ell+1} \frac{\ell(\ell+1)}{2\ell+1} c_\ell \tag{6.66}$$

and

$$\beta_\ell = (-i)^{\ell+1} \frac{\ell(\ell+1)}{2\ell+1} d_\ell \tag{6.67}$$

It may be noted that the formulae for calculating the cross sections and phase functions are the same as those developed in Chapter III for spherical particles.

CHAPTER VII

NONSPHERICAL PARTICLE CALCULATIONS:I

A computer code was generated to perform the calculations described in the previous chapter. This code is described in Appendix (I). Additionally, some special aspects of the numerical aspects are also described, in Appendix (II).

Any computer code or algorithm must be validated. This validation was approached in this investigation by a three part effort. The first part, described in Appendix (III), demonstrates analytically the reduction of the formalism developed in the previous chapter to the Mie solution when the particle is spherical.

The second part of the validation was to demonstrate the numerical equivalence of the code to a Mie code for a spherical particle. This demonstration was achieved by exercising the nonspherical code and a standard Mie code (Blattner, 1972) for the same single particles. Approximately fifty cases were considered. The c_ℓ, d_ℓ, cross sections, and phase functions were compared. In all cases, the agreement between the calculated quantities was within the roundoff error of the machine. This error was therefore significant only beyond the fourteenth figure.

While these two validation checks are heartening, they offer no real assurance that the formalism or the code is valid for nonspherical particles, only that it has the proper limiting behavior. To continue the validation, the code was exercised to provide calculations for comparison with exact calculations for prolate spheroids (Asano and Yamamoto, 1975).

The size parameter in this exact theory is

$$c = \frac{2\pi a}{\lambda} \left(1 - \frac{b^2}{a^2} \right)^{\frac{1}{2}} \qquad (7.1)$$

where: a = semimajor axis, and

b = semiminor axis of the ellipsoid.

In these calculations, a/b = 2 in all cases, and values of c = 1, 3, 5, 7 are used. The radius $a(\theta)$ and its derivative $\frac{\partial a(\theta)}{\partial \theta}$ are calculated both analytically and by expansion of $a(\theta)$ in Legendre polynomials as a further check on code accuracy. The calculated phase functions are shown in Figure (7.1).

Comparison of the approximate calculations using this formalism and the exact calculations evidenced minor differences in the fine structure of the phase functions. The positions of the relative maxima and minima and the relative magnitudes of the curves agreed very well, however. Although it is difficult to make an exact estimate of the accuracy of the calculation, an approximate comparison is made by comparing calculated values with exact values at 10° increments. This comparison gives an overall error bound of ± 2% with an average error of 8×10^{-2}%. Because some of this error may be attributed to the limited number of expansion coefficients calculated, to computer noise, and to the truncation error of the Gauss-Jordan integration, this error bound seems to be reasonable.

The overall conclusion of this validation exercise is that the agreement with limiting cases evidenced by the code indicates that it is useful despite the Rayleigh Hypothesis.

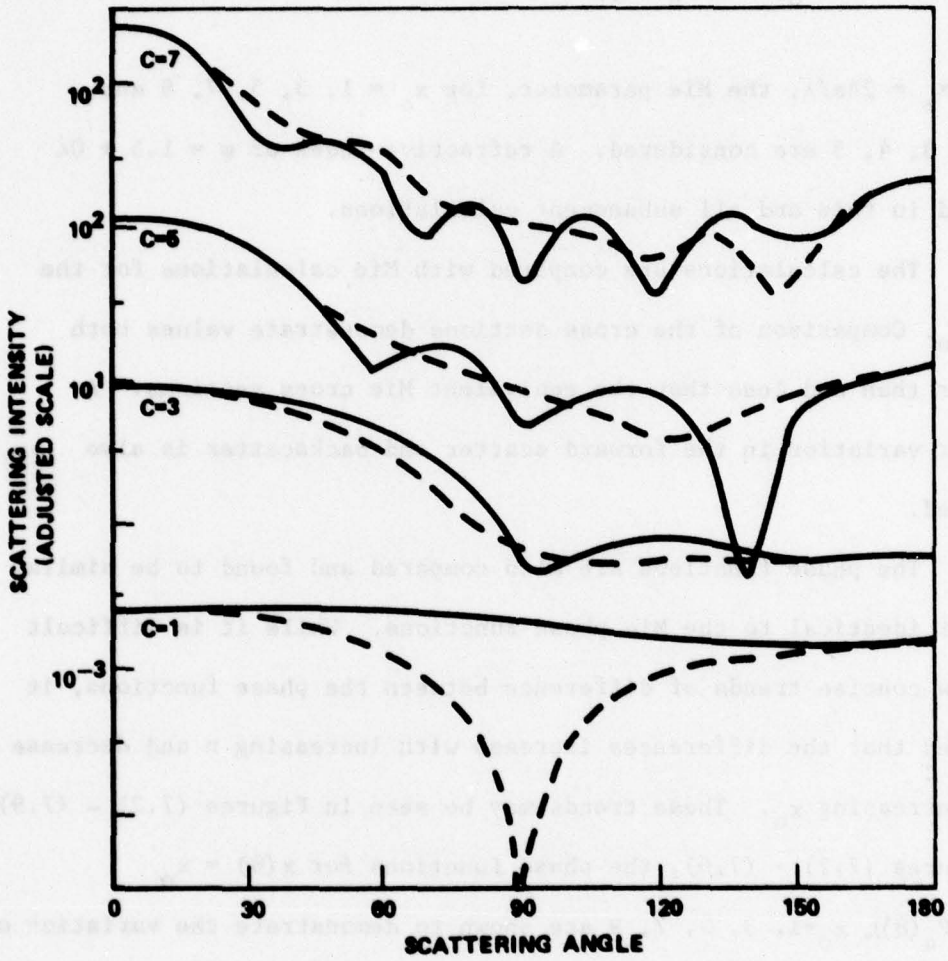

Figure (7.1) Calculated Phase Functions of Prolate Spheroids Used to Validate Code by Comparison with Exact Calculations (Asnao and Yamamoto, 1975). (Solid curve is parallel polarization, dotted is perpendicular polarization.)

Having validated the code, attention was next turned to the cross sections and phase functions of single, nonspherical particles. Individual particles of shape function

$$x(\theta) = 2\pi a(\theta)/\lambda$$

$$= x_o[1 \pm 0.1P_n(\theta)], \qquad (7.2)$$

where $x_o = 2\pi a/\lambda$, the Mie parameter, for $x_o = 1, 3, 5, 7, 9$ and $n = 2, 3, 4, 5$ are considered. A refractive index of $m = 1.5 + 0i$ is used in this and all subsequent calculations.

The calculations are compared with Mie calculations for the same x_o. Comparison of the cross sections demonstrate values both greater than and less than the equivalent Mie cross sections. A similar variation in the forward scatter and backscatter is also observed.

The phase functions are also compared and found to be similar but not identical to the Mie phase functions. While it is difficult to draw concise trends of difference between the phase functions, it is noted that the differences increase with increasing n and decrease with increasing x_o. These trends may be seen in Figures (7.2) - (7.9). In figures (7.2) - (7.6), the phase functions for $x(\theta) = x_o(1-0.1P_4(\theta))$, x_o=1, 3, 5, 7, 9 are shown to demonstrate the variation of difference of phase functions with x_o. The decreasing difference for x_o=1, 3, 5 is evident, although the trend appears to reverse for $x_o = 7$ and 9. This reversal is an indication of the inexactitude of the trend.

Figures (7.4) and (7.7) - (7.9) show the increase of difference in the phase functions with increasing n. In this case, the shape function $x(\theta) = x_o(1-0.1P_n(\theta))$, $n = 2, 3, 4, 5$, and $x_o = 5$ is used.

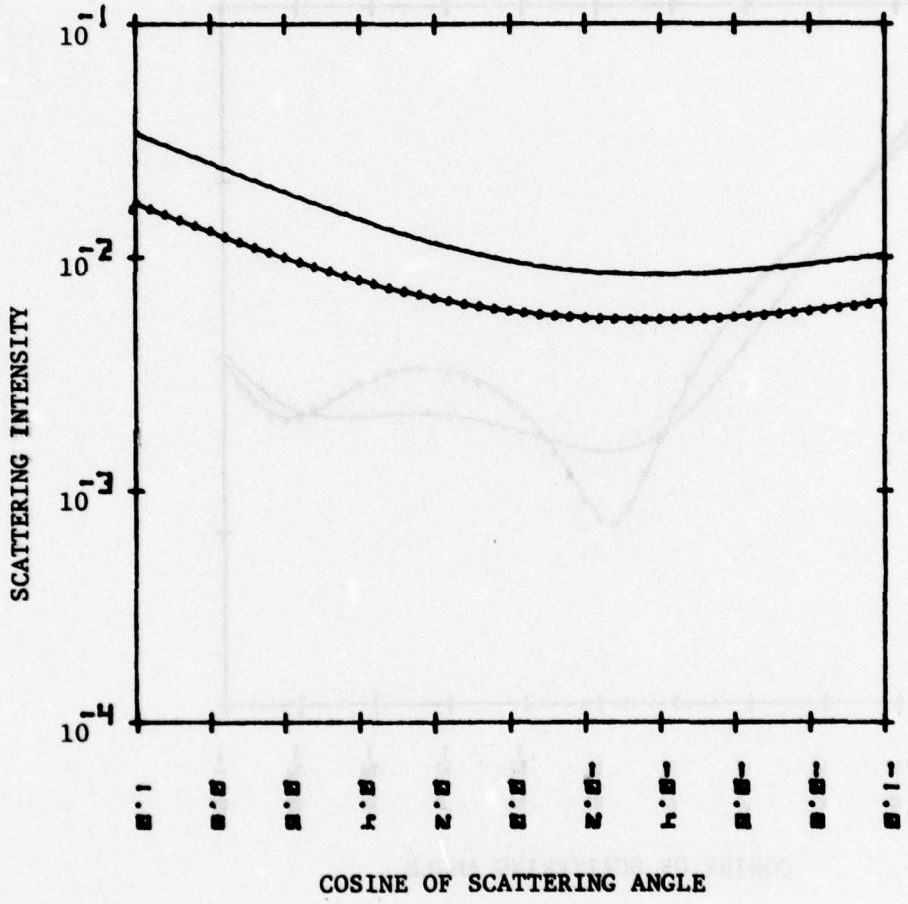

Figure (7.2) Unpolarized Phase Functions for Shape Functions $x(\theta) = x_o$ and $x(\theta) = x_o(1-0.1P_4(\theta))$ (Dotted), $x_o = 1$.

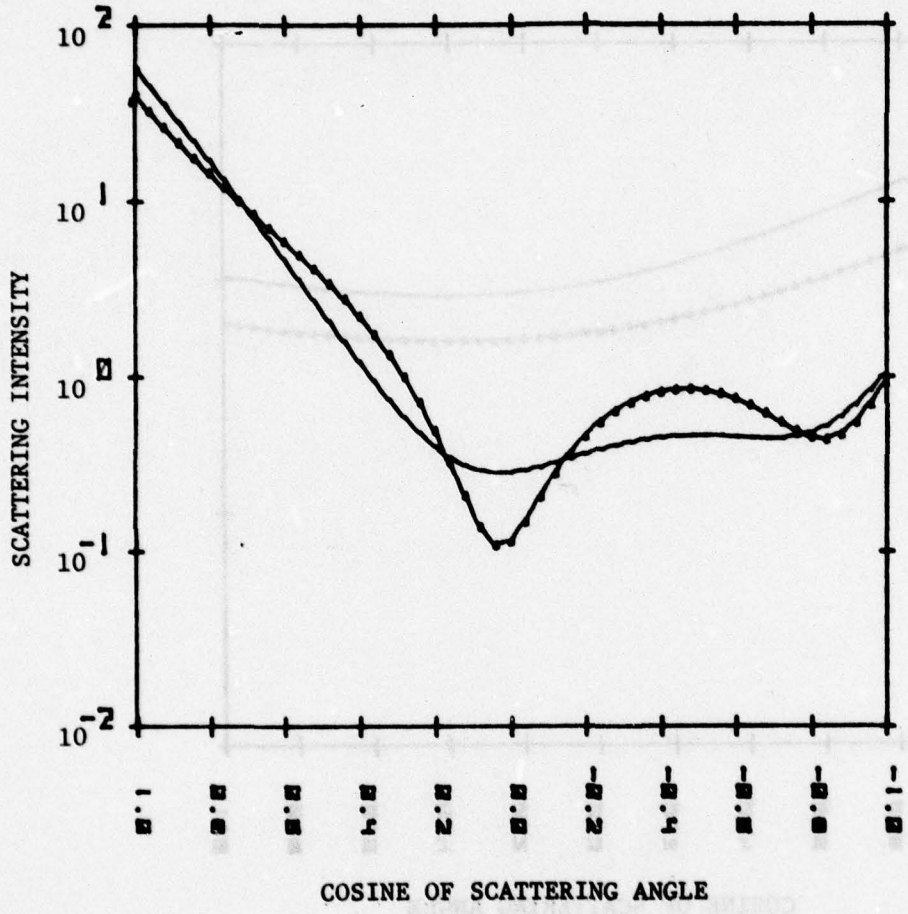

Figure (7.3) Unpolarized Phase Functions for Shape Functions $x(\theta) = x_o$ and $x(\theta) = x_o(1-0.1P_4(\theta))$ (Dotted), $x_o = 3$.

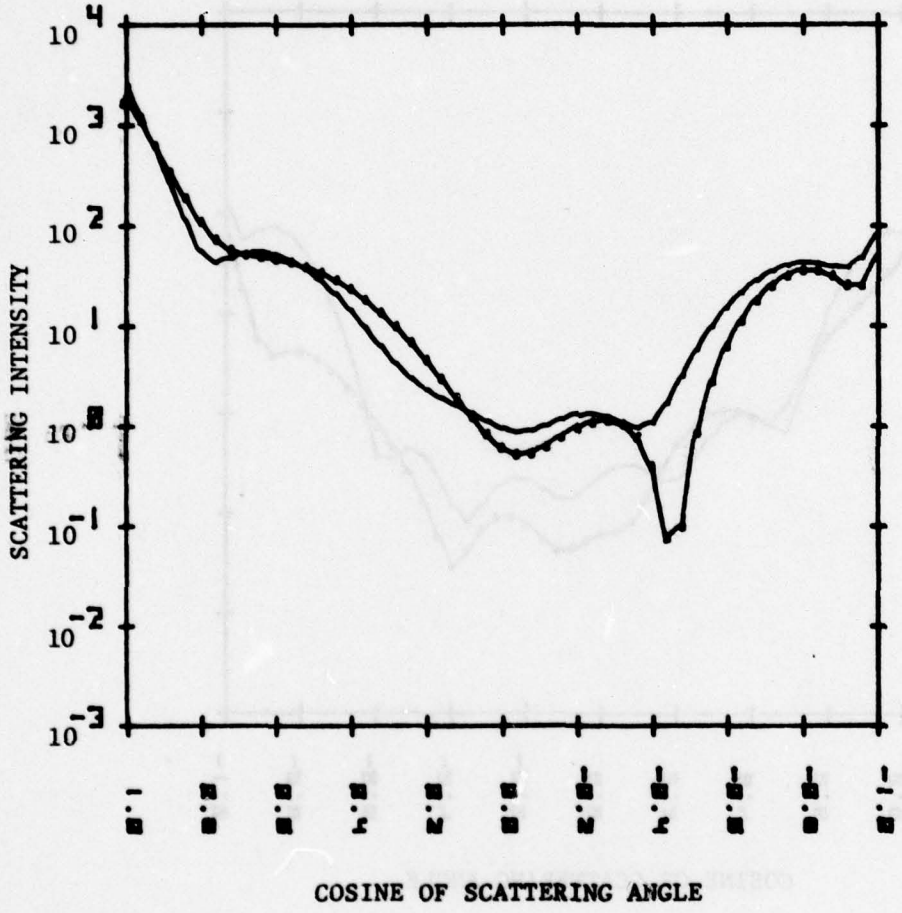

Figure (7.4) Unpolarized Phase Functions for Shape Functions $x(\theta) = x_o$ and $x(\theta) = x_o(1-0.1P_4(\theta))$ (Dotted), $x_o = 5$.

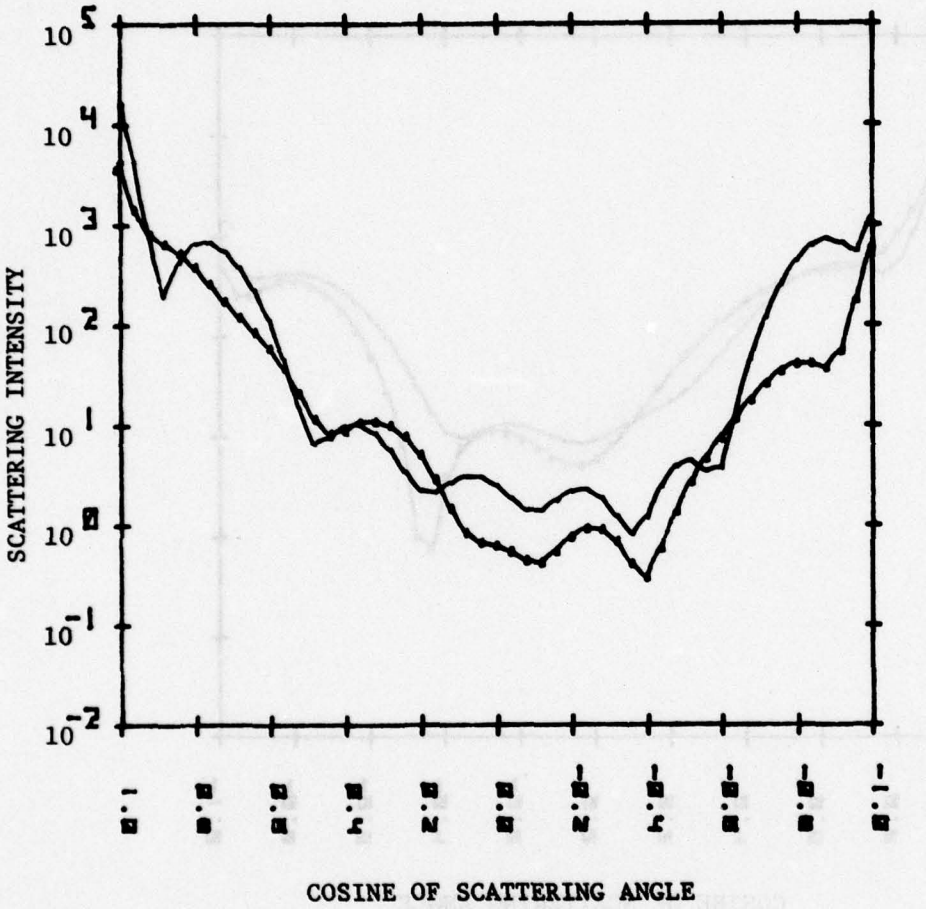

Figure (7.5) Unpolarized Phase Functions for Shape Functions $x(\theta) = x_o$ and $x(\theta) = x_o(1-0.1P_4(\theta))$ (Dotted), $x_o = 7$.

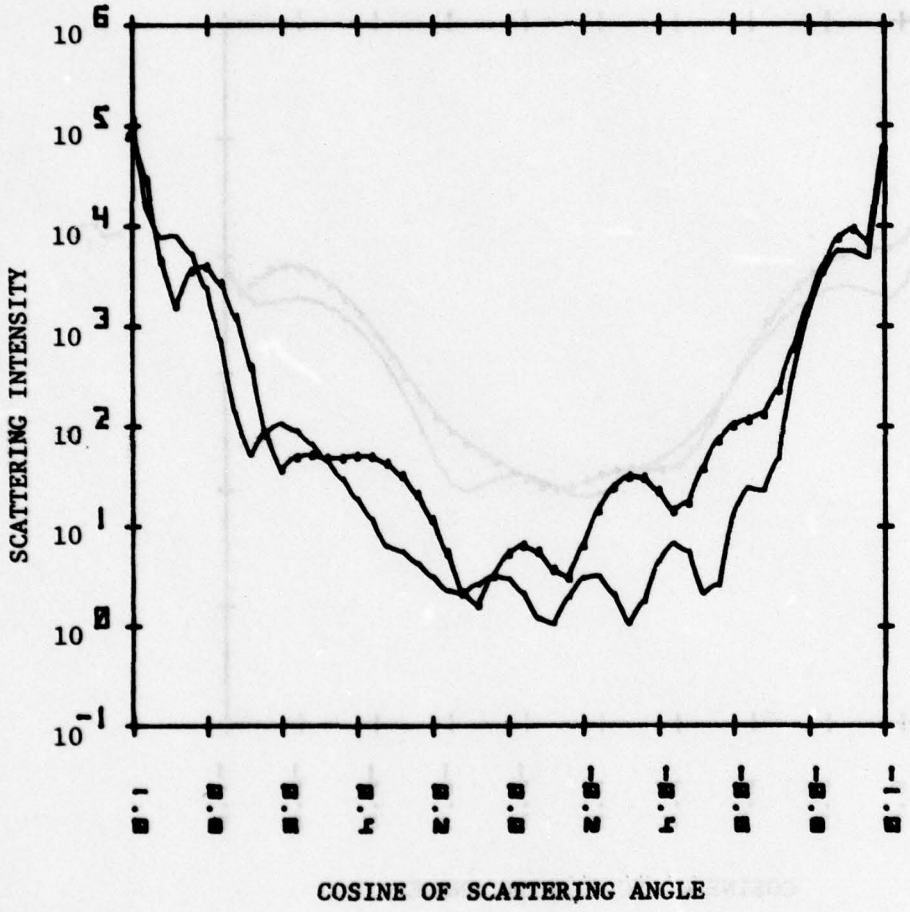

Figure (7.6) Unpolarized Phase Functions for Shape Functions $x(\theta) = x_o$ and $x(\theta) = x_o(1-0.1P_4(\theta))$ (Dotted), $x_o = 9$.

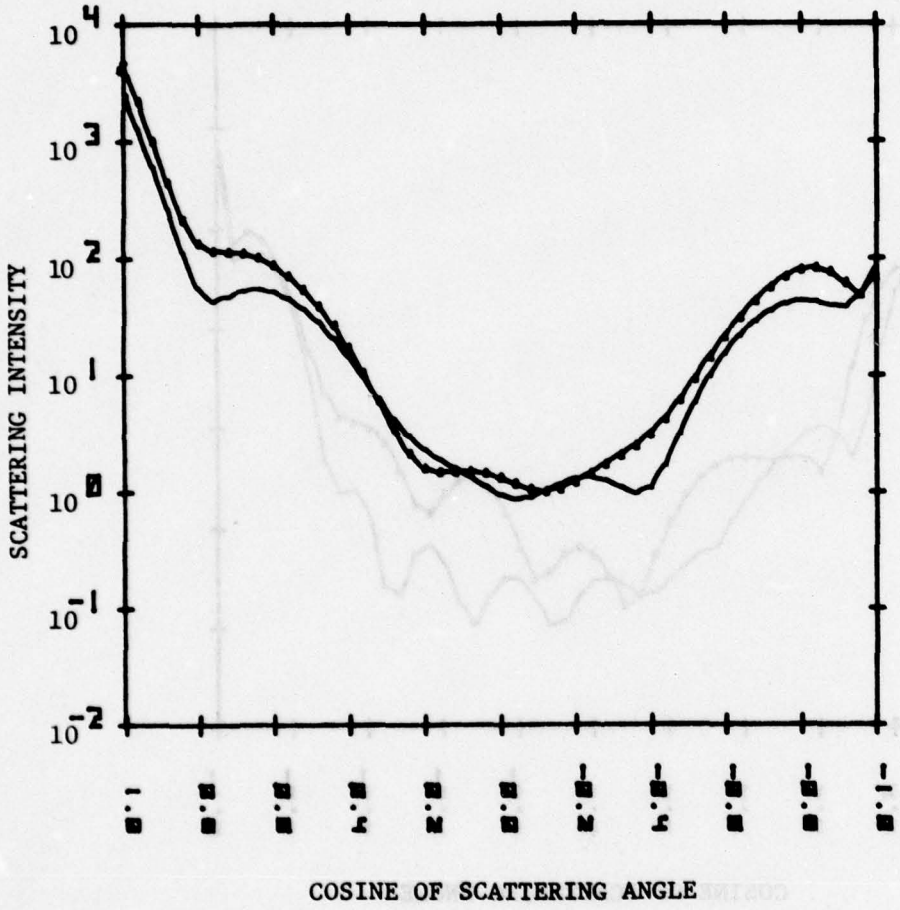

Figure (7.7) Unpolarized Phase Functions for Shape Functions $x(\theta) = x_o$ and $x(\theta) = x_o(1-0.1P_2(\theta))$ (Dotted), $x_o = 5$.

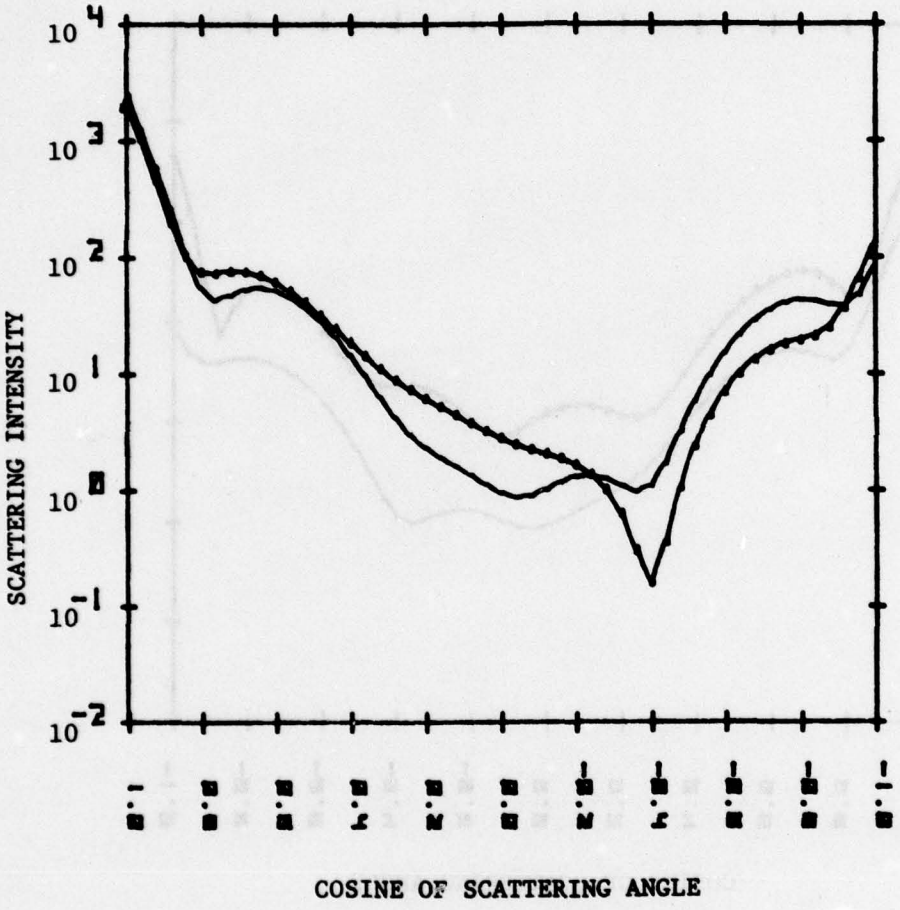

Figure (7.8) Unpolarized Phase Functions for Shape Functions $x(\theta) = x_o$ and $x(\theta) = x_o(1-0.1P_3(\theta))$ (Dotted), $x_o = 5$.

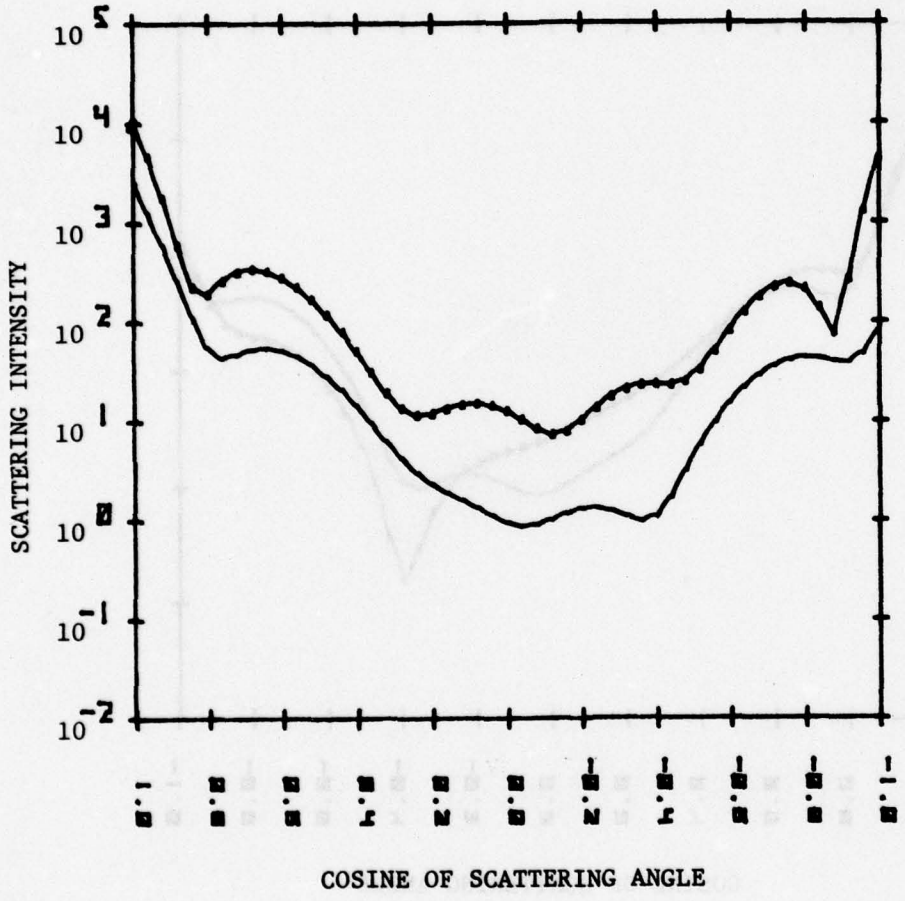

Figure (7.9) Unpolarized Phase Functions for Shape Functions $x(\theta) = x_o$ and $x(\theta) = x_o(1-0.1P_5(\theta))$ (Dotted), $x_o = 5$.

Additionally, the effect of varying the strength of the deformation is examined. Shape functions of the form

$$x(\theta) = x_o[1 \pm a_n P_n(\theta)] \tag{7.3}$$

for n = 2 and 3, a_n = 0.05, 0.01, and 0.15 are considered. Two effects of this variation of a_n are noted; the values of the relative maxima and minima vary by as much as a factor of five although the positions of the maxima and minima vary only slightly, and the amount of near forward scatter (scattering angle less than 30^o) varies by as much as a factor of five about the equivalent Mie curve. This latter effect would seem significant in terms of the experimental data reported by Chylek et al. since they demonstrate this frequently observed effect.

CHAPTER VIII

NONSPHERICAL PARTICLE CALCULATIONS: II

In Chapter V, a modification to the Mie solution to model nonspherical particle scattering was reviewed (Chylek, Grams and Pinnick, 1976). Because this modification is so attractive as a possible tool in radiation transfer analyses, part of this investigation is devoted to an estimate of the validity of the modification.

This modification is based on the correlation of the resonances of the c_ℓ and d_ℓ in the region $x \approx \ell$ with glories in the phase functions, glories not being commonly observed experimentally. As a result, Chylek et al. proposed the truncation of the resonances to model the effects of particle irregularity. This modification was implemented into a code, and calculations were presented that enjoyed better agreement with experimental data than did standard Mie calculations. This truncation was not applied to all c_ℓ and d_ℓ, but rather only to those for $\ell \geq 3$, otherwise the calculations do not exhibit good agreement with the data. This restriction is based on an argument that a certain minimum particle size is necessary for the validity of the modification.

The starting point for this effort is the calculation of the c_3 and d_3 in the region $x \approx \ell$. Shape functions of the form

$$x(\theta) = {}_o[1 \pm 0.1 P_n(\theta)] \tag{8.1}$$

for x_o = 3 to 4.5 by steps of 0.1 and for n=2,3,4,5 are considered. The real and imaginary parts of the c_3 and d_3 are compared with the c_3 and d_3 calculated using the Mie solution. In seven of these eight cases, the shape of the curves is preserved, although the resonance

sharpens in the sense that the real parts of the curve narrow by as much as a factor of two. This behavior is demonstrated in Figure (8.1) where the real part of c_3 is plotted for the Mie solution and for two shape functions. The imaginary parts of the curves also narrow. In one case, that of $x(\theta) = x_o(1+0.1P_3(\theta))$, the resonance curve is replaced by a slowly varying curve whose real parts have a mean of approximately 0.3, and whose imaginary parts have a mean of approximately zero.

Additionally, although the centers of the curves shift, apparently without trend, the real parts of the curves always fall under the Mie resonance curves. The extent of the narrowing or the curves seems to be approximately proportional to n. On the basis of these calculations, therefore, the modification of the c_ℓ and d_ℓ is not substantiated, but the numerical results of Chylek et al. may be justified in view of the narrowing of the resonance curves.

As a further step, calculations are performed for one of the polydisperse aerosol distributions reported by Chylek et al. (i.e. the first KCl). Nine phase functions are calculated using

$$x(\theta) = x_o$$

$$x(\theta) = x_o(1\pm0.05P_2(\theta))$$

$$x(\theta) = x_o(1\pm0.1P_2(\theta))$$

$$x(\theta) = x_o(1\pm0.15P_2(\theta))$$

$$x(\theta) = x_o(1-0.1P_2(\theta)\pm0.1P_4(\theta))$$

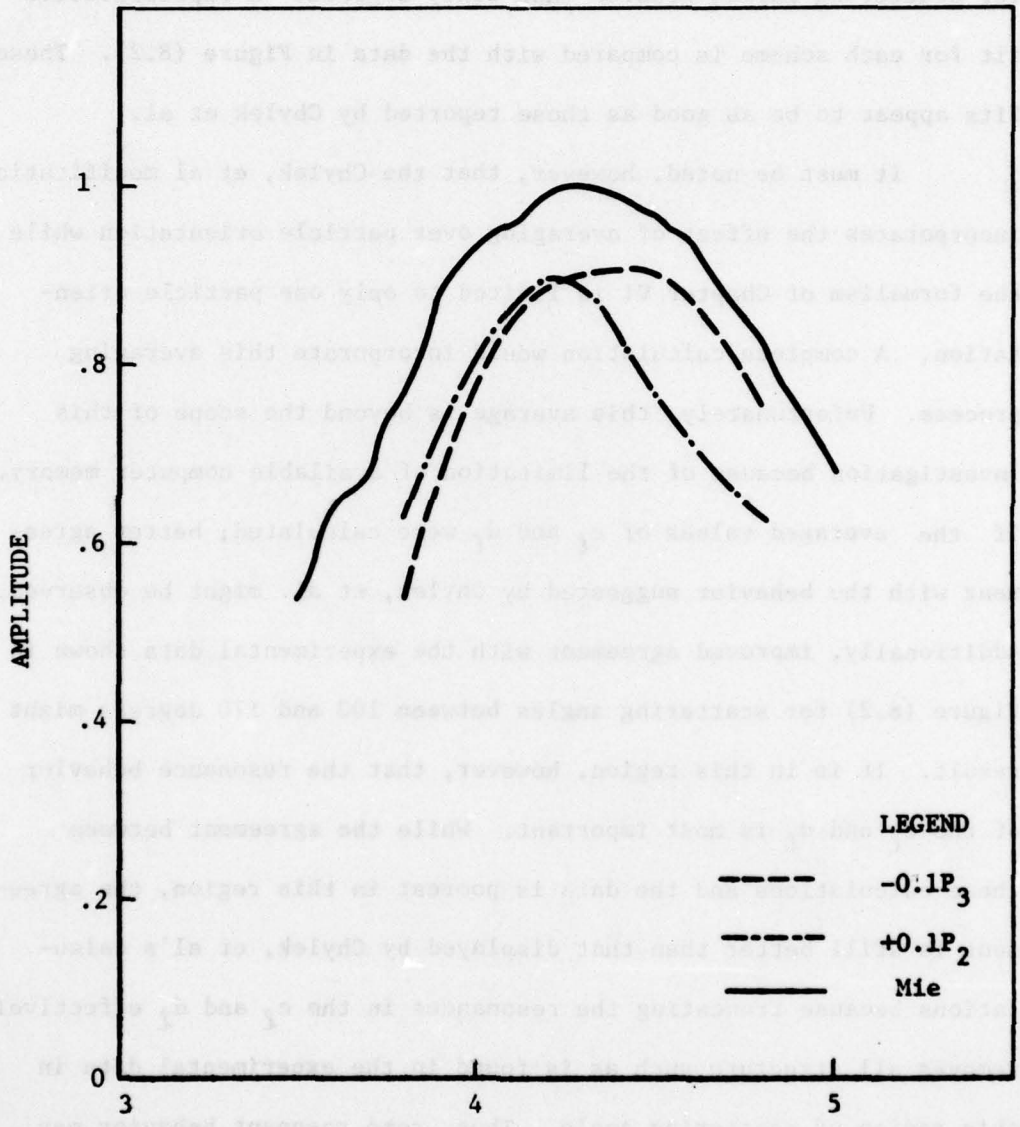

Figure (8.1) Comparison of real parts of c_3 for $x(\theta) = x_o(1-0.1P_2(\theta))$ (-.-), $x(\theta) = x_o(1-0.1P_3(\theta))$ (---), and Mie (solid).

and combined linerly with adjustable coefficients calculated using regression techniques to fit the data. Two different fitting schemes are used; one using all the data, and another using only those data for scattering angles greater than sixty degrees. A representative fit for each scheme is compared with the data in Figure (8.2). These fits appear to be as good as those reported by Chylek et al.

It must be noted, however, that the Chylek, et al modification incorporates the effect of averaging over particle orientation while the formalism of Chapter VI is limited to only one particle orientation. A complete calculation would incorporate this averaging process. Unfortunately, this average is beyond the scope of this investigation because of the limitation of available computer memory. If the averaged values of c_ℓ and d_ℓ were calculated, better agreement with the behavior suggested by Chylek, et al. might be observed. Additionally, improved agreement with the experimental data shown in Figure (8.2) for scattering angles between 100 and 170 degrees might result. It is in this region, however, that the resonance behavior of the c_ℓ and d_ℓ is most important. While the agreement between these calculations and the data is poorest in this region, the agreement is still better than that displayed by Chylek, et al's calculations because truncating the resonances in the c_ℓ and d_ℓ effectively removes all structure such as is found in the experimental data in this region of scattering angle. Thus, some resonant behavior may still be expected in the c_ℓ and d_ℓ after averaging over particle orientation, and the behavior suggested by Chylek, et al, should not be completely reproduced.

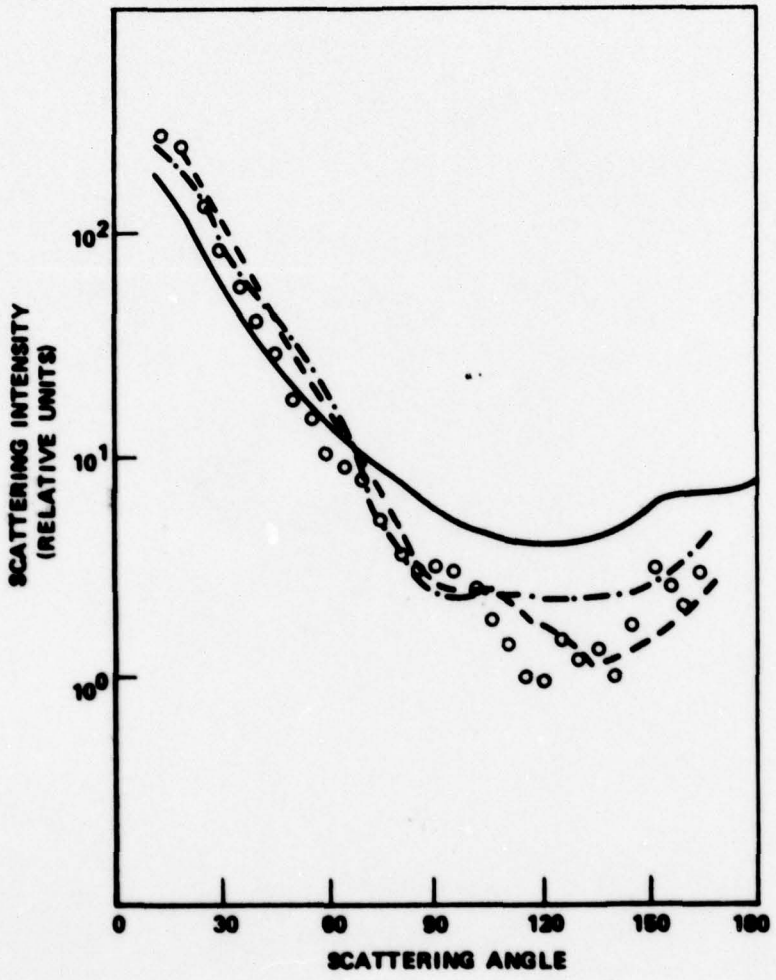

Figure (8.2) Comparison of Nonspherical Data (Circles) of Chylek, Grams, and Pinnick with Figurative Mie (Solid) and Two Combinations of Calculated Phase Functions. Both combinations use phase functions for the shape functions $x(\theta) = x_o(1-0.05P_2(\theta))$, $x(\theta) = x_o(1-0.1P_2(\theta))$, and $x(\theta) = x_o(1-0.15P_2(\theta))$. The curve (---) was fitted using all data, and the curve (-.-) was fitted using only data for scattering angles greater than sixty degrees.

CHAPTER IX

REVIEW OF RADIATIVE TRANSFER THEORY

The theory of Radiative Transfer (RT) has been developed to describe the transport of light in an extinguishing medium. The general four-dimensional form of the RT equation is (Chandrasekhar, 1960; Pomraning, 1973)

$$\left[\frac{1}{c}\frac{\partial}{\partial t} + \underline{k}\cdot\underline{\nabla}\right] I_j(\underline{r}, t, \underline{k}) = -\alpha(\underline{r}, t)\, I_j(\underline{r}, t, \underline{k}) \qquad (9.1)$$

$$+ \frac{\alpha(\underline{r}, t)\omega(\underline{r}, t)}{4\pi} \int_{j'=1}^{4} P_{jj'}(\underline{r}, t, \underline{k}\cdot\underline{k}') I_{j'}(\underline{r}, t, \underline{k}')\, d^2\underline{k}'$$

where: $I_j(\underline{r}, t, \underline{k})$ = the j^{th} component of the Stokes vector (Eqs. (3.43) - (3.46)),

c = the speed of light,

t = time,

$\underline{r}$ = position vector,

$\underline{k}$, $\underline{k}'$ = unit propagation vectors,

$\alpha(\underline{r}, t)$ = the extinction coefficient at $\underline{r}$ and t (Eq (4.2)),

$\omega(\underline{r}, t)$ = single scattering albedo at $\underline{r}$ and t (Eq. (4.6)),

$P_{jj'}(r, t, \underline{k}\cdot\underline{k}')$ = scattering phase function for the j'^{th} Stokes vector component into the j^{th} Stokes vector component at $\underline{r}$ and t through an angle,

$\underline{k}\cdot\underline{k}' = \cos(\theta)$, the cosine of the scattering angle.

The phase function $P_{jj'}(\underline{r}, t, \underline{k}\cdot\underline{k}')$ differs from the $P_j(\underline{r}, t, \theta)$ defined in Eq. (4.4) by a pair of rotations to correct for the change of orientation from $\underline{k}$ to $\underline{k}'$ (Chandrasekhar, 1960).

The RT equation is most commonly used in its unpolarized, time independent form

$$\underline{k}\cdot\nabla_{\underline{r}} I(\underline{r}, \underline{k}) = -\alpha(\underline{r})I(\underline{r}, \underline{k}) + \frac{\alpha(\underline{r})\omega(\underline{r})}{4\pi}\int p(\underline{r}, \underline{k}\cdot\underline{k}')I(\underline{r}, \underline{k}')d^2\underline{k}' \tag{9.2}$$

where: $I(\underline{r}, \underline{k})$ = the unpolarized intensity, and

$p(\underline{r}, \underline{k}\cdot\underline{k}')$ = phase function defined by Eq. (4.5).

Additionally, a source function $J(\underline{r}, \underline{k})$ is commonly defined as

$$J(\underline{r}, \underline{k}) = \frac{1}{4\pi}\int p(\underline{r}, \underline{k}\cdot\underline{k}')I(\underline{r}, \underline{k}')d^2\underline{k}', \tag{9.3}$$

which allows Eq. (9.2) to be rewritten as

$$\underline{k}\cdot\nabla_{\underline{r}} I(\underline{r}, \underline{k}) = -\alpha(\underline{r})[I(\underline{r}, \underline{k}) - \omega(\underline{r})J(\underline{r}, \underline{k})]. \tag{9.4}$$

Until recently, most of the work on RT has been performed in describing stellar or planetary atmospheres (Chandrasekhar, 1960). This work was concerned with plane or spherical parallel atmospheres with symmetry of medium and boundary conditions that allowed Eq. (9.4) to be reduced (in the plane parallel case) to

$$\mu\frac{d}{dZ}J(Z, \mu) = -\alpha(Z)[I(Z, \mu) - \omega(Z)J(Z, \mu)] \tag{9.5}$$

where Z = coordinate along which the medium varies,

$\mu = \underset{\sim}{k} \cdot \hat{Z}$, and

$$J(Z, \mu) = \frac{1}{2} \int P(Z, \underset{\sim}{k} \cdot \underset{\sim}{k}') I(Z, \mu') d\mu'.$$

Equation (9.5) is commonly referred to as the RT equation in the literature because of the interest it has enjoyed.

While Eq. (9.5) is useful for describing the brightness of a star or the amount of sunlight reaching the surface of a planet, it is limited to media varying along only one axis and uniform incident illuminations. Thus Eq. (9.5) cannot be used to treat problems where the media varies in more than one direction such as smoke (Friedlander, 1977; Greene and Lane, 1964) or clouds (Mason, 1971). Additionally, nonuniform incident illuminations such as are encountered in imaging and laser propagation problems cannot be treated.

To date, calculations performed on varying media and/or nonuniform incident illuminations have been limited to either few orders of scattering (Deepak and Green, 1970) or small angle scattering (Weinman and Shipley, 1972). Additionally, some Monte Carlo RT calculations have been performed for laser transmission through clouds (Bird, 1974), but these calculations are costly in terms of computer time required because the trajectory of each photon must be followed from source to absorption by either the medium or the detector, and a large number of photons must be counted to achieve

statistical significance. Thus, there have been no general numerical RT calculations performed to date from a general solution of the RT equation.

The RT equation, Eq. (9.1) may be rewritten by noting that the differential $(\frac{1}{c}\frac{\partial}{\partial Z} + \underset{\sim}{k}\cdot\underset{\sim}{\nabla})$ is essentially a directional derivative $\frac{\partial}{\partial \ell}$ where

$$\underset{\sim}{r} = \underset{\sim}{r}_o + \underset{\sim}{k}\ell$$
$$t = t_o + \ell/c \tag{9.6}$$

$\underset{\sim}{r}_o$ = boundary of the medium, and

t_o = time the light crosses the boundary.

Equation (9.1) may be rewritten as

$$\frac{\partial}{\partial \ell} I(\underset{\sim}{r}, t, \underset{\sim}{k}) = -\alpha(\underset{\sim}{r}, t) I(\underset{\sim}{r}, t, \underset{\sim}{k}) + \frac{\alpha(\underset{\sim}{r}, t)\omega(\underset{\sim}{r}, t)}{4\pi} \int p(\underset{\sim}{r}, t, \underset{\sim}{k}\cdot\underset{\sim}{k}') I(\underset{\sim}{r}, t, \underset{\sim}{k}') d^2\underset{\sim}{k}' \tag{9.7}$$

in an unpolarized form. Because most experimental data provide only the information of a concentration of total aerosol as a function of position and time and a constant particle size distribution, it is most useful to adopt the case where $N(\underset{\sim}{r}, a, t)$ is separable (Eqs. (4.1) - (4.4)), so that Eq. (9.7) may be rewritten as

$$\frac{\partial}{\partial \ell} I(\underset{\sim}{r}, t, \underset{\sim}{k}) = -\alpha(\underset{\sim}{r}, t) I(\underset{\sim}{r}, t, \underset{\sim}{k}) \tag{9.8}$$

$$+ \frac{\alpha(\underset{\sim}{r}, t)\omega}{4\pi} \int p(\underset{\sim}{k} \cdot \underset{\sim}{k}') I(\underset{\sim}{r}, t, \underset{\sim}{k}') d^2 \underset{\sim}{k}'$$

If the scattering events are independent, n^{th} order scattering is due to n consecutive single scatterings, and the intensity may be written as a sum of contributions for each order of scattering (Deepak and Green, 1970). That is,

$$I(\underset{\sim}{r}, t, \underset{\sim}{k}) = \sum_{n=0}^{N} \omega^n I_n(\underset{\sim}{r}, t, \underset{\sim}{k}) \tag{9.9}$$

where $I_n(\underset{\sim}{r}, t, k)$ is the intensity at $\underset{\sim}{r}$ at time t along $\underset{\sim}{k}$ due to n^{th} order scattering. While it is assumed that this series is convergent it may be noted that the series will converge in the limit $n \to \infty$ if $\omega I_{n+1}(\underset{\sim}{r}, t, \underset{\sim}{k}) / I_n(\underset{\sim}{r}, t, \underset{\sim}{k}) < 1$. Since $\omega < 1$, this assumption seems reasonable and is borne out numerically.

Equation (9.8) can be decomposed into N equations by substituting Eq. (9.0);

$$\frac{\partial}{\partial \ell} I_o(\underset{\sim}{r}, t, \underset{\sim}{k}) = -\alpha(\underset{\sim}{r}, t) I_o(\underset{\sim}{r}, t, \underset{\sim}{k}) \tag{9.10}$$

and

and

$$\frac{\partial}{\partial \ell} I_n(\underline{r}, t, \underline{k}) = -\alpha(\underline{r}, t) I_n(\underline{r}, t, \underline{k})$$

$$+ \frac{\alpha(\underline{r}, t)}{4\pi} \int p(\underline{k} \cdot \underline{k}') I_{n-1}(\underline{r}, t, \underline{k}') d^2\underline{k}', \quad n>o \tag{9.11}$$

It is convenient to extend the definition of the source function by combining Eqs. (9.3) and (9.9) to give

$$J_n(\underline{r}, t, \underline{k}) = \frac{1}{4\pi} \int p(\underline{k} \cdot \underline{k}') I_n(\underline{r}, t, \underline{k}') d^2\underline{k}') \tag{9.12}$$

Equation (9.11) may be rewritten as

$$\frac{\partial}{\partial \ell} I_n(\underline{r}, t, \underline{k}) = -\alpha(\underline{r}, t) I_n(\underline{r}, t, \underline{k}) + \alpha(\underline{r}, t) J_{n-1}(\underline{r}, t, \underline{k}) \tag{9.13}$$

The boundaries of the medium may be expressed as the set of vectors $\{\underline{r}_o\}$ and the initial times as $\{t_o\}$. The incident illuminations are defined as $I_o(\underline{r}_o, t_o, \underline{k})$. The solutions to Eqs. (9.10) and (9.13) may then be written as

$$I_o(\underline{r}, t, \underline{k}) = I_o(\underline{r}_o, t_o, \underline{k}) \exp\left(-\int_o^{\ell} \alpha(\underline{r}_o + \underline{k}\ell', t_o + \ell'/c) d\ell' \right) \tag{9.14}$$

and

$$I_n(\underline{r}, t, \underline{k}) = I_n(\underline{r}_o, t_o, \underline{k}) \exp\left(-\int_o^{\ell} \alpha(\underline{r}_o + \underline{k}\ell', t_o + \ell'/c) d\ell' \right) \tag{9.15}$$

$$+ \int \alpha(\underline{r}_o+\underline{k}\ell', t_o+\ell'/c) J_{n-1}(\underline{r}_o+\underline{k}\ell', t_o + \ell'/c, \underline{k})$$

$$\exp\left(-\int_{\ell'}^{\ell} \alpha(\underline{r}_o+\underline{k}\ell'', t_o+\ell'/c)d\ell''\right)d\ell', \quad n>0.$$

If the boundaries are nonreflecting, $I_n(\underline{r}_o, t_o, \underline{k}) = 0; n>0$, and Eq. (9.15) may be reduced to

$$I_n(\underline{r}, t, \underline{k}) = \int_0^{\ell} \alpha(\underline{r}_o+\underline{k}\ell', t_o+\ell'/c) J_{n-1}(\underline{r}_o+\underline{k}\ell', t_o+\ell'/c\ \underline{k}) \quad (9.16)$$

$$\exp\left(-\int_{\ell'}^{\ell} \alpha(\underline{r}_o+k\ell'', t_o+\ell''/c)d\ell''\right)d\ell'.$$

Equations (9.9), (9.12), (9.13), and (9.16) constitute the four basic equations for the general RT calculations to be performed. Chapter X describes the development of a numerical algorithm for the solution of the two-dimensional RT equation, and Chapter XI presents some calculations performed using the code implementing this algorithm.

CHAPTER X

TWO-DIMENSIONAL RADIATIVE TRANSFER EQUATION ALGORITHM

The RT equation is solved by introducing a quadrature approximation for the source function similar to that of Chandrasekhar (Chandrasekhar, 1960). The approximation for the source function, Eq. (9.12), is

$$J_n(\underline{r}, \underline{k}) \simeq \sum_{i=1}^{I} p(\underline{k} \cdot \underline{k}_i') W_i I_n(\underline{r}, \underline{k}_i') \tag{10.1}$$

where the W_i are approximate weighting factors chosen such that

$$\sum_{i=1}^{I} p(\hat{e}_3 \cdot \underline{k}) W_i = 1 \tag{10.2}$$

where $\hat{e}_3$ is the unit vector in the z direction. The phase function is now independent of position and time because the medium has been assumed to be separable. Additionally, because the RT equation of interest in this chapter will be essentially two-dimensional, all reference to the functional dependence on time t will be dropped; only steady state conditions will be admitted.

The aerosol medium will be represented by a rectangular array L by M points in extent. The positions of the points in the array are designated by the indices ℓ and m. Since the array is rectangular, the points in the array have eight first, second, and third nearest neighbors, defining eight directions (and $\underline{k}_i$). This geometry is shown in Figure (10.1).

AD-A058 385 ARMY MISSILE RESEARCH AND DEVELOPMENT COMMAND REDSTO--ETC F/G 20/3
AN INVESTIGATION OF RADIATION TRANSFER THROUGH AEROSOLS.(U)
JUN 78 B W FOWLER

UNCLASSIFIED DRDMI-C-78-3 NL

2 OF 3
AD
A058 385

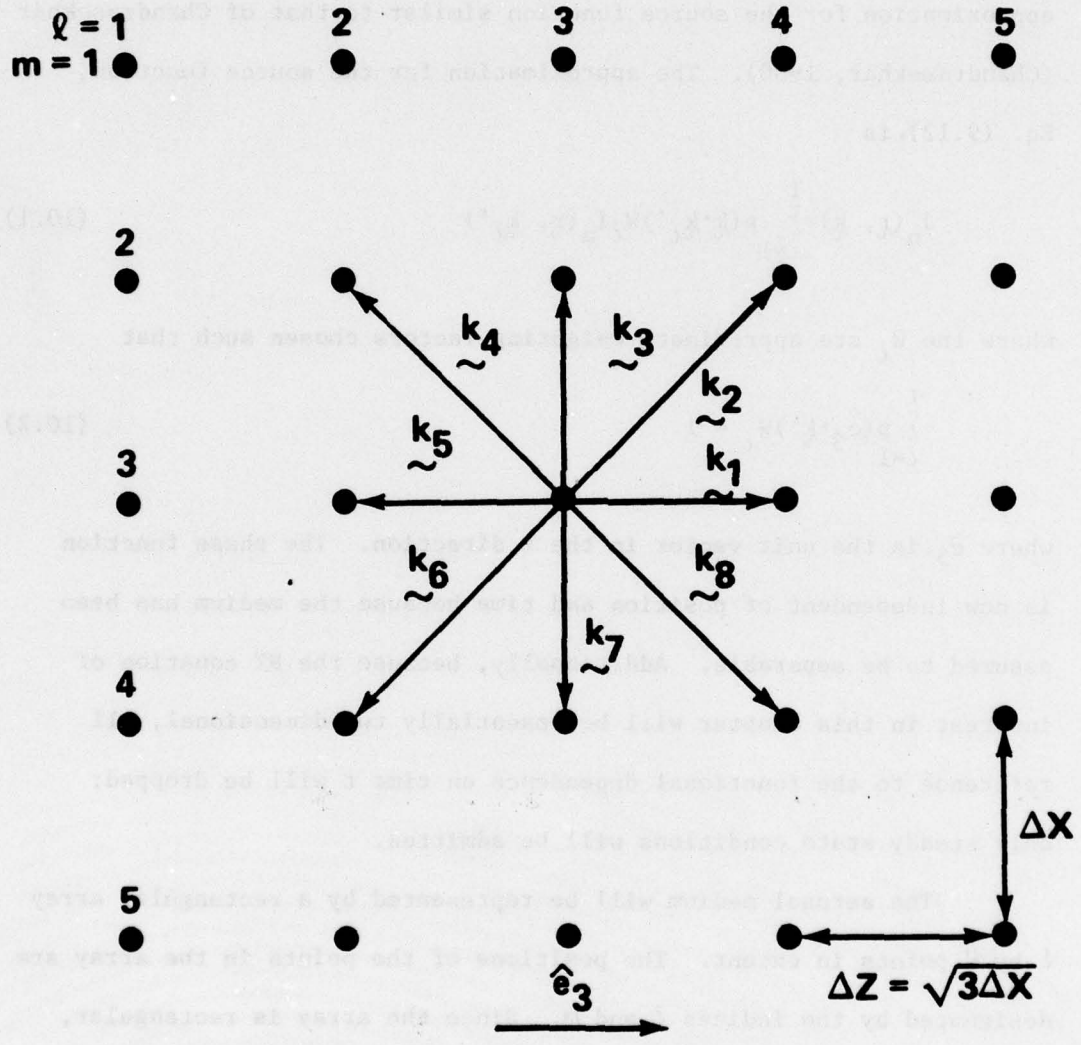

Figure (10.1). Eight Beam Geometry

The differential $d^2\underline{k}$ in Eq. (9.12) may be written as $d\cos\theta' d\phi'$ and Eq. (10.1) may be formed as the product of two trapezoid rule integrations (without derivitive terms)(Abramowitz and Stegun, 1964). One property of the trapezoid rule is that the weighting factors for all points except the end points are equal. The weighting factors for the end points are one-half of the other weighting factors. The ϕ' integration is approximated at the points $\phi' = 0$, π, and 2π. Since the integrand of Eq. (9.12) has the same value at $\phi' = 0$ and at $\phi' = 2\pi$, the integration effectively looks only at the points $\phi' = 0$ and $\phi' = \pi$ with equal weighting factors at both points. The $\cos\theta'$ integration is approximated at the points $\cos\theta' = \pm 1$, ± 0.5 and 0, but the end points, $\cos\theta' = \pm 1$ are counted twice because of the ϕ' approximation. As a result, the weighting factors W_i are the same for all i and are defined by reducing Eq. (10.2) to

$$W \sum_{i=1}^{I} p(\hat{e}_3 \cdot \underline{k}_i') = 1, \tag{10.3}$$

where W is the integration weighting factor.

Equation (10.1) allows the solution of the time-independent RT equation to be reduced to an eight-beam formalism, so that only those intensities needed for the source functions are calculated. Additionally, the approximation that the source functions and intensities are constant in the rectangular region about each point in the array is made.

Equation (10.1) may be rewritten as

$$J_n(\mathbf{r}_{\ell m}, \mathbf{k}_j) = \sum_{i=1}^{8} Q_{ji} I_n(\mathbf{r}_{\ell m}, \mathbf{k}_i) \tag{10.4}$$

where $Q_{ji} = Wp(\mathbf{k}_j \cdot \mathbf{k}_i)$ and $\mathbf{r}_{\ell m}$ is the position in the array. It is conceptually convenient to introduce the notation

$$J_n(\mathbf{r}_{\ell m}, \mathbf{k}_i) = J_{n,\ell m,j} \,, \tag{10.5}$$

$$I_n(\mathbf{r}_{\ell m}, \mathbf{k}_i) = I_{n,\ell m,i} \,, \tag{10.6}$$

and

$$\alpha(\mathbf{r}_{\ell m}) = \alpha_{\ell m} \,. \tag{10.7}$$

The incident illuminations are specified at all points on the boundary of the array ($\ell = 0$ and $\ell = L$ for all m, and $m = 0$ and $m = M$ for all ℓ) for all k_i interior to that ℓ,m point. The $I_{o,\ell m,j}$ are calculated from these boundary conditions by a point-to-point, along each path integration of Eq. (9.14). The $J_{o,\ell m,j}$ are calculated from the $I_{o,\ell m,j}$ using Eq. (10.4). Following this, the $I_{1,\ell m,j}$ are calculated from the $J_{o,\ell m,j}$ using Eq.(9.16) and the $J_{1,\ell m,j}$ are calculated from the $I_{1,\ell m,j}$. The intensities $I_{n,\ell m,j}$ and the source functions $J_{n,\ell m,j}$ for $n>1$ are calculated in a similar manner. The total intensity at any point in any direction may be

calculated from Eq. (9.9). For example, the forward intensity along the boundary $\ell = L$ is

$$I(\underset{\sim}{x}_{Lm}, \hat{e}_3) = \sum_{n=0} I_{n,\, Lm,\, 1}\, \omega^n \tag{10.8}$$

and the backscattered intensity along the boundary $\ell = 1$ is

$$I(\underset{\sim}{x}_{1}, -\hat{e}_3) = \sum_{n=0}^{N} I_{n,1m,5}\, \omega^n$$

These two quantities are calculated to the order of scattering N for which the Center Line of Sight (CLOS - the line between the source-detector system, being along varying ℓ for $m = M/2$) forward intensity varied with order of scattering by less than 1%. That is,

$$\sum_{n=o}^{N} I_{n,\, \ell M/2,\, 1}\, \omega^n - \sum_{n=o}^{N-1} I_{n,\, \ell M/2,\, 1}\, \omega^n < .01 \sum_{n=o}^{N} I_{n, \ell M/2,\, 1}\, \omega^n. \tag{10.10}$$

Another quantity calculated is the modulation contrast defined by

$$C(\underset{\sim}{x}_{\ell m}, \underset{\sim}{k}_i) = \frac{I(\underset{\sim}{x}_{\ell m}, \underset{\sim}{k}_i) - I(\underset{\sim}{x}_{\ell m}, \underset{\sim}{k}_i)_{\min}}{I(\underset{\sim}{x}_{\ell m}, \underset{\sim}{k}_i)_{\max} - I(\underset{\sim}{x}_{\ell m}, \underset{\sim}{k}_i)_{\min}} \tag{10.11}$$

where $I(\underset{\sim}{x}_{\ell m}, \underset{\sim}{k}_i)_{\max}$ and $I(\underset{\sim}{x}_{\ell m}, \underset{\sim}{k}_i)_{\min}$ are the maximum and minimum intensities along the path perpendicular to $\underset{\sim}{k}_i$. Specifically, the contrast for the forward intensity along m for $\ell = L$ is calculated

since this would be the contrast seen by a detector looking along the CLOS.

Available computer memory would only permit this two-dimensional algorithm to be coded and then by storing only the $J_{n,\ell m,j}$, the $J_{n-1,\ell m,j}$ and the forward scattered and backscattered intensities, Eqs. (10.8) and (10.9). The run time of the code was minimized by introducing an eight beam interlace integration scheme for the intensities and source functions.

The eight beam interlace integration scheme arises from noting that the quadrature approximation to the source function, Eq. (10.4) may be calculated sequentially by incrementing for each $I_{n,\ell m,j}$ as it is calculated rather than waiting until all eight $I_{n,\ell m,j}$ have been calculated and then summing them. The chief advantage of this scheme is that it allows the calculation of the source functions to be shifted from a consideration of each point in the array on a point by point basis to a consideration of each point in the array on a path by path basis, collecting points as they occur on each path to increment the source function at that point. The operation of this scheme is shown in Figure (10.2).

The advantage of Eqs. (9.9), (9.12), (9.14) and (9.16) in coding is that they allow the intensity for each order of scattering to be calculated from the source function for the previous order of scattering. The code may be structured so that the $I_{o,\ell m,j}$ are calculated from the boundary conditions, the $J_{o,\ell m,j}$ are calculated from the $I_{o,\ell m,j}$ and in general, the $I_{n,\ell m,j}$ are calculated from

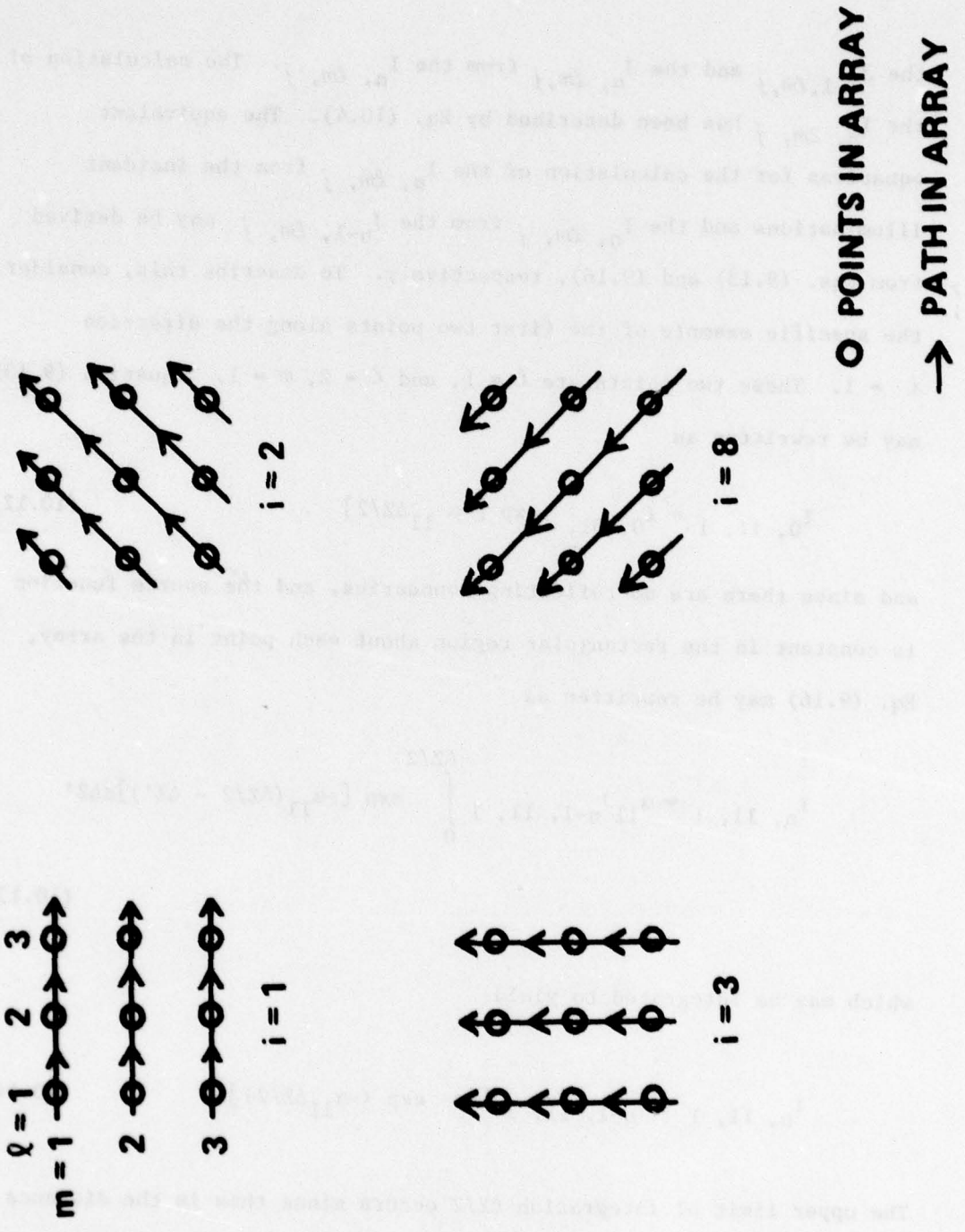

Figure (10.2). Eight Beam Interlace Integration Scheme

the $J_{n-1,\ell m,j}$ and the $J_{n,\ell m,j}$ from the $I_{n,\ell m,j}$. The calculation of the $I_{n,\ell m,j}$ has been described by Eq. (10.4). The equivalent equations for the calculation of the $I_{o,\ell m,j}$ from the incident illuminations and the $I_{n,\ell m,j}$ from the $J_{n-1,\ell m,j}$ may be derived from Eqs. (9.13) and (9.16), respectively. To describe this, consider the specific example of the first two points along the direction $i = 1$. These two points are $\ell = 1$, and $\ell = 2$, $m = 1$. Equation (9.13) may be rewritten as

$$I_{0,11,1} = I_{0,01,1} \exp\left[-\alpha_{11}\Delta Z/2\right] \tag{10.12}$$

and since there are no reflecting boundaries, and the source function is constant in the rectangular region about each point in the array, Eq. (9.16) may be rewritten as

$$I_{n,11,1} = \alpha_{11} J_{n-1,11,1} \int_0^{\Delta Z/2} \exp\left[-\alpha_{11}(\Delta Z/2 - \Delta Z')\right] d\Delta Z' \tag{10.13}$$

which may be integrated to yield

$$I_{n,11,1} = J_{n-1,11,1}\left[1 - \exp\left(-\alpha_{11}\Delta Z/2\right)\right] \tag{10.14}$$

The upper limit of integration $\Delta Z/2$ occurs since this is the distance from the boundary of the array to the point $\ell = 1$, $m = 1$ along the direction $i = 1$. The intensities $I_{0,11,1}$ and $I_{n,11,1}$ each

contribute one term $Q_{j1}I_{0,\ 11,\ 1}$ and $Q_{j1}I_{n,\ 11,\ 1}$ to the calculation of $J_{0,\ 11,\ j}$ and $J_{n,\ 11,\ j}$, respectively. The intensities at the point $\ell = 2$, $m = 1$ may also be calculated form Eqs. (9.13) and (9.16) as

$$I_{0,\ 21,\ 1} = I_{0,\ 01,\ 1}\ \exp\left(-\int_0^{\Delta Z}\alpha_{11}d\Delta Z' - \int_{\Delta Z}^{3\Delta Z/2}\alpha_{21}d\Delta Z'\right) \tag{10.15}$$

$$= I_{0,\ 11,\ 1}\exp\left(-\alpha_{11}\Delta Z - \alpha_{21}\Delta Z/2\right)$$

and

$$I_{n,\ 21,\ 1} = \alpha_{11}J_{n-1,\ 11,\ 1}\int_0^{\Delta Z}d\Delta Z'\ \exp\left(-\int_{\Delta Z'}^{\Delta Z}\alpha_{11}d\Delta Z''\right) \tag{10.16}$$

$$\exp\left(-\int_{\Delta Z}^{3\Delta Z/2}\alpha_{21}d\Delta Z''\right) + \alpha_{21}J_{n-1,\ 21,\ 1}\int_{\Delta Z}^{3\Delta Z/2}d\Delta Z'\exp\left(-\int_{\Delta Z'}^{3\Delta Z/2}\alpha_{21}d\Delta Z''\right),$$

which may be integrated to yield

$$I_{n,\ 21,\ 1} = J_{n-1,\ 11,\ 1}\left(1-\exp(-\alpha_{11}\Delta Z)\right)\exp(-\alpha_{21}\Delta Z/2)$$

$$+J_{n-1,\ 21,\ 1}\left(1-\exp(-\alpha_{21}\Delta Z/2)\right) \tag{10.17}$$

since the point $\ell = 2$, $m = 1$ is $3\Delta Z/2$ from the boundary, and the source function changes value is going from the first rectangular region about $\ell = 1$, $m = 1$ to the second rectangular region about $\ell = 2$, $m = 1$. Equation (10.15) may be rewritten as

$$I_{n,\,21,\,1} = I_{n,\,11,\,1} \exp\,[-(\alpha_{11} + \alpha_{21})\Delta Z/2] \tag{10.18}$$

by recognizing that $I_{0,\,21,\,1}$ is equal to the intensity $I_{0,\,11,\,1}$ degraded by extinction between the points $\ell = 1$, $m = 1$, and $\ell = 2$, $m = 1$, while Eq. (10.17) may be rewritten as

$$\begin{aligned} I_{n,\,21,\,1} = {} & J_{n-1,\,11,\,1}\,[1-\exp(-\alpha_{11}\Delta Z/2)]\exp[-(\alpha_{11}+\alpha_{21})\Delta Z/2] \\ & + J_{n-1,\,11,\,1}[1-\exp(-\alpha_{11}\Delta Z/2)]\exp(-\alpha_{21}\Delta Z/2) \\ & + J_{n-1,\,21,\,1}[1-\exp(-\alpha_{21}\Delta Z/2)] \end{aligned} \tag{10.19}$$

The first term of the right hand side of Eq. (10.19) may be recognized as the intensity $I_{n,\,11,\,1}$ degraded by extinction between the points $\ell = 1$, $m = 1$ and $\ell = 2$, $m = 1$. Equation (10.19) may then be rewritten as

$$I_{n,\,21,\,1} = I_{n,\,11,\,1}\exp[-(\alpha_{11}+\alpha_{21})\Delta Z/2]$$

$$+J_{n-1,\ 11,\ 1}[1-\exp(-\alpha_{11}\Delta Z/2)]\exp(-\alpha_{21}\Delta Z/2)$$

$$+J_{n-1,\ 21,\ 1}[1-\exp(-\alpha_{21}\Delta Z/2)]\ . \qquad (10.20)$$

Equations (10.18) and (10.20) are the specific forms for this example of the general numerical equations for the intensity at a point in the array along a path in terms of the intensity at the previous point in the array along the path and the previous order of scattering source functions at the two points on the path along the path, noting that $I_{n,\ \ell m,j} = 0$ for $n<0$ for all ℓ, m, j. It may also be noted that Eq. (10.20) may be derived from Eq. (9.15) if $\underset{\sim}{k} = \underset{\sim}{k}_1$, and $I_n(\underset{\sim}{r}_0, \underset{\sim}{k}) = I_{n,\ 11,\ 1}$. It is the combination of Eqs. (10.4), (10.12), (10.14), (10.15) and (10.20) that allows the order of scattering path-by-path calculation to be performed.

The derivation of these equations incorporated several approximations. Two approximations were used in deriving Eq. (10.4); that the extinguishing medium may be represented as planar, and that, within that plane, the radiation transport may be represented by eight beams. It is expected that computational errors will increase when the incident illumination varies greatly outside the plane, or when eight beams are not enough to represent accurately either the incident illumination or the scattering phase function. Equations (10.12), (10.14), (10.15), and (10.20) incorporate one major approximation, that the source function does not vary appreciably about each point

in the rectangular array representing the planar medium. The iterative form of the solution and the close computational connection between Eqs. (10.4), (10.12), (10.14), (10.15), and (10.20) makes an exact estimate of error difficult.

As an estimator of worse case error to be expected from the combination of these approximations, calculations were performed using this two-dimensional algorithm (a listing of the code is given in Appendix (IV)) and a three-dimensional Monte Carlo trajectory tracing code (House and Avery, 1969) for a Rayleigh scattering medium (Chandrasekhar, 1960) with an albedo of 0.5. The medium was assumed to be uniform ($\alpha_{\ell m}$ = constant). The Rayleigh phase function was chosen for this comparison because it represents the worse case of any situation of interest with regard to nonforward scattering, since polydisperse aerosol phase functions do not generally exhibit glories or rainbows (Van de Hulst, 1957; Deirmendjian, 1964). The incident illumination was a gaussian profile beam held constant with respect to the third dimension for the Monte Carlo calculations. The forward CLOS intensities at five optical depths are given in Table (10.1). The precent differences were calculated relative to the Monte Carlo results. It may be seen that while there are considerable differences between the two calculations (maximum 3.3%), the variation in the difference and the degree of approximations extant in the two-dimensional algorithm indicate that the agreement in this case may be considered to be quire good. Better agreement might be

TABLE (10.1). COMPARISON OF TWO-DIMENSIONAL ALGORITHM WITH THREE-DIMENSIONAL MONTE CARLO CODE.

OPTICAL DEPTH	TWO DIMENSIONAL ALGORITHM	MONTE CARLO CODE	% DIFFERENCE
1	0.4152	0.4152	0.0
2	0.1829	0.1770	3.3
3	0.0855	0.0848	0.8
4	0.0426	0.0436	-2.3
5	0.0224	0.0219	2.3

expected for most polydisperse aerosol phase functions, but worse agreement for incident illuminations with more variation outside the plane when the planar medium approximation becomes more inaccurate.

CHAPTER XI

RESULTS OF

TWO-DIMENSIONAL RADIATIVE TRANSFER CALCULATIONS

The calculations presented in this chapter are for a uniform Deirmendjian C.3 fog. Because the fog is uniform, the extinction coefficient $\alpha_{\ell m}$ is constant within the fog which encompasses the entire rectangular array. In terms of Eq. (4.9), D = 5.5556, B = 0.3333, δ = 3, γ = 8, and the concentration is $100/cm^3$ (Deirmendjian, 1964). Three wavelengths were considered; 1.06 μm, 3.0μm, and 10.6 μm, representing the near ir, the mid ir, and the far ir. Two of these wavelengths correspond to actual laser wavelengths (1.06 μm and 10.6 μm). The other wavelength was chosen close to the 3-5 μm window of the atmosphere, but just outside the window where the water absorption would be considerable (Selby and McClatchey, 1976). Additionally, the refractive index of water is well known at these wavelengths (Centeno, 1944; Pointer and Dechambenoy, 1966; Curcio and Petty, 1954).

The extinction coefficients, albedoes, and phase functions were calculated using an existing polydisperse Mie scattering code adapted to calculate the Q_{ji} (Blattner, 1972). A listing of this code is given in Appendix (IV). The wavelengths, refractive indices, calculated extinction coefficients, albedoes, and Q_{j1}'s for j = 1-5 are given in Table (11.1). The other Q_{j1}'s are not included in Table (11.1), since the symmetry of the unpolarized phase function requires that $Q_{21} = Q_{81}$, $Q_{31} = Q_{71}$, $Q_{41} = Q_{61}$.

Two sources were considered in these calculations -- a uniform intensity beam and a Gaussian profile beam. The uniform intensity

TABLE (11.1). PARAMETERS FOR RADIATIVE TRANSFER EQUATION

$\lambda(\mu m)$	m	$\alpha(km^{-1})$	ω	Q_{11}	Q_{21}	Q_{31}	Q_{41}	Q_{51}
1.06	$1.322-i.00001$	2.88	1.0	.168	.119	.118	.118	.120
3.0	$1.364-i.306$	3.25	.465	.246	.148	.066	.066	.214
10.6	$1.212-i.0601$	.393	.293	.213	.141	.109	.092	.102

beam was used to investigate the transmission of contrast. This beam was 1.9 km wide against a black background 5.2 km wide including the beam. The geometry of these calculations, showing the uniform intensity beam, is given in Figure (11.1). As defined by Eq. (10.11), this beam has an inherent contrast of one. Both beams were treated as plane waves traveling along the $\ell = 1$ direction for the purpose of establishing boundary conditions. The other boundary conditions were taken to be zero. For both beams, the incident illumination at the CLOS was one so that intensities along the CLOS could be directly interpreted as transmissions.

The depth of the fog was varied in 0.5 km increments from 0.5 to 5 km. The size of the array was $M = 31$ and $L = 50$, limited only by the available computer memory. The scale of Δz is determined by the depth of fog to be considered, the scale of Δx is determined by the scale of Δz, and the size of the beam is determined by the number of Δx needed to accurately represent it. Thus the beam diameter is directly constrained by the depth of fog considered.

The forward and backscattered intensities are calculated using Equations (10.8) and (10.9) for both beams at the three wavelengths and ten fog depths described. The forward intensities along the CLOS are shown in Figures (11.2) and (11.3) for the uniform profile and gaussian profile beams, respectively. Examination of these intensities reveals that the intensities fall off with fog depth z as approximately $\exp(-\alpha q z)$ where q is a diffusion exponent (always ≤ 1) similar to that found in traditional one-dimensional plane-parallel RT (Chandrasekhar, 1960; Kattawar and Plass, 1967). The intensity at 3.0μm falls off

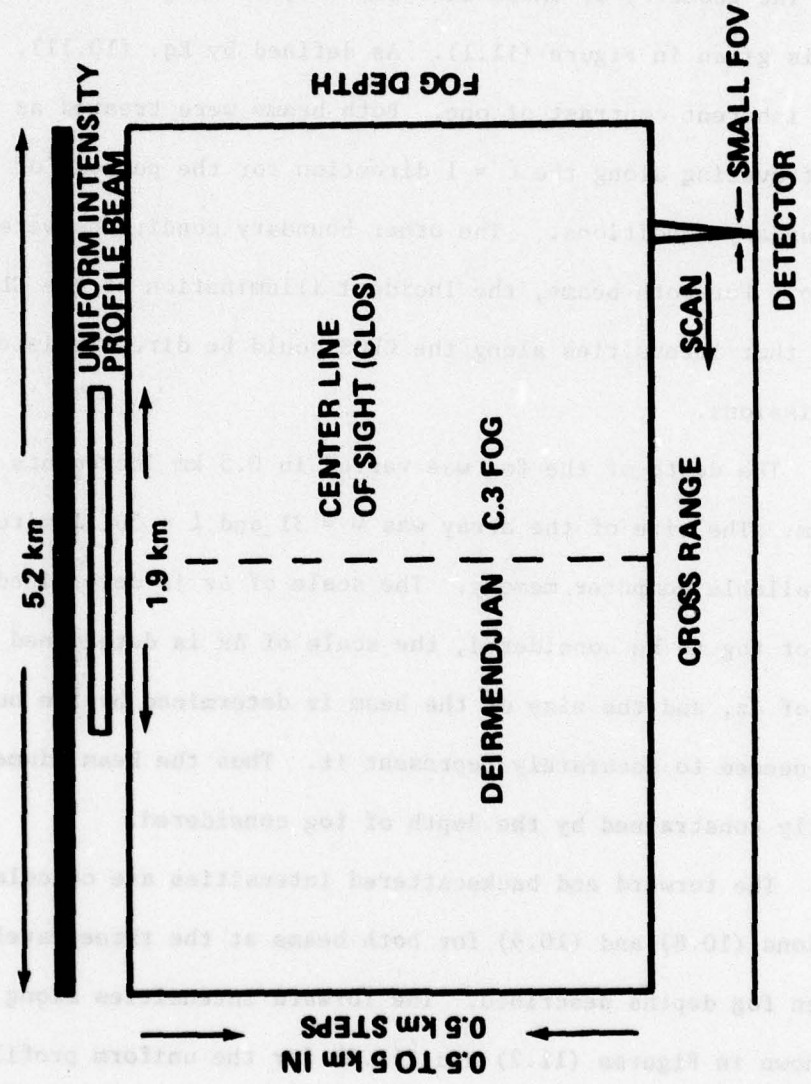

Figure (11.1). Geometry of Uniform Beam Calculations

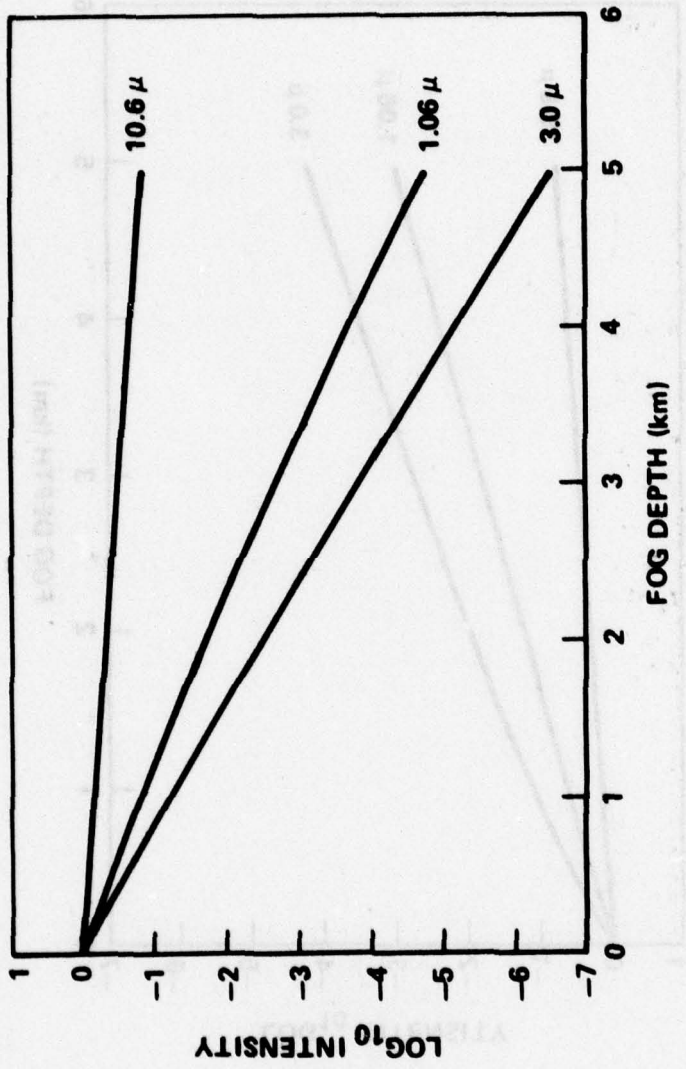

Figure (11.2) Forward CLOS Intensity of Uniform Beam.

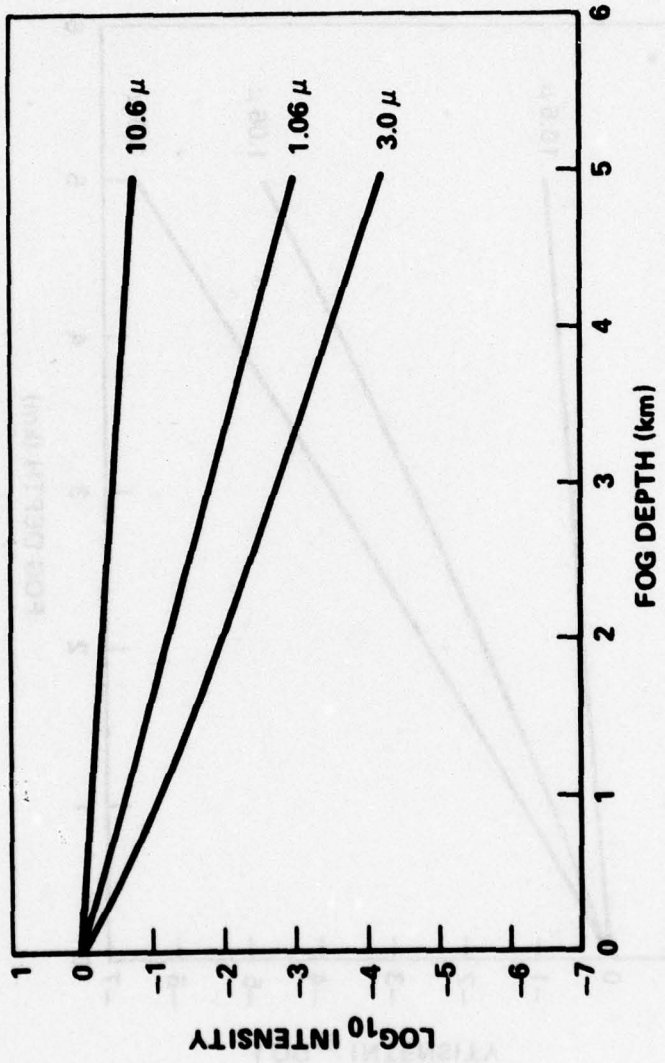

Figure (11.3) Forward CLOS Intensity of Gaussian Beam.

fastest because the extinction coefficient is largest at that wavelength due to the water absorption. While these Q's are not the same numerically as those encountered in one-dimensional RT because of the nonuniformity of the boundary conditions, this behavior of the intensity along the CLOS is not unexpected because of the symmetry of the boundary conditions. The intensity of the uniform beam falls off faster than the intensity of the gaussian beam for each wavelength, and the magnitude of the difference between the intensities for each wavelength decreases with increasing wavelength. This difference in intensities is due to both scattering and initial beam profile. The total orders of scattering N required to satisfy the convergence condition, Equation (10.10) is dependent on the depth of fog and the albedo, which is wavelength dependent. As the albedo or the fog depth increases, N increases. Experience with the two-dimensional code indicates that N is more strongly influenced by albedo value than by fog depth. Further, the value of Q decreases with increasing ω and/or N. This behavior of Q has been noted in plane-parallel one-dimensional RT (Kattawar and Plass, 1976).

The difference in transmission between the two beams is also due to the form of the initial beam profile. The uniform beam intensity falls off less rapidly adjacent to the CLOS than does the gaussian beam incident intensity. This condition affects the scattering of light away from the CLOS. The total scattering out from the CLOS is less for the uniform beam than for the gaussian beam for low orders of scattering since the intensity scattered out of the CLOS is largely

replaced by intensity scattered into the CLOS. For higher orders of scattering, the situation is reversed. At the edge of the uniform profile beam, intensity that scatters out into the background is not replaced, largely because there is little intensity to be scattered from the background into the beam. Some intensity is scattered into the edge of the beam from the interior of the beam, but there is a net scattering out from the beam into the background. As higher orders of scattering are considered, more intensity scatters into the background than out of it.

This net scattering out of the CLOS also occurs for the gaussian beam, but at a lesser rate since there are no regions of zero initial intensity for the gaussian beam. If the gaussian beam were truncated to the size of the uniform beam, the intensity of the truncated gaussian beam would fall off even faster than the intensity of the uniform beam.

The forward intensity is strongly influenced by the total orders of scattering N required to satisfy Equation (10.10). As previously stated, the value of N required is largely determined by the albedo. In practice, it is found that the relative value of N required goes at least as the square of the albedo. Since the value of the albedos used in this study decrease with increasing wavelength, N decreases with increasing wavelength. Thus shorter wavelengths evidence higher order intensities that fall off faster for the uniform beam than for the gaussian beam.

Comparison of the backscattered intensities, Figures (11.4) and (11.5), respectively, at each wavelength shows that the uniform beam intensities are greater than the gaussian beam intensities. Further, the magnitudes of the intensities decrease with increasing wavelength as do the differences between the intensities. This is because the backscattered intensity is largely due to low orders of scattering. This fact is demonstrated by the shape of the curves, being proportional to $1 - \exp(-2\alpha q' z)$, where q' is again a diffusion exponent. This curve may be calculated analytically for first order scattering, using Equation (9.15) for $n = 1$ and $\underset{\sim}{k} = -\hat{e}_3$. While q' could not be calculated as exactly as q for each wavelength-beam case because of the difficulty of accurately calculating the proportionality constant for each curve (essentially a total source term,) it was found that $q' < q$ in all cases by an amount consistent with the errors involved in the 1% criterion of Equation (10.10). This behavior is consistent with the contention that backscattered intensity is largely due to low orders of scattering since the 1% condition applies to the forward intensity and for equal numbers of forward and backscattered intensity terms contributing to the total intensities, the backscattered intensity should be more accurate and $q' < q$.

The increase in backscatter with decreasing wavelength may be seen by considering that the albedo decreases with increasing wavelength, and the product of albedo, extinction coefficient, and Q_{51} decreases with increasing wavelength. This latter quantity is the backscatter coefficient that determines the amount of first order backscatter back along the CLOS. Thus the backscatter coefficient

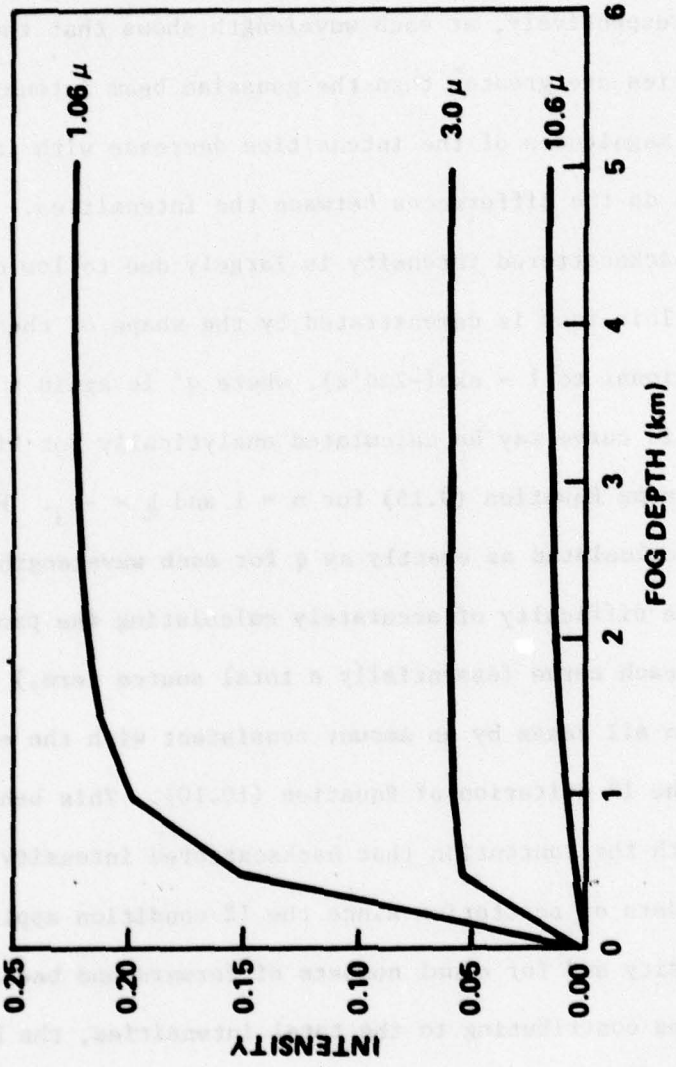

Figure (11.4) Backscatter CLOS Intensity of Uniform Beam.

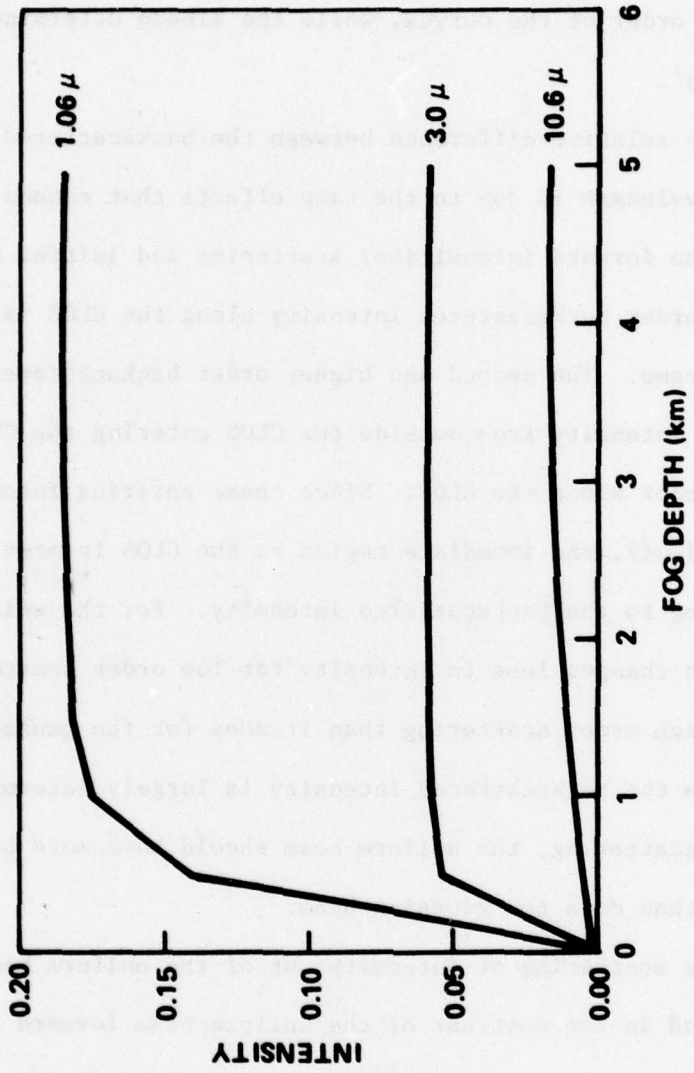

Figure (11.5) Backscatter CLOS Intensity of Gaussian Beam.

determines the first order backscatter, and, in this case, the relative wavelength order of the curves, while the albedo determines N and therefore ϱ'.

The relative difference between the backscattered intensities at each wavelength is due to the same effects that caused the differences in the forward intensities; scattering and initial beam profile. The first order backscattered intensity along the CLOS is the same for both beams. The second and higher order backscattered intensities are due to intensity from outside the CLOS entering the CLOS to be scattered back along the CLOS. Since these entering intensities fall off as $\exp(-\alpha\ell)$, the immediate region to the CLOS is most important in contributing to the backscattered intensity. For the uniform beam, this region changes less in intensity for low order scattering, and more for high order scattering than it does for the gaussian beam. Thus, since the backscattered intensity is largely determined by low orders of scattering, the uniform beam should have more backscattered intensity than does the gaussian beam.

The scattering of intensity out of the uniform beam is demonstrated in the contrast of the uniform beam forward intensity. The contrast for the three wavelengths, calculated using Equation (10.11), is shown in Figures (11.6) - (11.8), respectively. Since the contrast is symmetric about the CLOS, only one-half of the beam contrast is shown. Figure (11.6), the contrast of the uniform beam at 1.06μm clearly shows the decrease of the contrast of the beam, the increase of the contrast of the background, and the deformation of the

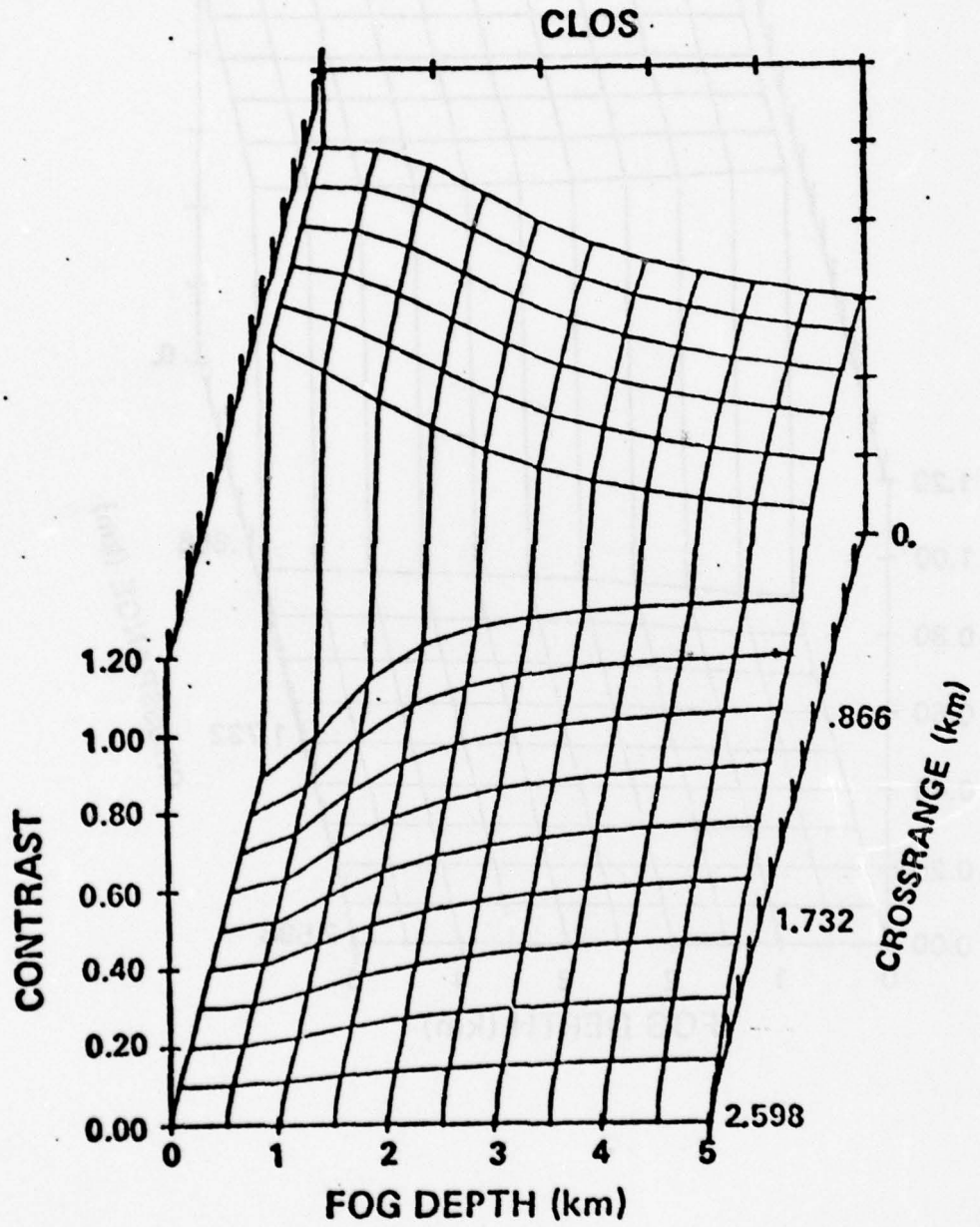

Figure (11.6) Uniform Beam Contrast Profile at 1.06μm.

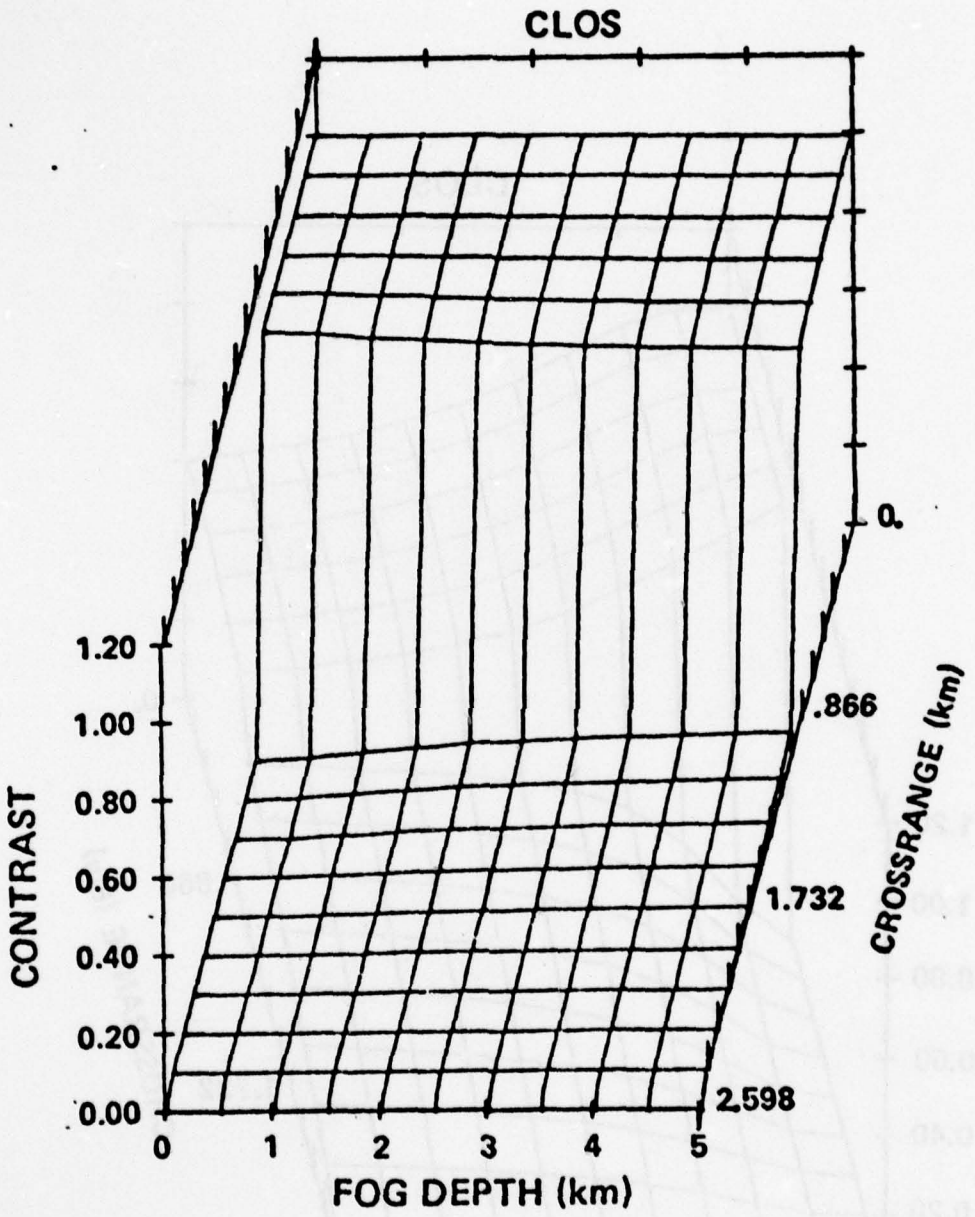

Figure (11.7) Uniform Beam Contrast Profile at 3.0μm.

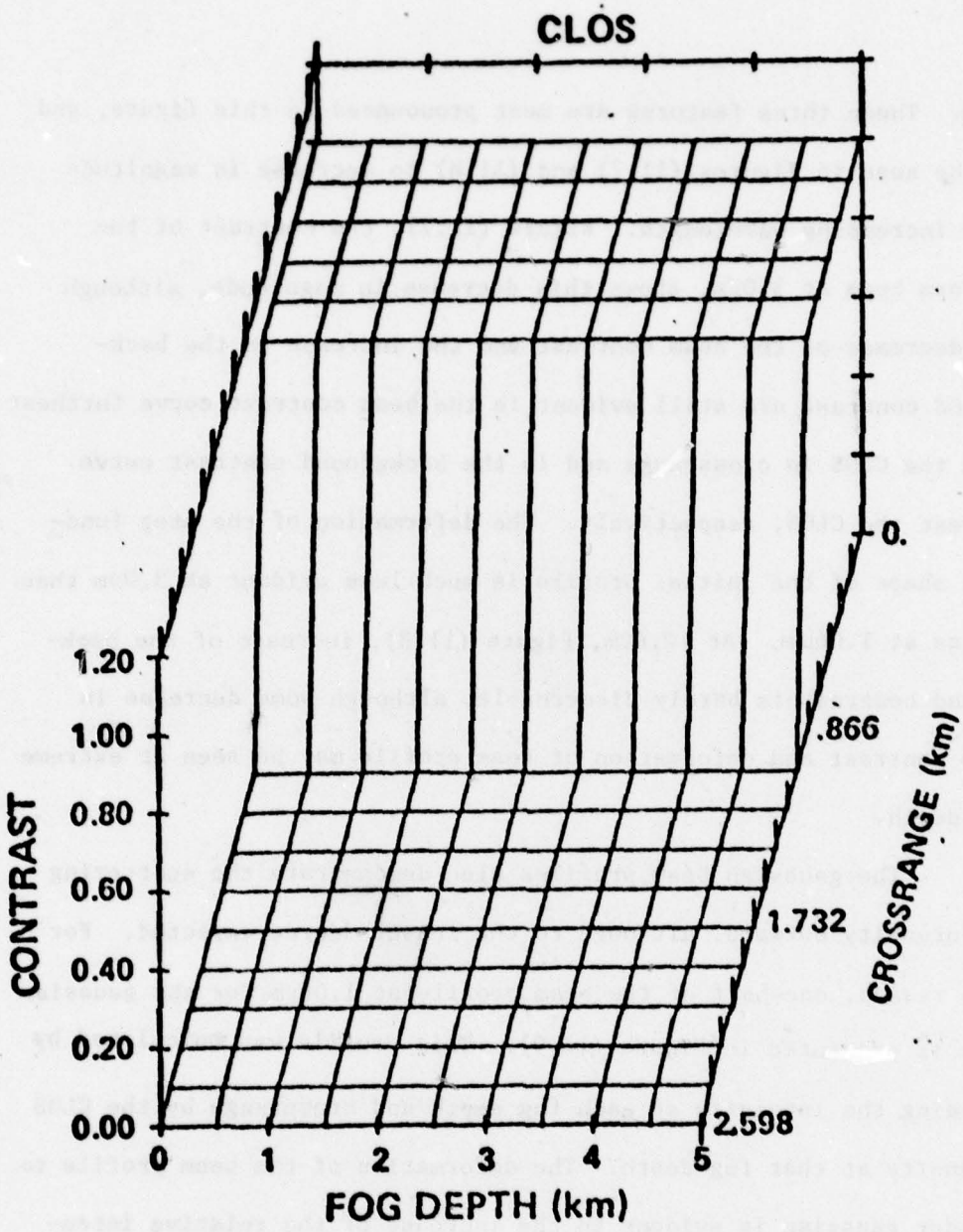

Figure (11.8). Uniform Beam Contract Profile at 10.6μm.

beam. These three features are most pronounced in this figure, and may be seen in Figures (11.7) and (11.8) to decrease in magnitude with increasing wavelength. Figure (11.7), the contrast of the uniform beam at 3.0μm, shows this decrease in magnitude, although the decrease of the beam contrast and the increase in the background contrast are still evident in the beam contrast curve furthest from the CLOS in crossrange and in the background contrast curve nearest the CLOS, respectively. The deformation of the step function shape of the initial profile is much less evident at 3.0μm than it was at 1.06μm. At 10.6μm, Figure (11.8), increase of the background contrast is barely discernable, although some decrease in beam contrast and deformation of beam profile may be seen at extreme fog depth.

The gaussian beam profiles also demonstrate the scattering of intensity outward, although to the lesser degree expected. For this reason, one-half of the beam profile at 1.06μm for the gaussian beam is presented in Figure (11.9). This profile was calculated by dividing the intensity at each fog depth and crossrange by the CLOS intensity at that fog depth. The deformation of the beam profile to a wider gaussian is evident in the increase of the relative intensity curves away from the CLOS with increasing fog depth. The deformation may be seen to be much less for this gaussian beam than in the comparable uniform beam, Figure (11.6). The beam profiles at 3.0μm and 10.6μm are not shown since they differ only qualitatively from Figure (11.9). Figure (11.10) shows the increase of

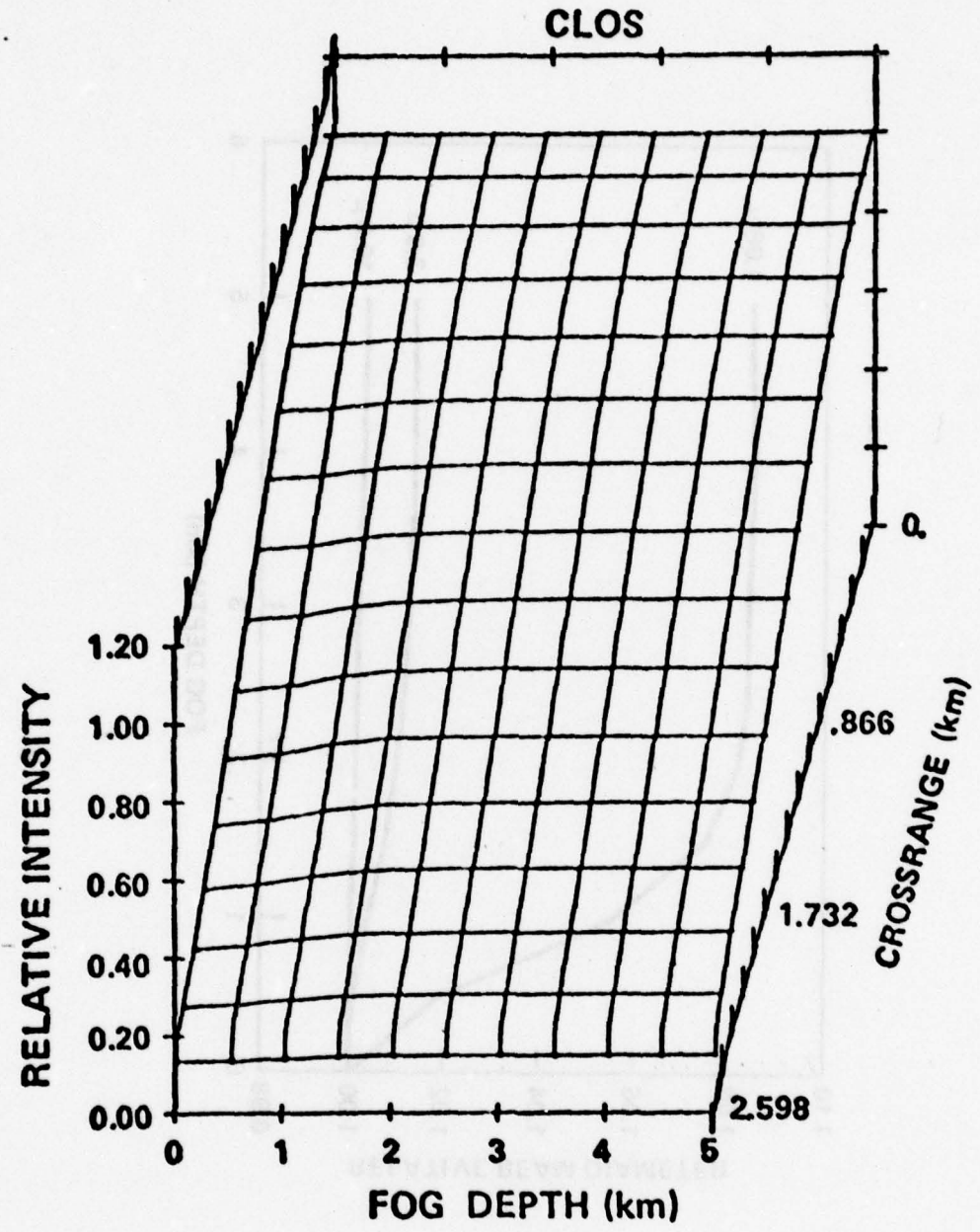

Figure (11.9) Gaussian Beam Profile at 1.06μm.

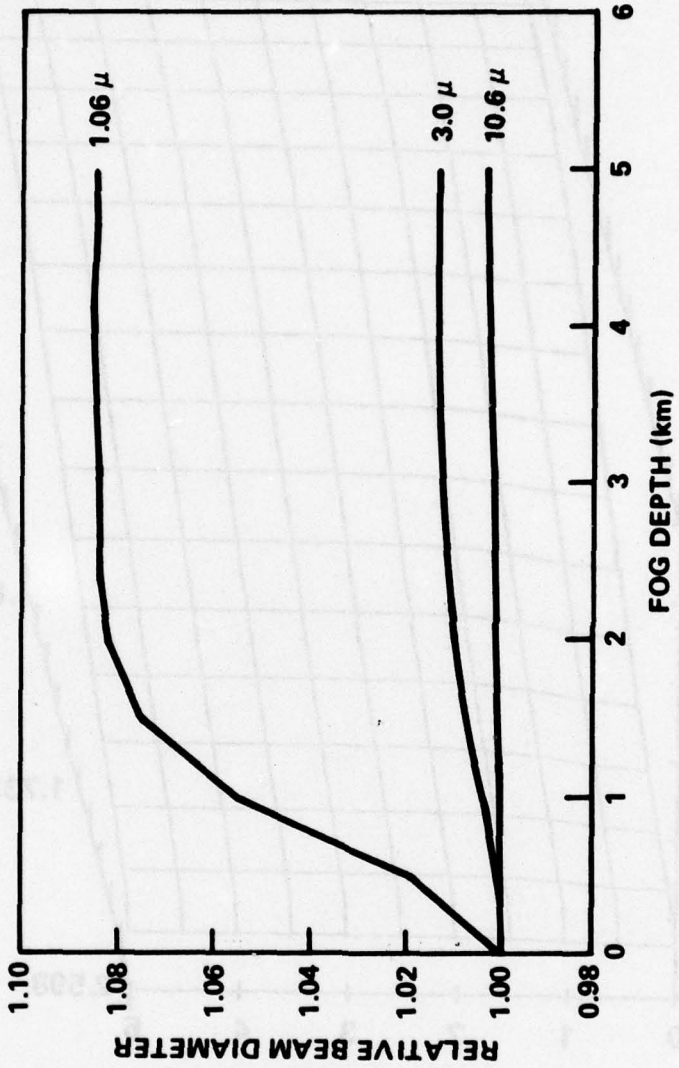

FIGURE (11.10): Gaussian Beam Spread

the beam diameter with fog depth at the three wavelengths. The relative effects of albedo value may be clearly seen.

CHAPTER XII

SUMMARY

This dissertation has described the results of an investigation of radiation transfer through aerosols. The first part of this investigation was concerned with single particle scattering. The scattering of light by a single spherical particle, the Mie solution, was reviewed by developing the Hertz vector solution for the Maxwell Equations in Chapter II and reproducing the Mie solution using the Hertz vectors in Chapter III. The extension of the Mie solution to describe the single scattering of light by a collection of independent particles, the usual case with aerosols, was reviewed as developed by Deirmendjian in a format compatible with performing radiative transfer (RT) calculations (Deirmendjian, 1964). This description of aerosol single scattering was given in Chapter IV.

The Mie solution is valid only for spherical dielectric particles so that it may treat most liquid aerosols and those solid aerosols that are spherical. Large liquid aerosol particles that have been deformed by gravity and aerodynamic drag, and most solid (irregular) aerosol particles cannot be treated. While dielectric particles of regular geometric shape may be treated by solving the Mie problem in other coordinate systems, no generally accepted solution for irregular particles is available. Much effort has been directed towards this problem, however, and several solutions have been developed to treat various aspects of the irregular particle problem. Several of these efforts were reviewed in Chapter V.

The central theme of the irregular particle scattering problem is the Rayleigh Hypothesis which limits the degree of irregularity of the particle if the scattered fields encorporate only outgoing spherical waves. Thus solutions that assume the Rayleigh Hypothesis are not valid for particles that are sufficiently irregular for light to be scattered from one part of the particle to another and then out. All of the solutions described in Chapter V assume the Rayleigh Hypothesis.

The previous efforts described in Chapter V satisfy the boundary conditions of electrodynamics approximately. The implication of these approximations is unclear. Recently, an integral equation solution has been advanced that accounts for the boundary conditions correctly and solves the vector Helmholtz equation rather than the scalar (Waterman, 1971). Unfortunately, only conducting particles have been treated numerically with this method although it is valid for dielectric particles.

Additionally, Chapter V reviews the Mie solution modification proposed by Chylek et al. (Chylek, Grams and Pinnick, 1976). This modification is based on the observation that glories are not commonly observed in the experimentally measured phase functions of polydisperse irregular particles. The mathematical source of glories in the Mie solution is the resonances in the scattered field expansion coefficients. Chylek et al. propose that these resonances be truncated to model the effects of particle irregularity on scattering. While the validity of this modification has been

questioned, Chylek et al. have demonstrated better agreement with experimental data for their calculated phase functions that for Mie phase functions.

Recognizing the limitations of previous efforts to treat the problem of irregular particle scattering, the Mie theory was extended to cylindrically symmetric irregular dielectric particles. This extension is presented in Chapter VI. The limitation of this extension to cylindrically symmetric particles was not prompted by an deficiency in the basic theory, but rather by the constraints of available computer memory. The only theoretical limitation on this solution is, in common with all other solutions described in this dissertation, the assumption of the Rayleigh Hypothesis, which permits only a small degree of particle irregularity.

A computer code was generated to calculate the scattering properties of these particles. This code is listed in Appendix (I). Analytic and numerical calculations were performed to demonstrate that the theory and code would reproduce the Mie solution when spherical particles were treated. These calculations are described in Appendix (III) and Chapter VII, respectively. The Mie solution has also been extended to nonspherical particles of regular geometric shape. Notable among these efforts is the solution for prolate and oblate ellipsoids (Asano and Yamamoto, 1975). Approximate calculations using the solution of Chapter VI were performed for prolate ellipsoids and compared with the exact calculations. Despite the Rayleigh Hypothesis,

the agreement evidenced by this comparison was quite good. In view of this agreement, the applicability of the code to large irregular particles is demonstrated. These calculations are described in Chapter VII.

This code was then used to investigate the scattering properties of single irregular particles, and to address the validity of the Mie solution modification of Chylek et al. Calculations were performed to determine the effect of particle irregularity on the resonant behavior of the scattered field expansion coefficients. While it was found that the resonances narrowed, the numerical method of Chylek et al. was not substantiated. This finding did not explain the agreement of the Chylek et al. calculations with the data, so the code was modified to treat polydisperse aerosols using the techniques described in Chapter IV. Calculations were then performed to generate polydisperse phase functions for nine shapes of particle using the particle size distribution and refractive index reported by Chylek et al. for one set of their data. These nine phase functions were then combined linearly in various combinations using regression techniques to fit the data. It was found that several combinations of calculated phase functions would fit the data as well as the calculations of Chylek et al., and that the choice of phase functions used in fitting the data was not especially crucial. The insensitivity of the data to particle shape indicates that calculations utilizing their modification may be adequate for most RT calculations. Chapter VIII is devoted to a description of these calculations.

The RT theory uses certain single scattering quantities, the extinction coefficient, the albedo of single scattering, and the phase functions, along with the appropriate boundary conditions to permit solution of the problem of describing the multiple scattering effects of aerosols. This theory, mainly developed by Chandrasekhar, had been primarily used to treat the problems associated with stellar and planetary atmospheres where the symmetry and time-independence of the boundary conditions and the extinguishing medium allow the general four-dimensional (3 space plus time) RT equation to be reduced to a one-dimensional RT equation (Chandrasekhar, 1960). This theory and the development of the one-dimensional equation are reviewed in Chapter IX.

The RT theory has most commonly been applied to practical problems such as the calculation of the brightness of a star or the amount of light that reaches the surface of a planet. A new set of practical problems, that of describing the propagation of low energy laser beams and images through the atmosphere with and without aerosol aerosols, has developed in recent years that cannot be treated by one-dimensional RT theory. These problems are characterized by non-uniform boundary conditions and/or asymmetric extinguishing media. Previous efforts to treat these problems have included Monte Carlo trajectory tracing codes that are exceedingly time consuming, small angle approximation developments of the four-dimensional RT equation that are valid for aerosols only in the visible and near-ir regions of the spectrum, and are not valid at all for atmospheres, and

general angle analyses that are limited to few orders of scattering. No general analytic or numerical solution of the four-dimensional RT equation has yet been developed.

In Chapter X, a numerical algorithm for the solution of the two-dimensional RT equation with nonuniform boundary conditions and asymmetric medium is developed. This algorithm is suitable for treating steady state laser beam and image propagation problems. The extinguishing medium used in this algorithm may incorporate both aerosol and atmospheric effects and the solution may be obtained to an arbitrary order of scattering. Thus, two limitations of previous efforts, the small angle approximation and the restriction to few orders of scattering, are removed.

A code was generated implementing this algorithm. A listing of the code is presented in Appendix (IV). While this code requires a large amount of computer memory to execute, it is rapidly executable. This speed advantage was demonstrated when the code was validated by comparison with a Monte Carlo trajectory tracing code that was much smaller in size but required much more execution time. The accuracy evidenced in the comparison of the results of the two codes and the speed of execution of the two-dimensional code demonstrate the utility of the code for steady state problems.

The two-dimensional code was then used to calculate the effects of aerosol multiple scattering on transmission, backscatter, and contrast transmission through an aerosol medium. Calculations were performed for a liquid (spherical) aerosol, a Deirmendjian C.3 fog

of uniform concentration. Two beams, one of uniform profile and the other of gaussian profile, were considered at wavelengths in the near, mid, and far-ir. These calculations are presented in Chapter XI.

In summary, two parts of the problem of radiation transfer through aerosols have been addressed in this dissertation investigation. The first part, that of single scattering by a single article, resulted in an extension of Mie theory to nonspherical particles. This extension is limited only by the ubiquitous Rayleigh Hypothesis and the current state-of-the-art in available computer memory. The code implementing this extension offers the capability to treat those solid, irregular aerosol particles that could not be treated by the Mie solution.

While the second part of the radiation transfer problem, that of single scattering by a collection of particles, was not addressed because most aerosols are comprised of independent particles and the basic work of Deirmendjian is valid, the third part of the problem, that of multiple scattering, was addressed. A numerical solution algorithm for the two-dimensional RT equation was developed and a computer code implementing it produced. This code is useful for treating steady state problems of low energy laser beam and image propagation through aerosol laden atmospheres.

This dissertation has suggested some interesting problems for future effort. One problem would be the comparison of the multiple scattering effects of liquid (spherical) and solid (nonspherical) aerosols. An example of this problem is the difference in

propagation through fog as compared to dust. This comparison could be addressed by using the single scattering quantities calculated with the nonspherical scattering code in solving the two-dimensional RT equation.

This second problem is an extension of the two-dimensional RT solution algorithm to four dimensions. The two-dimensional algorithm developed during the dissertation investigation is limited because it cannot treat time dependent problems such as calculating the stretching effect of multiple scattering on laser pulse propagation, nor problems in which the third spatial dimension is asymmetric. While the two-dimensional algorithm is adequate for some modern theories of detection and recognition, the four-dimensional RT equation solution is needed to consider problems with two-dimensional images and vertically varying media such as smoke and dust clouds. The extension of the two-dimensional algorithm may be effected by returning to the four-dimensional RT equations developed in Chapter IX. A numerical solution algorithm may then be developed for these equations by using the quadrature approximation and evaluating the path integrals numerically rather than analytically as is done in the two-dimensional algorithm.

LIST OF REFERENCES

Abramowitz, M., and I. A. Stegun, Handbook of Mathematical Functions, National Bureau of Standards, Washington, D.C., November 1964.

Asano, S., and G. Yamamoto, Appl. Opt., 14 29 (1975).

Bird, R. E., "Calculations of Multiple-Scattering Effects on Active Optical Sensors in Cloud Environments," Naval Weapons Center NWC-TP-5667, China Lake, CA, May 1974.

Blattner, W., "Utilization Instructions for Operation of the Mie Programs on the CDC-6600 at AFCRL," Radiation Research Associates Research Note RRA-N7240, contract F19628-70-c-0156, Radiation Research Associates, Inc., 1972.

Born, M., and E. Wolf, Principles of Optics, Pergamon Press, Oxford, 1975.

Cadel, R. D., Particle Size, Reinhold Publighing Corp., New York, 1965.

Carnahan, B., H. A. Luther, and J. C. Wilkes, Applied Numerical Methods, John Wiley and Sons, Inc., New York, 1969.

Centeno, M., J. Opt. Soc. Am., 31 244 (1944).

Chandrasekhar, S., Radiative Transfer, Dover Publications, Inc., New York, 1960.

Chylek, P., G. W. Grams, and R. G. Pinnick, Science, 193 480 (1976).

Corn, M., "Aerosols and the Primary Air Pollutants, Nonviable Particles, Their Occurrence, Properties and Effects" in A. C. Stern (ed.), Air Pollution, Vol. I, "Air Pollutants, Their Transformation and Transport," Academic Press, New York, 1976.

Curcio, J. A., and C. C. Petty, J. Opt Soc. Am., 44 302 (1951).

Davies, J. B., IEEE Trans. on Microwave Theory and Techniques MTT-21, 99 (1973).

Debye, P., Ann. Physik., 30 59 (1909).

Deepak, A., and A. E. S. Green, Appl. Opt., 9 2362 (1975).

Deirmendjian, D., Electromagnetic Scattering on Spherical Polydispersions, American Elsevier, New York, 1964.

Deirmendjian, D., "Far Infrared and Submillimeter Wave Attenuation by Clouds and Rain," Rand Report P-5419, The Rand Corporation, April 1975.

Draper, N. R., and H. Smith, Applied Regression Analysis, John Wiley and Sons, Inc., New York, 1967.

Eyres, L., and A. Nelson, Annals of Physics, 100 37 (1976).

Foldy, L. L., Phys. Rev., 67 107 (1945).

Friedlander, S. K., Smoke, Dust and Haze: Fundamentals of Aerosol Behavior, John Wiley and Sons, Inc., New York, 1977.

Fuchs, N. A., and A. G. Sutugin, Highly Dispersed Aerosols, Ann Arbor Science Publishers, Ann Arbor, Michigan, 1970.

Gans, R., Ann. Physik., 76 29 (1925).

Green, H. L., and W. R. Lane, Particulate Clouds: Dust, Smoke and Mists, E. and F. N. Spon, Ltd., London, 1964.

Holland, A. C., and G. Gagne, Appl. Opt., 9 1113 (1970).

House, L. L., and L. W. Avery, J. Quant. Spectrosc. Radiat. Transfer, 9 1579 (1969).

Jackson, J. D., Classical Electrodynamics, John Wiley and Sons, Inc., New York, 1962.

Junge, C. E., Air Chemistry and Radioactivity, Academic Press, New York, 1963.

Kattawar, G. W., and G. N. Plass, Appl. Opt., 15 3166 (1976).

Kerker, M., private communication, December 1977.

Mason, B. J., The Physics of Clouds, Clarendon Press, Oxford, 1971.

Mie, G., Ann. Physik., 25 377 (1908).

Millar, R. F., Radio Science, 8 785 (1973).

Miller, J. C. P., British Association for the Advancement of Science Bessel Functions, Part I Functions of order zero and unity, Mathematical Tables, Vol. X, Cambridge University Press, Cambridge, England, 1952.

Pinnick, R. G., D. E. Carroll, and D. J. Hoffman, Appl. Opt., 15 384 (1976).

Pomraning, G. C., The Equations of Radiation Hydrodynamics, Pergamon Press, Oxford, 1973.

Pontier, L., and C. Dechambenoy, Ann. Geophys., 22 633 (1966).

Lord Rayleigh, Phil. Mag., 41 274 (1871).

Lord Rayleigh, Phil. Mag., 12 81 (1881).

Reilley, Jr., E. D., J. Comp. Phys., 11 463 (1973).

Sedunov, Yu. S., Physics of Drop Formation in the Atmosphere, John Wiley and Sons, Inc., New York, 1974.

Selby, J. E. A., and R. A. McClatchey, "Atmospheric Transmittance from .025 to 28.5 μm: Computer Code LOWTRAN 3," Air Force Cambridge Research Laboratory, AFCRL-TR-75-0225, Bedford, Mass., April 1976.

Sellers, W. R., and B. G. Gibbs, "Descriptions-General Purpose Computer Subroutine," U. S. Army Missile Command Report No. TR-WS-75-2, January 1977.

Shifrin, K. S., Scattering of Light in a Turbid Medium, NASA TT F-477, Washington, D. C., 1968.

Tyras, G., Radiation and Propagation of Electromagnetic Waves, Academic Press, New York, 1969.

Uzonoglu, N. K., and A. R. Holt, J. Phys. A., 10 413 (1973).

Van de Hulst, H. C., Light Scattering by Small Particles, John Wiley and Sons, Inc., New York, 1957.

Voloshchuk, V. M., and Yu. S. Sedunov, Hydrodynamics and Thermodynamics of Aerosols, John Wiley and Sons, Inc., New York, 1973.

Waterman, P. C., Phys. Rev., D3 825 (1971).

Weinman, J. A., and S. Shipley, J. Geophys. Res., 77 7123 (1972).

Yeh, C., Phys. Rev., 135 A1193 (1964).

APPENDIX I

NONSPHERICAL PARTICLE SCATTERING CODE

The computer code described in this appendix was generated to implement the formalism developed in Chapter VI. Calculations performed using this code are presented in Chapters VII and VIII.

The integrals $A_{\ell\ell',,_n}$, Eqs. (6.43) - (6.57) are performed with a Gauss-Legendre Quadrature, (Carnahan, Luther, and Wilkes, 1969). Equation (6.62) is solved for the a_ℓ, b_ℓ, c_ℓ, and d_ℓ with a Gauss-Jordan elimination routine modified to treat complex entries (Sellers and Gibbs, 1977). The radial functions $\psi_\ell(x)$ and $\rho_\ell^1(x)$, Eqs. (2.45) and (2.47), and their derivatives are calculated with a special routine implementing the method of Miller (Miller, 1950). This method is described in Appendix (II). The cross sections and phase functions are calculated in the same manner as the Mie solution (Deirmendjian, 1964; Van de Hulst, 1957).

The formalism developed in Chapter VI is, of course, also valid for particles not cylindrically symmetric with respect to the incident plane wave. At this time, however, an extension of the formalism and computer code to consider more general geometries is not feasible due to computer limitations. If a general particle and/or incident direction were to be considered, Eqs. (3.3) - (3.8) would include terms $\cos(m\phi)$, $\sin(m\phi)$, and $P_\ell^m(\cos\theta)$, $m = 0$ to L. The size of the array B, Eq. (6.63), would increase by terms m and m'. Arrays G and F, Eqs. (6.64) and (6.65), would increase in size from 4L to $4L^2$. Thus the total storage required would increase from $16L^2 + 8L$ to $16L^4 + 8L^2$. For large value

of L, this is an approximate increase by a factor of L^2. The increase in computer memory required for operational code (as compared to array storage) should be approximately proportional. The present code requires 2×8^5 words to initiate compilation, so that $L^2 \sim 8^4$ words and a general code would require approximately 2×8^9 words to initiate compilation. Computer memory of this extent is available only on a very few machines so that the implementation is not feasible at this time.

It should be noted that while the code requires a large amount of computer memory for initial compilation (2×8^5 words), this does not restrict the utility of the code as much as might be expected. This code is normally executed on the MICOM CDC 6600 computer using the SCOPE 3.4.2 compiler. This is a two pass compiler that performs some optimization of the compiled code. In this case, the optimization is significant as the computer memory required for the compiled code is only 6.5×8^4 words. Additionally, execution of the compiled code is accomplished in about 15 seconds for a nominal particle with 19 expansion coefficients in each Debye potential, and Mie parameter (x_o) of nine. Compilation of the code requires about 60 seconds. Thus, the compiled code may be used to perform calculations with only moderate demands on computer memory and execution time.

This code consists of one driver routine and five subroutines. These routines are listed in Tables (I.1) - (I.6). The operation of each routine is described below.

NONSPH (Table (I.1))

This is the main driver routine. It accesses the five subroutines to perform the calculation of the nonspherical particle scattering. The version of the code shown here is the polydisperse aerosol code with provision for a log normal particle size distribution. The routine calls START to input the necessary parameters and load the arrays with the points and weights for the Gauss-Legendre quadrature. The value of the radius and its derivative at these points are calculated. The increments to the $A_{\ell\ell',,_n}$ integrals are calculated and the routine calls ADO to store these increments in the appropriate places in the B and F arrays. Once the B and F arrays have been calculated, CGAUSS is called to solve for the a_ℓ, b_ℓ, c_ℓ, and d_ℓ. Routine AP2 is then called to calculate the cross sections and phase functions from the c_ℓ and d_ℓ.

START (Table (I.2))

This subroutine performs two functions. It first loads the values of the weights and points for the Gauss-Legendre quadrature, and then inputs the necessary parameters for the calculation. These parameters include the refractive index, the wavelength of light, the minimum and maximum particle radii, the average particle radius and standard deviation for the log normal particle size distribution, and the number of terms in the particle radius expansion, the number of expansion terms in the Debye potentials, and the number of particle radii to be calculated. The routine also calculates the increment of particle radius.

AP2 (Table (I.3))

Subroutine AP2 performs the calculation of the cross sections and phase functions for both the individual particles and for the polydisperse aerosol. Additionally, it calculates the fraction of particles in each radius using a log-normal particle size distribution.

ADO (Table (I.4))

This routine receives the increments of the $A_{\ell\ell',,_n}$ integrals to form the B and F matrices. This routine is called once for each angle in the quadrature for each ℓ and ℓ' pair.

CGAUSS (Table (I.5))

Subroutine CGAUSS is modified version of a library Gauss-Jordan elimination routine (Sellers and Gibbs, 1977). The only modifications performed to it were to permit consideration of complex rather than only real numbers.

BESSL (Table (I.6))

This subroutine implements the method of Miller described in Appendix (II) to calculate the radial functions $\psi_\ell(x)$ and $\psi_\ell(mx)$. The radial function $\rho_\ell^1(x)$ and the derivatives of the radial functions $\psi_\ell(x)$, $\psi_\ell(mx)$, and $\rho_\ell^1(x)$ are calculated using the method described in Appendix (II). This routine has an upper limit on x due to the use of the backwards recursion method of Miller (Miller, 1950). Should larger values of x be required, another version of BESSL impelmenting both Miller's method and the standard forward recursion method is

available. This additional capability is not generally required because values of x that result in divergence were not needed in this investigation.

TABLE (I.1). LISTING OF ROUTINE NONSPH

```
      PROGRAM NONSPH(INPUT,OUTPUT,TAPE5=INPUT,TAPE6=OUTPUT)
      COMMON/ONE/X(20),W(20),AM,ALAM,NM,NN,AN(15)
      COMMON/TWO/A(80,81),CI(15),AI
      DIMENSION RK(20),RM(20)
 5    COMMON/THREE/AM(20),AJ(20),BM(20),DAJ(20),DAM(20),DBM(20)
      COMPLEX AJ,AM,BM,DAJ,DAM,DBM
      COMMON/FOUR/NT,NP,RMIN,DR,SD,SR,AXX(15),NXX
      COMPLEX A
      COMPLEX CI
10    COMPLEX AM,RKM
      COMPLEX AI,ALP
      DATA PI/3.1415927/
C     ***************************************************************
C     NON-SPHERICAL PARTICLE MIE SCATTERING
15    C     ASCO PROGRAM
C     CODED BY B. W. FOWLER
C     VERSION OF 1 AUGUST 1977
C     METHOD OS SOLUTION IS BOUNDARY VALUE OF TANGENTIAL E AND H FIELDS
C     USING COEFFICIENT OF EQUATION SOLUTION
20    C     REFERENCE IS BORN AND WOLF
C     PROJECTION USING LEGENDRE PLOYNOMIALS OF FIRST ASSOCIATED TYPE
C     CODE LIMITED TO PARTICLES WITH CYLINDRICAL SYMMETRY
C     RADIUS SURFACE EXPANDED IN ZEROTH LEGENDRE PLOYNOMIALS
C     EXTERIOR REGION ASSUMED VACUUM
25    C     ***************************************************************
C     X = POINTS IN GAUSS-LEGENDRE QUADRATURE
C     W = WEIGHTS IN GAUSS-LEGENDRE QUADRATURE
C     RK = RADIUS AT X(I)
C     A IS MATRIX OF COEFFICIENT INTEGRALS
30    C     CI IS CURRENT CONTRIBUTION TO L,N INTEGRAL I
C     NM = NUMBER OF LEGENDRE COMPONENTS IN RADIUS
C     ALAM IS WAVELENGTH IN MICRONS
C     ***************************************************************
C     SUBROUTINE TO LOAD VARIOUS PARAMETERS
35    CALL START
C     CALCULATION OF K VALUE (WAVENUMBER)
      AK=2.*PI/ALAM
C     AI IS SQUARE ROOT OF -1
      AI=CMPLX(0.,1.)
40    WRITE(6,91)AM,AI,AK
C     CODE TO CALCULATE THE VALUES OF THE RADIUS AT EACH G-L INTEGRATION
      DO 98 N=1,NT
      AN(1)=RMIN+FLOAT(N-1)*DR
      IF(NXX.LT.2)GOTO 42
45    DO 41 II=2,NXX
   41 AN(II)=AN(1)*AXX(II)
   42 CONTINUE
      NM=NXX
      NP=N
50    DO 1 I=1,20
C     P VARIABLES ARE ZEROTH LEGENDRES
      P0=1.
      P1=X(I)
C     T VARIABLES ARE DERIVATIVES OF ZEROTH LEGENDRES = VAN DE HULST'S P
55    T0=0.
      T1=X(I)
C     PP VARIABLES ARE VAN DE HULST'S PI FNCS
```

TABLE (I.1). CONTINUED

```
                PP0=0.
                PP1=1.
60              RK(I)=AN(1)*P0+AN(2)*P1
                RH(I)=AN(2)*T1
                DO 2 J=3,NM
                AJJ=FLOAT(J)
                P2=((2.*AJJ-1.)*X(I)*P1-AJJ*P0)/(AJJ-1.)
65              P0=P1
                P1=P2
                PP=((2.*AJJ-1.)*X(I)*PP1-AJJ*PP0)/(AJJ-1.)
                TT=X(I)*(PP-PP0)-(2.*AJJ-1.)*(1.-X(I)*X(I))*PP1+T0
                PP0=PP1
70              PP1=PP
                T0=T1
                T1=TT
                RK(I)=RK(I)+AN(J)*P2
                RH(I)=RH(I)+AN(J)*TT
75            2 CONTINUE
                RK(I)=RK(I)*AK
              1 CONTINUE
             91 FORMAT(5X,2E20.8)
          C     ZERO OUT INTEGRAL ARRAY
80              NNN=4*NN
                NNNP=NNN+1
                DO 3 L1=1,NNN
                DO 3 N1=1,NNNP
              3 A(L1,N1)=CMPLX(0.,0.)
85        C     CALL EQUATION ROUTINE
          C     MUST EITHER BE COMPLEX OR DO IN TWO STAGES
                DO 4 I=1,20
          C     INTEGRATION LOOP - REFERS TO 10 PT G-L QUADRATURE
                RK4=RK(I)*AM
90        C     AM IS REFRACTIVE INDEX
          C        ROUTINE TO CALCULATE BESSEL FUNCTIONS J SUB L1 OF KX AND KMX AN
          C        H SUB L1 OF KR AND THEIR DERIVATIVES
                CALL BESSL(RK(I),RKM)
          C     J SUB N OF KMR - NOT PSI FNC OF MIE SCATTERING SOLUTION
95        C     SET UP OF VDH PI FNC
                P0=0.
                P1=1.
                P2=3.*X(I)
          C     VDH TAU FNC SET UP
100             T0=0.
                T1=X(I)
                T2=3.*(2.*X(I)*X(I)-1.)
          C     P SUB L SUPER 1 SET UP
                PL1=SQRT(1.-X(I)*X(I))
105             PL2=3.*X(I)*PL1
          C     NN IS NUMBER OF TERMS IN FIELD EXPANSION
                DO 5 L1=1,NN
                AL=FLOAT(L1)
                ALL=AL*(AL+1.)
110             ALP=AL**(L1-1)*(2.*AL+1.)/AL/(AL+1.)
                L2=NN+L1
                L3=2*NN+L1
                L4=3*NN+L1
                IF(L1.GT.1)GOTO 51
```

TABLE (I.1). CONTINUED

```
                  P=P1
                  T=T1
                  PL=PL1
                  GOTO 59
               51 IF(L1.GT.2)GOTO 52
                  P=P2
                  T=T2
                  PL=PL2
                  GOTO 59
               52 P=(2.+1./(AL-1.))*X(I)*P2-P1*(1.+1./(AL-1.))
                  T=X(I)*(P-P1)-(2.*AL-1.)*(1.-X(I)**(I))*P2+T1
                  P1=P2
                  P2=P
                  T1=T2
                  T2=T
                  PL=(2.+1./(AL-1.))*X(I)*PL2-PL1*(1.+1./(AL-1.))
                  PL1=PL2
                  PL2=PL
               59 CONTINUE
            C        ZEROTH LEGENDRE PROJECTORS
            C     PLL1=X(I)
            C     PLL2=(3.*X(I)*X(I)-1.)/2.
            C        PI FUNCTION PROJECTORS
            C     PLL1=1.
            C     PLL2=3.*X(I)
            C        FIRST LEGENDRE POLYNOMIALS
                  PLL1=SQRT(1.-X(I)*X(I))
                  PLL2=3.*X(I)*PLL1
                  DO 5 N1=1,NN
                  ANN=FLOAT(N1)
                  N2=NN+N1
                  N3=2*NN+N1
                  N4=3*NN+N1
                  IF(N1.GT.1)GOTO 61
                  PLL=PLL1
                  GOTO 62
               61 IF(N1.GT.2)GOTO 63
                  PLL=PLL2
                  GOTO 62
            C  63 PLL=((2.*ANN-1.)*X(I)*PLL2-(ANN-1.)*PLL1)/ANN
            C        FIRST LEGENDRES
            C  63 PLL=((2.*ANN-1.)*X(I)*PLL2-ANN*PLL1)/(ANN-1.)
               63 PLL=(2.+1./(ANN-1.))*X(I)*PLL2-PLL1*(1.+1./(ANN-1.))
                  PLL1=PLL2
                  PLL2=PLL
            C     CI ARE ALPHA SUB L,N+1 INTEGRALS
               62 CI(1)=ALP*ALL*AM(L1)/RK(I)/RK(I)*PL*PLL*W(I)*AK*RM(I)
                  CI(2)=ALP*AM(L1)*P*PLL*W(I)
                  CI(3)=ALP*(AM(L1)/RK(I)+DAM(L1))*T*PLL*W(I)
                  CI(4)=ALP*AM(L1)*T*PLL*W(I)
                  CI(5)=ALP*(AM(L1)/RK(I)+DAM(L1))*P*PLL*W(I)
                  CI(6)=AJ(L1)/RKM*ALL*RM(I)*PL*PLL*W(I)/RK(I)*AK
                  CI(7)=AJ(L1)*P*PLL*W(I)
                  CI(8)=(AJ(L1)/RKM+DAJ(L1))*T*PLL*W(I)
                  CI(9)=AJ(L1)*T*PLL*W(I)
                  CI(10)=(AJ(L1)/RKM+DAJ(L1))*P*PLL*W(I)
                  CI(11)=RM(L1)/RK(I)/RK(I)*AK*ALL*RM(I)*PL*PLL*W(I)
```

TABLE (I.1). CONTINUED

```
                  CI(12)=HM(L1)*P*PLL*W(I)
                  CI(13)=(HM(L1)/RK(I)+DHM(L1))*T*PLL*W(I)
                  CI(14)=HM(L1)*T*PLL*W(I)
175               CI(15)=(HM(L1)/RK(I)+DHM(L1))*P*PLL*W(I)
                  CALL ADD(L1,L2,L3,L4,N1,N2,N3,N4)
            C     WRITE(6,93)L1,N1,ALP,AJ,AM,HM,DAJ,DAM,DHM,X(I),P,T,PLL,PL
           93 FORMAT(5X,2I10,2(5X,2E20.8)/3(5X,2E20.8)/,2(5X,2E20.8),
             15X,5E20.8)
180           5 CONTINUE
              4 CONTINUE
            C     CALL AP1
                  CALL CGAUSS(NNN,1.0,NNN,0,IR,E,A)
                  WRITE(6,90)F
185           90 FORMAT(/5X,F20.8)
                  CALL AP2
              98 CONTINUE
              99 STOP
                  END
```

TABLE (I.2). LISTING OF ROUTINE START

```
      SUBROUTINE START
      COMMON/ONE/X(20),W(20),AM,ALAM,NM,NN,AN(15)
      COMMON/THREE/AM(20),AJ(20),BM(20),DAJ(20),DAM(20),DBM(20)
      COMPLEX AJ,AM,BM,DAJ,DAM,DBM
      COMMON/FOUR/NT,NP,RMIN,DR,SD,SR,ANX(15),NXX
      COMPLEX AM
      NAMELIST/INTO/AM,ALAM,RMIN,RMAX,SD,SR,NN,NT,NXX,ANX
C     ******************************************************************
C     SUBROUTINE START
C     SUBROUTINE TO SET UP NECESSARY PARAMETERS FOR MAIN PROGRAM
C     ******************************************************************
C     X IS ARRAY OF GAUSS-LEGENDRE COSINE THETA VALUES
C     W IS ARRAY OF CORRESPONDING WEIGHTS
C     20 POINT G-L QUADRATURE
C     EXPECTED UPPER LIMIT THEREFORE ORDER IS
C     AM IS COMPLEX INDEX OF REFRACTION OF PARTICLE
C     AN IS ARRAY OF SURFACE COEFFICIENTS
C     MUST BE IN FORM OF ZEROTH LEGENDRE POLYS
C     ALAM IS WAVELENGTH IN UNITS OF MICRONS
C     NM IS NUMBER OF TERMS IN SURFACE EXPANSION
C     NN IS NUMBER OF TERMS TO BE CONSIDERED IN EXPANSION
C     ******************************************************************
      DATA(X(I),I=1,10)/.0765265211,.2277858511,.3737060887,.5108670019,
     1.6360536807,.7463319064,.8391169718,.9122344282,.9639719272,
     2.9931285991/
      DATA(W(I),I=1,10)/.1527533871,.1491729864,.1420961093,.1316886384,
     1.1181945319,.1019301198,.0832767415,.0626720483,.0406014298,
     2.0176140071/
      DO 1 I=11,20
      II=21-I
      X(I)=-X(II)
    1 W(I)=W(II)
      READ(5,INTO)
      WRITE(6,INTO)
      DR=(RMAX-RMIN)/FLOAT(NT-1)
      RETURN
      END
```

TABLE (I.3). LISTING OF ROUTINE AP2

```
      SUBROUTINE AP2
      COMMON/ONE/X(20),W(20),AM,ALAM,NM,NN,AN(15)
      COMMON/TWO/A(80,81),CI(15),AI
      COMMON/FOUR/NT,NP,WMIN,DW,SU,SR,AXX(15),NXX
      DIMENSION P1T(101),P2T(101),P3T(101),P4T(101)
      COMPLEX A,AI,CI
      COMPLEX AM,GN
      COMPLEX SUM,ST,T0
      IF(NP.NE.1)GOTO 52
      ST=0.
      ET=0.
      FT=0.
      DO 53 I=1,101
      P1T(I)=0.
      P3T(I)=0.
      P4T(I)=0.
   53 P2T(I)=0.
   52 WRITE(6,92)
      FP=EXP(-((ALOG(AN(1))-ALOG(SR))/(ALOG(SU))**2/2.))/AN(1)
      FT=FT+FP
      NNN=4*NN
      DO 2 I=1,NNN
      WRITE(6,90)I,A(I,1)
   90 FORMAT(5X,I10,2E20.8)
    2 CONTINUE
   92 FORMAT(1H1)
      DO 3 I=1,NN
      N=2*NN+I
      NA=3*NN+I
      FN=FLOAT(I)
      GN=(-AI)**(I+1)*FN*(FN+1.)/(2.*FN+1.)
      A(N,1)=A(N,1)*GN
      A(NA,1)=A(NA,1)*GN
      WRITE(6,92)
      NNNP=2*NN+1
      DO 4 I=NNNP,NNN
      WRITE(6,90)I,A(I,1)
    4 CONTINUE
      NNNX=0
      S=0.
      E=0.
      DO 5 I=1,NN
      N=2*NN+I
      NA=3*NN+I
      AH=FLOAT(I)
      AX=2.*AH+1.
      F=(CABS(A(N,1))**2+CABS(A(NA,1))**2)/AH
      NNNX=I
      S=S+F*AH*AX
      E=E+(REAL(A(N,1))+REAL(A(NA,1)))*AX
      IF(F.LE.1.E-14)GOTO 51
    5 CONTINUE
   51 FAC=ALAM*ALAM/2./3.1415927
      S=S*FAC
      E=E*FAC
      AB=E-S
      WRITE(6,93)E,S,AB
```

TABLE (I.3). CONTINUED

```
      ST=ST+S*FP
      ET=ET+E*FP
   93 FORMAT(/5A,"EXTINCTION = ",E20.8,/5X,"SCATTERING = ",E20.8,/5X,
     1"ABSORPTION = ",E20.8)
      DO 6 I=1,101
      AMU=1.-.02*FLOAT(I-1)
      SONE=CMPLX(0.,0.)
      STWO=CMPLX(0.,0.)
      P0=0.
      T0=0.
      P1=1.
      T1=AMU
      DO 61 J=1,NNNX
      N=2*NN+J
      NA=3*NN+J
      AJ=FLOAT(J)
      AJJ=(2.*AJ+1.)/AJ/(AJ+1.)
      IF(J.GT.1)GOTO 62
      P=P1
      T=T1
      GOTO 63
   62 P=(AMU*(2.*AJ+1.)*P1-AJ*P0)/(AJ+1.)
      T=AMU*(P-P0)-(2.*AJ-1.)*(1.-AMU*AMU)*P1+T0
      P0=P1
      P1=P
      T0=T1
      T1=T
   63 SONE=SONE+AJJ*(A(N,1)*P+A(NA,1)*T)
      STWO=STWO+AJJ*(A(N,1)*T+A(NA,1)*P)
   61 CONTINUE
      SONE=SONE*ALAM/2./3.1415927
      STWO=STWO*ALAM/2./3.1415927
      SIG1=CABS(SONE)**2
      SIG2=CABS(STWO)**2
      SIG3=REAL(SONE*CONJG(STWO))
      SIG4=-AIMAG(SONE*CONJG(STWO))
      SIG5=(SIG1+SIG2)/2.
      P1T(I)=P1T(I)+SIG1*FP
      P2T(I)=P2T(I)+SIG2*FP
      DP=1.-2./(1.+SIG1*SIG2/(SIG3**2+SIG4**2))
      P3T(I)=P3T(I)+SIG3*FP
      P4T(I)=P4T(I)+SIG4*FP
      WRITE(6,94)AMU,SIG1,SIG2,SIG3,SIG4,SIG5,DP
   94 FORMAT(5X,F10.3,6E15.6)
    6 CONTINUE
      IF(NP.NE.NT)RETURN
      ST=ST/FT
      ET=ET/FT
      AT=ET-ST
      WRITE(6,92)
      WRITE(6,93)ET,ST,AT
      DO 71 I=1,101
      P1T(I)=P1T(I)/FT
      P2T(I)=P2T(I)/FT
      P3T(I)=P3T(I)/FT
      P4T(I)=P4T(I)/FT
      PAVG=(P1T(I)+P2T(I))/2.
```

TABLE (I.3). CONTINUED

```
115                OP=1.-2./(1.+P1T(I)*P2T(I)/(P3T(I)**2+P4T(I)**2))
                   AMU=1.-2.*FLOAT(I-1)/100.
                   WRITE(6,94)AMU,P1T(I),P2T(I),P3T(I),P4T(I),PAV...,DP
                71 CONTINUE
                   RETURN
120                END
```

TABLE (I.4). LISTING OF ROUTINE ADO

```
      SUBROUTINE ADO(L1,L2,L3,L4,N1,N2,N3,N4)
      COMMON/ONE/X(20),W(20),AM,AL,AM,ANM,V,AN(15)
      COMMON/TWO/A(80,81),CI(15),AI
      COMPLEX AM,A,AI,CI
    5 C     MATRIX A IS COMPLEX ARRAY OF COEFFICIENT MULTIPLIERS
      NNNP=4*NN+1
      A(N1,L1)=A(N1,L1)+CI(10)
      A(N1,L2)=A(N1,L2)+AI*CI(9)
      A(N1,L3)=A(N1,L3)-CI(15)
   10 A(N1,L4)=A(N1,L4)-AI*CI(14)
      A(N2,L1)=A(N2,L1)-AI*CI(9)*AM
      A(N2,L2)=A(N2,L2)-CI(10)*AM
      A(N2,L3)=A(N2,L3)+AI*CI(14)
      A(N2,L4)=A(N2,L4)+CI(15)
   15 A(N3,L1)=A(N3,L1)-CI(6)-CI(8)
      A(N3,L2)=A(N3,L2)-AI*CI(7)
      A(N3,L3)=A(N3,L3)+CI(13)+CI(11)
      A(N3,L4)=A(N3,L4)+AI*CI(12)
      A(N4,L1)=A(N4,L1)-AI*CI(7)*AM
   20 A(N4,L2)=A(N4,L2)-(CI(6)+CI(8))*AM
      A(N4,L3)=A(N4,L3)+AI*CI(12)
      A(N4,L4)=A(N4,L4)+CI(13)+CI(11)
      A(N1,NNNP)=A(N1,NNNP)+CI(5)+AI*CI(4)
      A(N2,NNNP)=A(N2,NNNP)-CI(5)-AI*CI(4)
   25 A(N3,NNNP)=A(N3,NNNP)-CI(1)-CI(3)-AI*CI(2)
      A(N4,NNNP)=A(N4,NNNP)-CI(1)-CI(3)-AI*CI(2)
      RETURN
      END
```

TABLE (I.5). LISTING OF ROUTINE CGAUSS

```
      SUBROUTINE CGAUSS(N,NH,MS,MN1,D,IE,E,ID)
      COMMON/TWO/X(80,81),CI(15),A1
      COMPLEX CI,A1
      COMPLEX X,X1,Y
      A1=CMPLX(1.,0.)
      L1=1
      E=0.
      D=1.
      IF(ID.EQ.0)D=0.
      NN=N+NH
      IF(MS.EQ.0)GOTO 21
      K=N+1
      DO 22 I=1,N
      DO 23 J=K,NN
   23 X(I,J)=CMPLX(0.,0.)
      J=I+N
   22 X(I,J)=CMPLX(1.,0.)
   21 NM1=N-1
      DO 1 I=1,N
      K=I+1
      IF(K.GT.N)GOTO 31
      IJJ=I
      Y=X(I,I)
      DO 2 II=K,N
      IF(CABS(Y).GE.CABS(X(II,I)))GOTO 2
      IJJ=II
      Y=X(II,I)
    2 CONTINUE
      IF(IJJ.EQ.I)GOTO 31
      D=-D
      DO 3 J=I,NN
      Y=X(I,J)
      X(I,J)=X(IJJ,J)
    3 X(IJJ,J)=Y
   31 D=D*X(I,I)
      IF(CABS(X(I,I)).EQ.0.)GOTO 10
      GOTO(5,13),L1
   13 IF(CABS((A1-X(I,I)/A1)-1.).LT.1.E-7)E=2
      X1=X(I,I)
    5 L1=2
      DO 4 J=K,NN
    4 X(I,J)=X(I,J)/X(I,I)
      IF(I.EQ.N)GOTO 6
      DO 1 II=K,N
      Y=X(II,I)
      DO 1 J=K,NN
    1 X(II,J)=X(II,J)-X(I,J)*Y
    6 DO 8 L=K,NN
      M=NM1
      DO 7 I=1,NM1
      M1=M+1
      K1=N
      DO 9 J=M1,N
      X(M,L)=X(M,L)-X(M,K1)*X(K1,L)
    9 K1=K1-1
    7 M=M-1
    8 CONTINUE
```

TABLE (I.5). CONTINUED

```
      IR=K-1
      DO 12 I=1,N
      L=K
      DO 11 J=1,NN
      X(I,J)=X(I,L)
   11 L=L+1
   12 CONTINUE
      RETURN
   10 E=1.
      IR=K-1
      RETURN
      END
```

TABLE (I.6). LISTING OF ROUTINE BESSL

```
      SUBROUTINE BESSL(Z,ZZ)
      COMMON/THREE/AH(20),AJ(20),BH(20),DAJ(20),DAH(20),DBH(20)
      COMPLEX AJ,AH,BH,DAJ,DAH,DBH
      COMMON/FOUR/NT,NP,RMIN,DR,SD,SR,AXX(15),NXX
      COMPLEX ZZ,BA,BB,BC,P1,P2,P3
      Z2=1./Z**2
      AA=0.
      BA=CMPLX(0.,0.)
      BB=CMPLX(1.,0.)
      AB=1.
      DO 1 I=1,39
      II=40-I
      FI=FLOAT(II)
      FF=2.*FI+1
      AC=FF*BB/Z-AA
      AA=AB
      AB=AC
      BC=FF*BB/ZZ-BA
      BA=BB
      BB=BC
      IF(II.GT.21)GOTO 1
      IF(II.EQ.1)GOTO 2
      IJ=II-1
      AH(IJ)=AC
      AJ(IJ)=BC
    1 CONTINUE
    2 P1=CSIN(ZZ)/ZZ/BC
      P2=CMPLX(SIN(Z)/Z,0.)
      P2=P2/AC
      P3=CMPLX(SIN(Z)/Z,COS(Z)/Z)
      P3=P3/AC
      DO 3 I=1,20
      AJ(I)=P1*AJ(I)
      AH(I)=P2*AH(I)
    3 BH(I)=AH(I)
      P4=(Z2+AH(1)*COS(Z)/Z)*Z/SIN(Z)
      BH(1)=BH(1)+CMPLX(0.,P4)
      DO 31 I=2,20
      II=I-1
      P4=(Z2+AH(I)*P4)/AH(II)
   31 BH(I)=BH(I)+CMPLX(0.,P4)
      DAJ(1)=P1*BC-2.*AJ(1)/ZZ
      DAH(1)=P2*AC-2.*AH(1)/Z
      DBH(1)=P3*AC-2.*BH(1)/Z
      DO 4 I=2,20
      FF=FLOAT(I+1)
      DAJ(I)=AJ(I-1)-FF*AJ(I)/ZZ
      DAH(I)=AH(I-1)-FF*AH(I)/Z
    4 DBH(I)=BH(I-1)-FF*BH(I)/Z
      RETURN
      END
```

APPENDIX II

SPHERICAL BESSEL FUNCTION GENERATION; NUMERICAL ASPECTS

One of the difficulties experienced in this investigation was the calculation of the radial functions $\psi_\ell(x)$ and $\rho_\ell^1(x)$, Eqs. (2.45) and (2.47), and their derivatives. This difficulty is not new, and in the early days of the implementation of the Mie solution, it was necessary to derive recursion relations for the c_ℓ and d_ℓ to effect their calculation (Deirmendjian, 1964). Since that time, however, advances in the construction of compilers has permitted more fundamental calculations of the radial functions if sufficient safeguards are taken. Because of the special dependency of this investigation on calculating the values of these radial functions, this appendix describes the numerical considerations of calculating these quantities.

The radial function $\psi_\ell(x)$ and $\rho_\ell^1(x)$ are related to the spherical bessel functions and spherical hankel functions of the first kind by

$$\psi_\ell(x) = x j_\ell(x) \tag{II.1}$$

and

$$\rho_\ell^1(x) = x h_\ell^1(x) = x[j_\ell(x) - i y_\ell(x)] \tag{II.2}$$

where $y_\ell(x)$ = spherical Neuman function. The first two $\psi_\ell(x)$ and $\rho_\ell^1(x)$ (i.e. ℓ = 0 and 1) are

$$\psi_o(x) = \sin(x) \tag{II.3}$$

$$\psi_1(x) = \frac{\sin(x)}{x} - \cos(x) \tag{II.4}$$

$$\rho_0^1(x) = \sin(x) + i\cos(x) \tag{II.5}$$

and

$$\rho_1^1(x) = \frac{\sin(x)}{x} - \cos(x) + i\left(\frac{\cos(x)}{x} + \sin(x)\right) \tag{II.6}$$

Additionally, the $j_\ell(x)$, $y_\ell(x)$, and $h_\ell^1(x)$ all satisfy the same recursion relation

$$f_{\ell+1}(x) = (2\ell+1)\frac{f_\ell(x)}{x} - f_{\ell-1}(x) \tag{II.7}$$

and derivative formula

$$\frac{d}{dx}f_\ell(x) = f_{\ell-1}(x) - \frac{n+1}{x}f_\ell(x) \tag{II.8}$$

where $f_\ell(x)$ may be any of the three functions. Additionally, the $j_\ell(x)$ and $y_\ell(x)$ have a cross product relation

$$j_\ell(x)y_{\ell-1}(x) - j_{\ell-1}(x)y_\ell(x) = \frac{1}{x^2} \tag{II.9}$$

The recursion relation for $\psi_\ell(x)$ or $\rho_\ell^1(x)$ may be obtained from Eq. (II.7) by multiplying by x to yield,

$$\psi_{\ell+1}(x) = (2\ell+1)\frac{\psi_\ell(x)}{x} - \psi_{\ell-1}(x) \tag{II.10}$$

and the derivative relation may be similarly obtained as

$$\frac{d}{dx}\psi_\ell(x) = \psi_{\ell-1}(x) - \frac{n}{x}\psi_\ell(x) \tag{II.11}$$

In principle, Eqs. (II.10), (II.11) and (II.3) - (II.6) may be used to calculate the value of $\psi_\ell(x)$ and $\rho_\ell^1(x)$ for any x and ℓ by

forward recursion. In practice, however, the forward recursion tends to diverge numerically when $|x|<1$, causing problems with overflow as well as inaccuracy due to roundoff errors.

To circumvent this difficulty, the calculational procedure of Miller may be used (Miller, 1950). This procedure operates as a backwards recursion. The algorithm operates in the following manner: some maximum value L for ℓ is established. An upper limit for the algorithm L* at least twice L in value is established. The larger L* is, the greater the accuracy of the method. A series of factors F_ℓ are calculated using Eq. (II.10) in a backwards recursion subject to the conditions

$$F_{L^*} = 1 \tag{II.12}$$

and

$$F_{L^*+1} = 0 \tag{II.13}$$

The ψ_ℓ may then be calculated from the F_ℓ by

$$\psi_\ell(x) = \psi_o(x)F_\ell/F_o \tag{II.14}$$

where $\psi_o(x)$ is defined by Eq. (II.3)

It may be noted that this method also suffers from divergence problems in a like manner as the forward recursion technique. Fortunately, this does not occur within the bounds of the Mie solution or this investigation for $|x| \lesssim 18$. In practice, the two methods, forward and backward recursion, overlap so that values of $\psi_\ell(x)$ may be calculated for any except very small values of x where Rayleigh or Rayleigh-Gans theory is valid.

The $\rho_\ell^1(x)$ could also be calculated using Miller's method, but are not because it is easier to rewrite Eqs. (II.2) and (II.9) as

$$\rho_\ell^1(x) = \psi_\ell(x) - i\eta_\ell(x) \tag{II.15}$$

and

$$\eta_\ell(x) = \frac{\psi_\ell(x)\eta_{\ell-1}(x)-1}{\psi_{\ell-1}(x)} \tag{II.16}$$

where: $\eta_\ell(x) = x_\ell(x)$, and

$\eta_o(x) = -\cos(x)$.

The $\eta_\ell(x)$ may then be calculated from the $\psi_\ell(x)$, and the $\rho_\ell^1(x)$ from the $\psi_\ell(x)$ and the $\eta_\ell(x)$.

The routine BESSEL uses this recipe to calculate the values of the radial functions:

1.) Calculate the F_ℓ.

2.) Calculate the $\psi_\ell(x)$ from the F_ℓ.

3.) Calculate the $\rho_\ell^1(x)$ (via the $\eta_\ell(x)$) from the $\psi_\ell(x)$.

4.) Calculate the $\psi_\ell'(x)$ and the $\rho_\ell^{1'}(x)$ from the $\psi_\ell(x)$ and the $\rho_\ell^1(x)$ via Eq. (II.11).

Based on a survey of the literature, it appears that Miller's method had previously been validated only for real value of x. During this investigation, therefore, its validity for complex values of x was demonstrated through the numerical validation of the entire code.

APPENDIX III

REDUCTION OF THE NONSPHERICAL FORMALISM TO MIE THEORY FOR THE SPHERICAL PARTICLE CASE

As a matter of course, the nonspherical formalism developed in Chapter VI must reduce to Mie theory when the particle is spherical. This appendix will demonstrate that reduction.

In terms of Eq. (6.1), the radius of a spherical particle reduces to

$$a(\theta) = S_o P_o(\cos\theta). \tag{III.1}$$

and has angular derivative

$$\frac{\partial a(\theta)}{\partial \theta} = 0. \tag{III.2}$$

Additionally, the radial functions ψ_ℓ and ρ_ℓ^1 and their derivatives are independent of θ, so that Eqs. (6.43) - (6.57) reduce to

$$A_{\ell\ell',1} = 0 \tag{III.3}$$

$$A_{\ell\ell',2} = \gamma_\ell \frac{\psi_\ell(ka)}{ka} I_{1\ell\ell'} \tag{III.4}$$

$$A_{\ell\ell',3} = \gamma_\ell \frac{\psi_\ell'(ka)}{ka} I_{2\ell\ell'} \tag{III.5}$$

$$A_{\ell\ell',4} = \gamma_\ell \frac{\psi_\ell(ka)}{ka} I_{2\ell\ell'} \tag{III.6}$$

$$A_{\ell\ell',5} = \gamma_\ell \frac{\psi_\ell'(ka)}{ka} I_{1\ell\ell'} \qquad \text{(III.7)}$$

$$A_{\ell\ell',6} = 0 \qquad \text{(III.8)}$$

$$A_{\ell\ell',7} = \frac{\psi_\ell(kma)}{kma} I_{1\ell\ell'} \qquad \text{(III.9)}$$

$$A_{\ell\ell',8} = \frac{\psi_\ell'(kma)}{kma} I_{2\ell\ell'} \qquad \text{(III.10)}$$

$$A_{\ell\ell',9} = \frac{\psi_\ell(kma)}{kma} I_{2\ell\ell'} \qquad \text{(III.11)}$$

$$A_{\ell\ell',10} = \frac{\psi_\ell'(kma)}{kma} I_{1\ell\ell'} \qquad \text{(III.12)}$$

$$A_{\ell\ell',11} = 0 \qquad \text{(III.13)}$$

$$A_{\ell\ell',12} = \frac{\rho_\ell^1(ka)}{km} I_{1\ell\ell'} \qquad \text{(III.13)}$$

$$A_{\ell\ell',13} = \frac{\rho_\ell^{1'}(ka)}{ka} I_{2\ell\ell'} \qquad \text{(III.15)}$$

$$A_{\ell\ell',14} = \frac{\rho_\ell^1(ka)}{ka} I_{2\ell\ell'} \qquad \text{(III.16)}$$

$$A_{\ell\ell',15} = \frac{\rho_\ell^{1'}(ka)}{ka} I_{2\ell\ell'} \qquad \text{(III.17)}$$

where

$$I_{2\ell\ell'} = \int \frac{P_\ell^1 P_{\ell'}^1}{\sin(\theta)} d\cos\theta \qquad \text{(III.18)}$$

$$I_{2\ell\ell'} = \int \frac{\partial P_\ell^1}{\partial\theta} P_{\ell'}^1 d\cos\theta \qquad \text{(III.19)}$$

Equation (6.63) may then be written as

$$B = \begin{bmatrix} \frac{\psi_{\ell'}(kma)}{kma} I_{1\ell\ell'} & i\frac{\psi_\ell(kma)}{kma} I_{2\ell\ell'} & -\frac{\psi_{\ell'}(ka)}{ka} I_{1\ell\ell'} & \frac{-i\rho_\ell^1(ka)}{ka} I_{2\ell\ell'} \\ -\frac{\psi_{\ell'}'(kma)}{kma} I_{2\ell\ell'} & -\frac{\psi_\ell(kma)}{kma} I_{\ell\ell'} & \frac{i\rho_\ell^1(ka)}{ka} I_{2\ell\ell'} & \frac{\rho_\ell^{1'}(ka)}{ka} I_{1\ell\ell'} \\ -\frac{\psi_{\ell'}(kma)}{kma} I_{2\ell\ell'} & -i\frac{\psi_\ell(kma)}{kma} I_{1\ell\ell'} & \frac{\rho_\ell^{1'}(ka)}{ka} I_{2\ell\ell'} & \frac{i\rho_\ell^1(ka)}{ka} I_{1\ell\ell'} \\ -\frac{\psi_\ell(kma)}{kma} I_{1\ell\ell'} & -\frac{\psi_\ell(kma)}{kma} I_{2\ell\ell'} & \frac{i\rho_\ell^1(ka)}{ka} I_{1\ell\ell'} & \frac{\rho_\ell 1'(ka)}{ka} I_{2\ell\ell'} \end{bmatrix} \qquad \text{(III.20)}$$

and Eq. (6.64) as

$$F = \begin{pmatrix} \sum_{\ell} \gamma_{\ell} [i\psi_{\ell}(ka) I_{2\ell\ell'} + \psi_{\ell}'(ka) I_{1\ell\ell'}]/ka \\ -\sum_{\ell} \gamma_{\ell} [i\psi_{\ell}(ka) I_{2\ell\ell'} + \psi_{\ell}'(ka) I_{2\ell\ell'}]/ka \\ -\sum_{\ell} \gamma_{\ell} [i\psi_{\ell}(ka) I_{1\ell\ell'} + \psi_{\ell}'(ka) I_{2\ell\ell'}]/ka \\ -\sum_{\ell} \gamma_{\ell} [i\psi_{\ell}(ka) I_{1\ell\ell'} + \psi_{\ell}'(ka) I_{2\ell\ell'}]/ka \end{pmatrix} \qquad \text{(III.21)}$$

To simplify the demonstration, two restrictions may be made without compromise: first, that the particle is small enough that only the first term $\ell = 1$ need be retained, and second, that ℓ' be chosen such that

$$I_{1\ell\ell'} = I \qquad \text{(III.22)}$$

and

$$I_{2\ell\ell'} = 0 \qquad \text{(III.23)}$$

This reduces Eq. (III.20) to

$$E = \begin{pmatrix} \frac{\psi_1'(kma)}{m} & 0 & -\rho_1^{1'}(ka) & 0 \\ 0 & -\psi_1'(kma) & 0 & \rho_1^{1'}(ka) \\ 0 & \frac{-i\psi_1(kma)}{m} & 0 & i\rho_1^{1}(ka) \\ -i\psi_\ell(kma) & 0 & i\rho_1^{1}(ka) & 0 \end{pmatrix} \qquad \text{(III.24)}$$

and Eq. (III.21) to

$$F = \begin{pmatrix} \gamma_1 \psi_1'(ka) \\ -\gamma_1 \psi_1'(ka) \\ -i\gamma_1 \psi_1(ka) \\ -i\gamma_1 \psi_1(ka) \end{pmatrix} . \qquad \text{(III.25)}$$

It may be noted that Eq. (III.24) is now separated in terms of pairing a_1 with c_1, and b_1 with d_1. If Eq. (III.24) and (III.25) are combined, the result is

$$\frac{a_1}{m}\psi_1'(kma) - c_1\rho_1^{1'}(ka) = \gamma_1 \psi_1'(ka) \qquad \text{(III.26)}$$

$$-b_1\psi_1'(kma) + d_1\rho_1^{1'}(ka) = \gamma_1\psi_i^{-}(ka) \qquad \text{(III.27)}$$

$$-\frac{ib_1}{m}\psi_1(kma) + id_1\rho_1^{1}(ka) = -i\gamma_1\psi_1(ka) \qquad \text{(III.28)}$$

$$-ia_1\psi_1(kma) + ic_1\rho_1^{1}(ka) = -i\gamma_1\psi_1(ka). \qquad \text{(III.29)}$$

Equation (III.26) may be rewritten as

$$a_1 = m[c_1\rho_1^{1'}(ka) + \gamma_1\psi_1'(ka)]/\psi_1'(kma) \qquad \text{(III.30)}$$

and combined with Eq. (III.29) to yield

$$-\frac{i\psi_1(kma)}{\psi_1'(kma)}\, m[c_1\rho_1^{1'}(ka) + \gamma_1\psi_1'(ka)] + ic_1\rho_1^{1}(ka) =$$

$$-i\gamma_1\psi_1(ka) \qquad \text{(III.31)}$$

$$-imc_1\rho_1^{1'}(ka)\psi_1(kma) - i\gamma_1 m\psi_1(kma)\psi_1'(ka) + ic_1\rho_1^{1}(ka)\psi_1'(kma)$$

$$= -i\gamma_1\psi_1(ka)\psi_1'(kma) \qquad \text{(III.32)}$$

$$ic_1[\rho_1^1(ka)\psi_1'(kma) - m\rho_1^{1'}(ka)\psi_1(kma)] =$$

$$i\gamma_1[m\psi_1(kma)\psi_1'(ka) - \psi_1'(kma)\psi_1(ka)] \qquad \text{(III.33)}$$

$$c_1 = \gamma_1 \frac{[m\psi_1(kma)\psi_1'(ka) - \psi_1'(kma)\psi_1(ka)]}{[\rho_1^1(ka)\psi_1'(kma) - m\rho_1^{1'}(ka)\psi_1(kma)]} \qquad \text{(III.34)}$$

which is identical to Eq. (3.17) for $\ell = 1$.

In a like manner Eqs. (III.27) and (III.28) may be combined to yield Eq. (3.18) for $\ell = 1$.

APPENDIX IV

TWO-DIMENSIONAL RADIATIVE TRANSFER CODE

The computer code described in this appendix implements the algorithm of Chapter X. Calculations performed using this code are presented in Chapter XI. The version of the code presented here is for a constant extinction coefficient.

The computer memory requirement for this code is approximately 1.25×8^5 words. This requirement is not decreased appreciably by compilation using the SCOPE 3.4.2 compiler. Run time for a nominal run in the near-ir requiring 24 orders of scattering to satisfy the 1% self-consistency requirement is about five seconds. The same calculation for varying medium would require about twice as much time.

The code consists of a driver routine and five subroutines. These routines are described individually below, and are listed in Tables (IV-1) - (IV.6).

RT2 (Table (IV.1))

This is the driver routine. It inputs the extinction coefficient, the albedo of single scattering, and the phase function for directions i = 1 to 5, sets the scale of the calculations, and normalizes the phase function. The calculation is performed for incremental ranges or optical depths. Routine LSTART is called to generate the zeroth order of scattering source functions. Routines UPDOWN, ACROSS, and ACCOUNT are called for each order of scattering to calculate the source functions. Finally, CTRST is called to calculate to modulation contrast for the total intensities.

LSTART (Table (IV.2))

This subroutine uses the incident illumination beam profile, the extinction coefficient, and the phase function to calculate the zeroth order of scattering source functions. This routine is specific for beam type sources with light propagating only along the $i = 1$ direction. More general incident illuminations are not considered by this routine because only this type of incident illumination was needed in this investigation.

UPDOWN (Table (IV.3))

Subroutine UPDOWN calculates the n^{th} order of scattering source function contributions for directions $i = 1, 3, 5, 7$ *from the* $n\text{-}1^{th}$ order of scattering source functions. Additionally, it calculates the n^{th} order of scattering intensities for directions $i = 1$ and 5 at the edges of the medium. These are the forward scattered and back-scattered intensities, respectively.

ACROSS (Table (IV.4))

This routine performs the same source function calculations as UPDOWN except for directions $i = 2, 4, 6, 8$.

ACCOUNT (Table (IV.5))

Surboutine ACCOUNT transfers the n^{th} order of scattering source function array into the $n\text{-}1^{th}$ array in preparation for the next order of scattering calculation. Additionally, it zeroes out the n^{th} order array.

CTRST (Table (IV.6))

This routine calculates the forward scattered and backscattered modulation contrasts.

TABLE (IV.1). LISTING OF ROUTINE RT2


```
      PROGRAM RT2(INPUT,OUTPUT,TAPE5=INPUT,TAPE6=OUTPUT,TAPE7,TAPE8)
      COMMON/ONE/A(5,31,8),A1(5,31,8),CI(31),DI(31),T(31),PP(8),
     1  PO(8),OP(8),OO(8),PM(8),PS(8),O-(8),OS(8)
      COMMON/TWO/DX,DY,DR,AL,W,SMU,CMU,NR,N
      COMMON/AL/TITLE
      DIMENSION X(31),Y(31)
      NAMELIST/RTR/AL,ALL,W,PP
      DX=1.
      DY=1.155
      DY = 1.732
      DR=SQRT(DX*DX+DY*DY)

      CMU=DX/DR
      SMU=DY/DR
      DO 1 I=1,31
    Y(I)=FLOAT(I-1)
  1 T(I)=EXP(-FLOAT(I-16)**2*3./25.)
    CALL CINST(Y,T,T,1)
    READ(5,RTR)
    IF(AL.NE.0.)GOTO 4
    AL=.05
    GOTO 41
  4 ALL=AL
 41 IF(PP(6).GT.0.)GOTO 5
C
C       N=2 LEGENDRE
C
    DO 3 I=6,8
    II=10-I
  3 PP(I)=PP(II)
  5 PSS=0.
    DO 31 I=1,8
 31 PSS=PSS+PP(I)
    DO 32 I=1,8
 32 PP(I)=PP(I)/PSS
    WRITE(6,RTR)
     0 99 NR=10,50,10
    OO=AL*FLOAT(NR)
    RNGE=OO/ALL
    WRITE(6,95)RNGE,OO
 95 FORMAT(5X," RANGE = ",F15.5,5X," OPT. DEPTH = ",F15.5)
      CALL LSTART
      N=0
      CO=CI(16)
    WRITE(6,92)
    WRITE(6,91)((Y(I),CI(I),DI(I)),I=1,31)
    WRITE(6,93)
 90 FORMAT(5X," DEFAULT END ")
 91 FORMAT(5X,F10.2,2E15.5)
 92 FORMAT(12X,"X",7X,"FORWARD",8X,"BACKWARD")
 93    FORMAT(/////)
 94 FORMAT(/5X,I10)
    10    CONTINUE
      CALL UPDOWN
      CALL ACROSS
      CALL ACCOUNT
```

TABLE (IV.1). CONTINUED


```
      WRITE(6,91)((Y(I),CI(I),DI(I)),I=1,31)
         CF=ABS(CO-CI(16))/CO
50       IF(N.LT.3)GOTO 98
         IF(CF.LE..01)GOTO 999
      IF(N.GT.50)GOTO 999
   98    N=N+1
      WRITE(6,94)N
65       CO=CI(16)
         GOTO 10
  999 CONTINUE
      CALL CPST(Y,CI,DI,2)
   99    CONTINUE
70       STOP
         END
```

TABLE (IV.2). LISTING OF ROUTINE LSTART


```
      SUBROUTINE LSTART
      COMMON/ONE/A(51,31,8),H(51,31,8),CI(31),DI(31),T(31),PP(8),
     1 PQ(8),QP(8),QQ(8),PR(8),PS(8),QR(8),QS(8)
      COMMON/TWO/DX,DY,DR,AL,W,SMU,CM1,NR,N
      DO 1 I=1,51
      DO 1 J=1,31
      DO 1 K=1,8
        A(I,J,K)=0.
      H(I,J,K)=0.
    1 CONTINUE
      CX=EXP(-AL*DX)
      C=1./SQRT(CX)
      DO 10 I=1,NR
      C=C*CX
      DO 10 J=1,31
      D=C*T(J)
      DO 10 K=1,8
      A(I,J,K)=D*PP(K)
   10 CONTINUE
      C=EXP(-AL*DX*NR)
      DO 20 I=1,31
      DI(I)=0.
   20 CI(I)=T(I)*C
      RETURN
      END
```

TABLE (IV.3). LISTING OF ROUTINE UPDOWN

```
      SUBROUTINE UPDOWN
      COMMON/ONE/A(51,31,8),B(51,31,8),CI(31),DI(31),  (31),PP(8),
     1 PQ(8),QP(8),QQ(8),PM(8),PS(8),QM(8),QS(8)
      COMMON/TWO/DX,DY,DK,AL,W,SMU,CMU,NR,N
C
C     MESH IN 1,3,5,7 DIRECTIONS
C
      E=EXP(-AL*DX)
      EE=EXP(-AL*DX/2.)
      EF=1.-EE
C
C  1,5 DIRECTIONS
C
      DO 10 J=1,31
      VV=A(1,J,1)*EF
      UU=A(NR,J,5)*EF
      U=UU
      V=VV
      DO 11 K=1,8
      B(1,J,K)=B(1,J,K)+V*PP(K)
      IZ=K-4
      IF(IZ.GT.0)GOTO 11
      IZ=IZ+8
   11 B(NR,J,K)=B(NR,J,K)+U*PP(IZ)
      DO 1 I=2,NR
      V=V*E+VV*EE
      U=U*E+UU*EE
      VV=A(I,J,1)*EF
      UU=A(NR+1-I,J,5)*EF
      U=U+UU
      V=V+VV
      DO 12 K=1,8
      B(I,J,1)=B(I,J,1)+PP(K)*V
      IZ=K-4
      IF(IZ.GT.0)GOTO 12
      IZ=IZ+8
   12 B(NR+1-I,J,K)=B(NR+1-I,J,K)+PP(IZ)*U
    1 CONTINUE
C
C     NTH ORDER INTENSITIES
C
      DI(J)=DI(J)+(U*EE+UU)*W**N
      CI(J)=CI(J)+(V*EE+VV)*W**N
   10 CONTINUE
      E=EXP(-AL*DY)
      EE=EXP(-AL*DY/2.)
      EF=1.-EE
C
C     3,7 DIRECTIONS
C
      DO 2 I=1,NR
      VV=A(I,1,7)*EF
      UU=A(I,31,3)*EF
      V=VV
      U=UU

      DO 21 K=1,8
```

TABLE (IV.3). CONTINUED


```
      IZ=K-6
      I (IZ.GT.0)GOTO 211
60    IZ=17+8
  211 B(I,J,K)=B(I,J,K)+PP(IZ)*V
      IZ=K-2
      IF(IZ.GT.0)GOTO 21
      IZ=IZ+8
65    B(I,31,K)=B(I,31,K)+PP(IZ)*U
   21 DO 2 J=2,31

      V=V*F+VV*EE
      U=U*E+UU*EE
70    UU=A(I,32-J,3)*EF
      VV=A(I,J,7)*EF
      U=U+UU
      V=V+VV
      DO 22 K=1,8
75    IZ=K-6
      IF(IZ.GT.0)GOTO 221
      IZ=IZ+8
  221 B(I,J,K)=B(I,J,K)+PP(IZ)*V
      IZ=K-2
80    IF(IZ.GT.0)GOTO 22
      IZ=IZ+8
   22 B(I,32-J,K)=B(I,32-J,K)+PP(IZ)*...
    2 CONTINUE
      RETURN
85    END
```

TABLE (IV.4). LISTING OF ROUTINE ACROSS

```
      SUBROUTINE ACROSS
      COMMON/ONE/A(51,31,8),B(51,31,8),CI(31),DI(31),EI(31),PP(8),
     1 PQ(8),QP(8),QQ(8),PR(8),PS(8),QR(8),QS(8)
      COMMON/TWO/DX,DY,DR,AL,W,SMU,CMU,NR,N
C
C     MESH FOR 2,4,6,8 DIRECTIONS
C
      E = EXP(-AL*DR)
      EE=EXP(-AL*DR/2.)
      EF=1.-EE
C     DIRECTION 8 DOWN
      DO 1 J=1,31
      JP=J+1
      IP=2
      VV=A(1,J,8)*EF
      V=VV
      DO 111 K=1,8
      IZ=K-7
      IF(IZ.GT.0)GOTO 111
      IZ=IZ+8
  111 B(1,J,K)=B(1,J,K)+PP(IZ)*V
      IF(JP.GT.31)GOTO 1
   11 V=V*E+VV*EE
      VV=A(IP,JP,8)*EF
      V=V+VV
      DO 112 K=1,8
      IZ=K-7
      IF(IZ.GT.0)GOTO 112
      IZ=IZ+8
  112 B(IP,JP,K)=B(IP,JP,K)+PP(IZ)*V
      JP=JP+1
      IP=IP+1
      IF(IP.LT.(NR+1).AND.JP.LT.32)GOTO 11
    1 CONTINUE
C     DIRECTION 8 ACROSS
      DO 2 I=2,NR
      IP=I+1
      JP=2
      V=A(I,1,8)*EF
      VV=V
      DO 211 K=1,8
      IZ=K-7
      IF(IZ.GT.0)GOTO 211
      IZ=IZ+8
  211 B(I,1,K)=B(I,1,K)+PP(IZ)*V
      IF(IP.GT.NR)GOTO 2
   21 V=V*E+EE*VV
      VV=A(IP,JP,8)*EF
      V=V+VV
      DO 212 K=1,8
      IZ=K-7
      IF(IZ.GT.0)GOTO 212
      IZ=IZ+8
  212 B(IP,JP,K)=B(IP,JP,K)+PP(IZ)*V
      JP=JP+1
      IP=IP+1
      IF(IP.LT.(NR+1).AND.JP.LT.32)GOTO 21
```

TABLE (IV.4). CONTINUED

```
      2     CONTINUE
      C     DIRECTION 6 DOWN
            DO 3 J=2,31
            JP=J+1
            IP=NR-1
            UU=A(NR,J,6)*EF
            U=UU
            DO 311 K=1,8
            IZ=K-5
            IF(IZ.GT.0)GOTO311
            IZ=IZ+8
     311    B(NR,J,K)=B(NR,J,K)+PP(IZ)*U
            IF(JP.GT.31)GOTO 3
      31    U=U*E+UU*EE
            UU=A(IP,JP,6)*EF
            U=U+UU
            DO 312 K=1,8
            IZ=K-5
            IF(IZ.GT.0)GOTO 312
            IZ=IZ+8
     312    B(IP,JP,K)=B(IP,JP,K)+PP(IZ)*U
            IP=IP-1
            JP=JP+1
            IF(IP.GT.0.AND.JP.LT.32)GOTO 31
      3     CONTINUE
      C     DIRECTION 6 ACROSS
            DO 4 I=1,NR
            JP=2
            IP=I-1
            UU=A(I,1,6)*EF
            U=UU
            DO 411 K=1,8
            IZ=K-5
            IF(IZ.GT.0)GOTO 411
            IZ=IZ+8
     411    B(I,1,K)=B(I,1,K)+PP(IZ)*U
            IF(IP.LT.1)GOTO 4
      41    U=U*E+UU*EE
            UU=A(IP,JP,6)*EF
            U=U+UU
            DO 412 K=1,8
            IZ=K-5
            IF(IZ.GT.0)GOTO 412
            IZ=IZ+8
     412    B(IP,JP,K)=B(IP,JP,K)+PP(IZ)*U
            IP=IP-1
            JP=JP+1
            IF(IP.GT.0.AND.JP.LT.32)GOTO 41
      4     CONTINUE
      C     DIRECTION 4 UP
            DO 5 J=1,30
            JP=J-1
            IP=NR-1
            UU=A(NR,J,4)*EF
            U=UU
            DO 511 K=1,8
            IZ=K-3
```

TABLE (IV.4). CONTINUED

```
      IF(IZ.GT.0)GOTO 511
      IZ=IZ+8
  511 B(NR,J,K)=B(NR,J,K)+PP(IZ)*U
      IF(JP.LT.1)GOTO 5
   51 U=U*E+UU*EE
      UU=A(IP,JP,4)*EF
      U=U+UU
      DO 512 K=1,8
      IZ=K-3
      IF(IZ.GT.0)GOTO 512
      IZ=IZ+8
  512 B(IP,JP,K)=B(IP,JP,K)+PP(IZ)*U
      IP=IP-1
      JP=JP-1
      IF(IP.GT.0.AND.JP.GT.0)GOTO 51
    5 CONTINUE
C     DIRECTION 4 ACROSS
      DO 6 I=1,NR
      IP=I-1
      JP=30
      UU=A(I,31,4)*EF
      U=UU
      DO 611 K=1,8
      IZ=K-3
      I (IZ.GT.0)GOTO 611
      IZ=IZ+8
  611 B(I,31,K)=B(I,31,K)+PP(IZ)*U
      IF(IP.LT.1)GOTO 6
   61 U=U*E+UU*EE
      UU=A(IP,JP,4)*EF
      U=U+UU
      DO 612 K=1,8
      IZ=K-3
      IF(IZ.GT.0)GOTO 612
      IZ=IZ+8
  612 B(IP,JP,K)=B(IP,JP,K)+PP(IZ)*U
      IP=IP-1
      JP=JP-1
      IF(IP.GT.0.AND.JP.GT.0)GOTO 61
    6 CONTINUE
C     DIRECTION 2 UP
      DO 7 J=1,31
      IP=2
      JP=J-1
      UU=A(1,J,2)*EF
      U=UU
      DO 711 K=1,8
      IZ=K-1
      IF(IZ.GT.0)GOTO 711
      IZ=IZ+8
  711 B(1,J,K)=B(1,J,K)+PP(IZ)*U
      IF(IP.LT.1)GOTO 7
    7 U=U*E+UU*EE
      UU=A(IP,JP,2)*EF
      U=U+UU
      DO 712 K=1,8
      IZ=K-1
```

TABLE (IV.4). CONTINUED

```
                IF(IZ.GT.0)GOTO 712
                IZ=IZ+8
          712   B(IP,JP,K)=B(IP,JP,K)+PP(IZ)*U
175             JP=JP-1
                IP=IP+1
                IF(IP.LT.(NR+1).AND.JP.GT.0)GOTO 71
            7   CONTINUE
          C     DIRECTION 2 ACROSS
180             DO 8 I=2,NR
                IP=I+1
                JP=J0
                UU=A(I,3,2)*EF
                U=UU
185             DO 811 K=1,8
                IZ=K-1
                IF(IZ.GT.0)GOTO 811
                IZ=IZ+8
          811   B(I,3,K)=B(I,3,K)+PP(IZ)*U
190             IF(IP.GT.NR)GOTO 8
           81   U=U*F+UU*EE
                UU=A(IP,JP,2)*EF
                U=U+UU
                DO 812 K=1,8
195             IZ=K-1
                IF(IZ.GT.0)GOTO 812
                IZ=IZ+8
          812   B(IP,JP,K)=B(IP,JP,K)+PP(IZ)*U
                JP=JP-1
200             IP=IP+1
                IF(IP.LT.(NR+1).AND.JP.GT.0)GOTO 81
            8   CONTINUE
                RETURN
                END
```

TABLE (IV.5). LISTING OF ROUTINE ACCOUNT

```
      SUBROUTINE ACCOUNT
      COMMON/ONE/A(51,31,8),B(51,31,8),CI(41),DI(31),EI(31),PP(8),
     1 PQ(8),QP(8),QQ(8),PR(8),PS(8),QR(8),QS(8)
      COMMON/TWO/DX,DY,DR,AL,N,SMU,CMU,NR,N
C
C     SUBROUTINE TO INSERT B INTO A, THAT IS J(N-1) IS GOTTEN FRO
C     J(N)
C
      DO 1 I=1,NR
      DO 1 J=1,31
      DO 1 K=1,8
      A(I,J,K)=B(I,J,K)
      B(I,J,K)=0.
    1 CONTINUE
      RETURN
      END
```

TABLE (IV.6). LISTING OF ROUTINE CTRST

```
      SUBROUTINE CTRST(X,Y,Z,IZ)
      COMMON/AL/TITLE
      DIMENSION A(31),Y(31),Z(31),C(31),CC(31)
      D=Y(1)
      E=Y(1)
      DO 1 I=2,31
      D=AMAX1(D,Y(I))
    1 E=AMIN1(E,Y(I))
      DO 2 I=1,31
    2 C(I)=(Y(I)-E)/(E-D)
      TITLE="CONTRAST F"
      IF(IZ.EQ.1)GOTO 98
      D=Z(1)
      E=Z(1)
      DO 20 I=2,31
      D=AMAX1(D,Z(I))
   20 E=AMIN1(E,Z(I))
      DO 30 I=1,31
   30 CC(I)=(Z(I)-E)/(E-D)
      TITLE="CONTRAST B"
   91 FORMAT(5X,F10.2,2F15.5)
   92 FORMAT(12X,"X",7X,"FORWARD",8X,"BACKWARD")

      WRITE(6,92)
      WRITE(6,91)((X(I),C(I),CC(I)),I=1,31)
      RETURN
   98 WRITE(6,92)
      WRITE(6,91)((X(I),C(I)),I=1,31)
      RETURN
      END
```

LIST OF SYMBOLS

A	Parameter for Deirmendjian particle size distribution function.
$A_{\ell\ell'',n}$	Integrals used in non-spherical particle scattering solution.
A_m	Field expansion coefficient in Rayleigh Hypothesis.
$A(r)$	Reilly integral.
$\underset{\sim}{A}$	Arbitrary vector function.
$\mathbf{A}$	Matrix in least-squares technique.
$\mathbf{A}^+$	Transpose of matrix $\mathbf{A}$.
$(\mathbf{A}^+\mathbf{A})^{-1}$	Inverse of matrix $\mathbf{A}^+\mathbf{A}$.
a	Constant used in relating $\underset{\sim}{E}$ to $\underset{\sim}{\Pi}$, the specific particle radius, and the semimajor axis of the ellipsoid/spheroid.
a_ℓ	Interior electric Debye potential expansion coefficient.
a_η	Shape function parameter.
$a(\theta,\phi)$	Radius of particle as a function of θ and ϕ.
B	Parameter for Deirmendjian particle size distribution function.
$\mathbf{B}$	$A_{\ell\ell'',\eta}$ matrix representing interior and scattered fields.
$B(r)$	Reilly integral.
$\underset{\sim}{B}$	Magentic flux intensity.
$\mathbf{B}$	Matrix in least-squares technique.

b	Constant used in relating $\underset{\sim}{H}$ to $\underset{\sim}{\Sigma}$, effective particle radius in Rayleigh-Gans theory, and simimajor axis of the ellipsoid/spheroid.
b_ℓ	Interior magnetic Debye potential expansion coefficient.
C	Coupling constant for Junge particle size distribution function.
$C(r)$	Reilly integral.
$C(\underset{\sim}{r}_{\ell m}, \underset{\sim}{k}_i)$	Modulation contrast at $\underset{\sim}{r}_{\ell m}$ along $\underset{\sim}{k}_i$.
C	Matrix in least-square technique.
c	Speed of light, speroidal/ellipsoidal particle size parameter.
c_ℓ	Scattered electric Debye potential expansion coefficient.
cos	Cosine function.
D	Coupling constant for log-normal particle size distribution function.
$\underset{\sim}{D}$	Electric displacement.
d_ℓ	Scattered magnetic Debye potential expansion coefficient.
E_ℓ, E_r	Left and right components.
E_r, E_θ, E_ϕ	Spherical components of $\underset{\sim}{E}$ (also used for other vectors).
$\underset{\sim}{E}$	Electric field.
$\hat{e}_1, \hat{e}_2, \hat{e}_3$	Cartesian unit vectors.
F	$A_{\ell\ell',\eta}$ matrix representing incident fields.
$f(\underset{\sim}{r}, t)$	Particle concentration.
$\underset{\sim}{f}^i(r)$	Symbolic incident field solution in least-squares technique.
$f(\theta, \phi)$	Radius function for non-spherical particle.

$G(r,\theta,\phi)$	Reilly's test function.
G	Matrix of a_ℓ, b_ℓ, c_ℓ, and d_ℓ.
$g^s(r)$	Symbolic scattered field solution in least-squares technique.
$H_m^1(r)$	Hankel function of 1st kind and order m.
H_r, H_θ, H_ϕ	Spherical components of $\underset{\sim}{H}$.
$\underset{\sim}{H}$	Magnetic field.
h_ℓ^1, h_ℓ^2	Spherical Hankel function of the 1st and 2nd kinds of order ℓ.
$h^w(\underset{\sim}{r})$	Symbolic interior field solution in the least-squares technique.
I_ℓ, I_r	Left and right polarized Stokes vector components, Intensities.
$I(\underset{\sim}{r},t,\underset{\sim}{k})$	Intensity at $\underset{\sim}{r}$ at time t along $\underset{\sim}{k}$.
$I_n(\underset{\sim}{r},t,\underset{\sim}{k})$	n^{th} order of scattering intensity.
$I_{n,\ell m,i}$	n^{th} order of scattering intensity at $\underset{\sim}{r}_{\ell m}$ along $\underset{\sim}{k}_i$.
"i"	Superscript, indicating incident wave or field.
$J(\underset{\sim}{r},\underset{\sim}{k})$	Source function.
$J_n(\underset{\sim}{r},t,\underset{\sim}{k})$	n^{th} order of scattering source function.
$J_{n,\ell m,i}$	n^{th} order of scattering source function at $\underset{\sim}{r}_{\ell m}$ along $\underset{\sim}{k}_i$.
$J_\ell(x)$	Spherical Bessel function of the 1st kind of order ℓ.
$\underset{\sim}{k},\underset{\sim}{k}'$	Propagation direction unit vectors.
$\underset{\sim}{k}_i,\underset{\sim}{k}'$	i^{th} propagation direction unit vectors.
k	Wave number.

ℓ,ℓ'	Summation indices.
ℓ	Path length.
ln	Natural logarithm.
m	Refractive index, summation index.
m_1, m_o	Refractive indices inside and outside particle.
$N(\underline{r},a,t)$	Particle distribution function.
$\underline{n}$	Surface normal vector.
$\hat{n}$	Unit surface normal vector.
n	Index of order of scattering, summation index.
$n(r), n(a)$	Particle size distribution function.
$P(\underline{r},t,\theta), P(\theta)$	Unpolarized phase function.
$P_\ell(\cos\theta)$	Legendre polynomial of order ℓ.
$P_\ell^m(\cos\theta)$	m^{th} associated Legendre polynomial of order ℓ.
$p_j(\underline{r},t,\theta)$	Scattering phase function corresponding to j^{th} Stokes vector component.
$P_{jj'}(\underline{r},t,\underline{k}\cdot\underline{k}')$	Polarized phase function used in radiative transfer.
Q_{ji}	Weighted quadrature approximation phase function value for scattering from k_i to k_j.
$Q(\underline{r},t,\theta)$	Modified unpolarized phase function.
R(r)	Reilly's unknown function.
$\hat{r}$, $\underline{r}_o$	Radial unit vector.
$\underline{r},\underline{r}$	Position vector.
$\underline{r}_{\ell m}$	Position of the ℓ,m point in L x M array.

r	Particle radius, radial coordinate.
S, S'	General solution of the Helmholtz equation.
$S_1(\theta), S_2(\theta)$	Angular scattering function.
"s"	Superscript indicating scattered wave or field.
S_n	Expansion coefficient in $a(\theta,\phi)$.
sin	Sine function.
t, t_o	Time variable.
U	Stokes vector component.
u^s	Scalar scattered field.
V	Stokes vector component.
"w"	Superscript indicating interior ("within") wave or field.
x, x_o	Mie size parameter ($= 2\pi a/\lambda$).
$x(\theta)$	Irregular particle shape function.
$y_\ell(x)$	Spherical Bessel function of the 2nd kind of order ℓ.
$\hat{z}$	Unit vector in the z direction, identical with $\hat{e}_3$.
z	Cartesian coordinate.
α_ℓ	Angular scattering function expansion coefficient.
$\alpha_{\ell m}$	Extinction coefficient ar $\chi_{\ell m}$.
$\alpha(\chi, t)$	Extinction coefficient at χ at time t.
β_ℓ	Angular scattering function expansion coefficient.
$\beta(\chi, t)$	Scattering coefficient at χ at time t
γ	Parameter for Deirmendjian particle size distribution function.

γ_ℓ	Incident Debye potential expansion coefficient.
δ	Parameter for Deirmendjian particle size distribution function, phase difference.
ε	Dielectric function (constant) total fitting error.
$\varepsilon_{i1}, \varepsilon_{i2}$	Fitting errors in least-squares technique.
η	Exponent coefficient in Junge particle size distribution function.
$\eta_\ell(x)$	Radial function, = $xy_\ell(x)$.
$\eta_\ell(\theta)$	Angular function used in $S_1(\theta)$ and $S_2(\theta)$.
κ	Real part of m.
λ	Wavelength.
μ	Permeability.
μ	Cos(θ), $\underset{\sim}{k} \cdot \hat{z}$.
ν	Negative imaginary part of m.
ω	Angular frequency.
ω^*	Effective albedo.
$\omega(\underset{\sim}{r},t), \omega$	Albedo.
Φ	Magnetic scalar potential.
Φ, Φ^i, Φ^s	Scalar Helmholtz equation solution of Keilly.
$\Phi_n(r,\theta,\phi)$	Symbolic linearly independent function of least-squares technique.
ϕ	Azimuthal angle.
$\underset{\sim}{\Pi}$	Electric Hertz vector.

π	Electric Debye potential, ratio of circle circumference to diameter.
Ψ	Electric scalar potential.
$\Psi_n(r,\theta,\phi)$	Symbolic linearly independent function of least-squares technique.
$\psi_\ell(x)$	Radial function, = $xj_\ell(x)$.
ρ	Charge density.
$\rho_\ell^1(x)$, $\rho_\ell^2(x)$	Radial function, = $xh_\ell^1(x)$ and $xh_\ell^2(x)$
$\underset{\sim}{\Xi}$	Magnetic Hertz vector.
σ	Standard deviation used in log-normal particle size distribution function, conductivity, magnetic Debye potential.
$\sigma_{ex}(a,\lambda,m)$	Extinction cross section.
$\sigma_i(a,\lambda,m,\theta)$	Stokes vector component i differential cross section.
$\sigma_{sc}(a,\lambda,m)$	Total scattering cross section.
$\sigma_{sc}(a,\lambda,m,\theta)$	Unpolarized differential scattering cross section.
$\tau_\ell(\theta)$	Angular function used in $S_1(\theta)$ and $S_2(\theta)$.
θ	Polar angle and scattering angle.
$\hat{\theta}$	Unit polar vector.
$\underset{\sim}{\nabla}$	Gradient operator.
$\Delta\underset{\sim}{E}$	Boundary condition $\underset{\sim}{E}$ function.
$\Delta\underset{\sim}{H}$	Boundary condition $\underset{\sim}{H}$ function.
$\langle r \rangle$	Average particle size used in log-normal particle size distribution function.
∞	Infinity.

DISTRIBUTION

	No. of Copies
Commander USATRADOC Attn: ATCD-TEC, Dr. Pastel Ft. Monroe, VA 23651	1
Commander USAMERADCOM Attn: DRXFB-RT, Mr. Kezer Ft. Belvior, VA 22060	2
Commander Naval Weapons Center Attn: R. Bird Dr. A. Shlanta China Lake, CA 93555	1 1
Director NVEOL Attn: DRSEL-NV-VI, R.J. Bergmann , T. Cassady Ft. Belvoir, VA 22043	1 1
Commander Naval Air Systems Command Code Air-310C, Dr. H. Rossenwasser Washington, DC 20361	1
Director AMSAA Attn: Mr. T. Dolce Mr. P. Frosell Aberdeen Proving Grounds, MO 20783	1 1
Commander Naval Intelligence Support Center Attn: NISC Code 433, Mr. St. Aubin 4301 Suitland Road Suitland, MD 20930	1
Director USATRADOC System Analysis Activity Attn: ATAA, Dr. Payne ATAA-TDS, MAJ Allen ATAA-TGA, Dr. Domingus White Sands Missle Range, NM 88002	1 1 1

	No. of Copies
PM Smoke/ Obscurants Attn: DRCPM-SMK Aberdeen Proving Grounds, MD 21005	1
Director Chemical Systems Laboratory Attn: DRDAR-CYL-A, R. Pennsyle DRDAR-CLB-P, J. Vervier DRDAR-CLB-P, Dr. Stuebing Aberdeen Proving Grounds, MD 21010	 1 1 1
Commander Harry Diamond Laboratory Attn: DRXDO-RAF, Dr. Giglio 2800 Powder Mill Road Adelphi, MN 20783	 1
The Pentagon Attn: Dr. Walsh, Rm 3D1079 DUSA(OR), Dr. Fallin Washington, DC 20301	 1 1
Commander DARCOM Attn: DRCBSI/COL C. Gearin 5001 Eisenhower Road Alexandria,VA 22304	 1
General Research Corporation Attn: Dr. R. Zirkind 7655 Old Springhouse Road West Gate Park McKlean, VA 22101	 1
SAI Attn: F. G. Smith Ann Arbor, MI 48105	 1
Oklahoma State University Field Office Attn: Dr. C. Arpke Mr. B. Chancey Eglin AFB, FL 32542	 1 1
Oklahoma State University Attn: Dr. M. Smith School of Technology Stillwater, OK 74074	 1

	No. of Copies
Commander Wright- Patterson AFB Attn: AFAL-WRP-3, Mr. Huffman ASD/ENASC, L. J. Beasley Dayton, OH 45433	 1 1
Commander Naval Weapons Support Center Attn: C. Lokhamp, Code 502 L. Hitchcock D. Johnson C. Dinerman Crane, IN 47522	 1 1 1 1
Commander Dugway Proving Grounds Attn: Lothar Saloman Dugway, UT 84022	 1
Commander OMEW Attn: DRSEL-WLM-SE, A. Davenport DRSEL-WLM-SL, K. Larson DRSEL-WLM-ST, S. Hoihjelle White Sands Missile Range, NM 88002	 1 1 1
Director Atmospheric Sciences Laboratory Attn: F.V. Hansen AMSEL-BL-SY, F. Horning AMSEL-BL-SY, Dr. Gomez White Sands Missile Range, NM 88002	 1 1 1
Commander Eglin AFB Attn: AFATL-DCMT, Mr. Burnett Eglin AFB, FL 32542	 1
Commander Naval Support Weapons Center Attn: Code DG-302, D. L. Shamblin Dahlgren, VA 22448	 1
Defense Documentation Cameron Station Alexandria, VA 33214	 12

AD-A058 385 ARMY MISSILE RESEARCH AND DEVELOPMENT COMMAND REDSTO--ETC F/G 20/3
AN INVESTIGATION OF RADIATION TRANSFER THROUGH AEROSOLS.(U)
JUN 78 B W FOWLER

UNCLASSIFIED DRDMI-C-78-3 NL

3 OF 3
AD
A058 385

END
DATE
FILMED
-11-78
DDC

	No. of Copies
The University of Tennessee Space Institute	
Attn: Dr. R. Kohl	1
Dr. K. E. Harwell	1
Tullahoma, TENN 37388	
Louisiana Technical University	
Department of Physics	
Attn: Dr. N. Witriol	1
P. O. Box 5296	
Ruston, LA 71270	
Lockhead Missile and Space Co., Inc.	
Huntsville Research and Engineering Center	
Attn: L. R. Baker	1
Dr. L. Pinkley	1
4800 Bradford Dr.	
Huntsville, AL 35804	
Clarkson College	
Attn: Dr. M. Kerker	1
Potsdam, NY 13676	
Pacific-Sierra Research Corporation	
Attn: Dr. R. Lutomurski	1
1456 Colverfield Blvd	
Santa Monica, CA 90404	
Institute for Atmoshperic Optics and Remote Sensing	
Attn: Dr. A. Deepak	1
P. O. Box P	
Hampton, VA 23666	
Hughes Aircraft Company	
Attn: D. Allen, MS E182	1
Culver City, CA 90230	
Hughes Aircraft Company	
Attn: J. Baer	1
3322 Memorial Pkwy	
Huntsville, AL 35801	
General Dynamics	
Pomona Division	1
Attn: W. M. Harborth	
P. O. Box 2507	
Pomona, CA 91766	

	No. Of Copies
The University of Alabama in Huntsville Department of Physics Attn: Dr. L. Smalley Huntsville, AL 35806	1
Dynetics, Inc. Attn: Dr. S. Gilbert P. O. Box Drawer B Huntsville, AL 35805	1
Raytheon Company Equipment Divison Equipment Development Laboratories Attn: Dr. A. Jelalian Dr. C. Sonnenshein 528 Boston Post Road Sudbury, MASS 01776	1 1
Analytics Attn: Dr. R. Goldman 2500 Maryland Road Willow Grove, PA 19090	1
DRCPM-HEL, Dr. Sepucha	1
-VI, Mr. Havchanka	1
-MP, COL DeFatta	1
-ROL, CPT Cox	1
-CF, Mr. Kay	1
-DT, COL Williamson	1
-	
DRSMI-LP	1
DRDMI-T, Dr. Kobler	1
-TEO, Mr. Anderson	1
-TE, Mr. Widenhofer	1
- Mr. T. Jackson	1
-Y, Mr. May	1
-C, COL Cranford	1
Mr. Atkins	1
TRADOC LN OF, LTC Johnson	1
-CGA, Dr. Fowler	50
-CA, Dr. McDaniel	1
-CE, Mr. Johnston	1
-HS, Dr. Honeycutt	1
-I, Mr. Fowler	1
-TI (Record Copy)	1
(Reference Copy)	1
-TB	3